Joint FAO/IAEA Programme
Nuclear Techniques in Food and Agriculture

COSMIC RAY NEUTRON SENSING

APPLICATIONS IN AGRICULTURAL WATER MANAGEMENT

Cosmic ray neutron sensing

Applications in agricultural water management

Hami Said, Emil Fulajtár, Trenton Franz, Gabriele Baroni, Rafael Rosolem, Modou Mbaye, Gerd Dercon & Lee Heng

Hami Said – Joint FAO/IAEA Centre of Nuclear Techniques in Food and Agriculture, International Atomic Energy Agency, Vienna, Austria.

Emil Fulajtár – Joint FAO/IAEA Centre of Nuclear Techniques in Food and Agriculture, International Atomic Energy Agency, Vienna, Austria; Soil Science and Conservation Research Institute, National Agricultural and Food Centre, Bratislava, Slovakia

Trenton Franz – School of Natural Resources, University of Nebraska-Lincoln, USA.

Gabriele Baroni – Department of Agricultural and Food Sciences (DISTAL), Alma Mater Studiorum – University of Bologna, Italy.

Rafael Rosolem – School of Civil, Aerospace, and Design Engineering, University of Bristol. Cabot Institute for the Environment, University of Bristol, United Kingdom.

Modou Mbaye – Centre d'Étude Régionale pour l'Amélioration de l'Adaptation à la Sècheresse (CERAAS), Senegal.

Gerd Dercon – Joint FAO/IAEA Centre of Nuclear Techniques in Food and Agriculture, International Atomic Energy Agency, Vienna, Austria.

Lee Heng – Joint FAO/IAEA Centre of Nuclear Techniques in Food and Agriculture, International Atomic Energy Agency, Vienna, Austria.

Food and Agriculture Organization of the United Nations
Vienna, 2025

Required citation:
Said, H., Franz, T., Baroni, G., Rosolem, R., Mbaye, M., Fulajtár, E., Dercon, G. & Heng, L. 2025. *Cosmic ray neutron sensing – Applications in agricultural water management.* Vienna, FAO. https://doi.org/10.4060/cd2650en

ISBN 978-92-5-139147-1

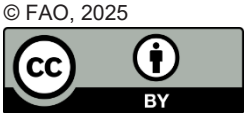

Contents

Preface

Characterisation of soil moisture temporal dynamics and its spatial distribution has become a key issue for improving agricultural land management. Agriculture is very demanding for water, and it consumes approximately seventy percent of water used by human society. Water is a major limiting factor for optimizing food production. While soil properties can be improved by careful land management and nutrients can be supplied relatively easily at reasonable costs, the water availability is a key limiting factor as water is needed in great quantities, which cannot be easily transported for large distances and agriculture depends on local water sources. Therefore, optimizing the water use management is a crucial condition for improving crop production and securing food supply for growing population. For this reason, the data on soil moisture, its spatial distribution and temporal dynamics is needed and the techniques enabling a systematic monitoring of soil moisture across scales should be improved.

The assessment of soil moisture is a complex task because of its remarkable spatial and temporal variability. The major problem is to obtain spatial soil moisture data representing territorial units corresponding to the spatial scale of agricultural fields. Conventional soil moisture methods (such as gravimetric method, electronic sensors, thermal sensors, pressure sensors, etc.) provide point data only. To characterize the soil moisture of spatial units a great number of point measurements are needed what makes soil moisture assessment costly and labour demanding, the interpolation of point data is difficult. Most conventional methods (except for capacitance sensors) are invasive (i.e. the soil is disturbed by measurements and the next measurement should be taken at different places) what makes the systematic monitoring of moisture temporal dynamics problematic. After all effort the information obtained by conventional methods is not satisfactory.

Using cosmic ray neutron technique to detect soil water is a promising approach with great potential enabling to overcome the problems of point data obtained by conventional techniques. The cosmic ray neutron technique measuring soil moisture was introduced approximately a decade ago and during last years it developed to a well-established technique using commercially accessible cosmic ray neutron sensors and algorithm for converting neutron data to soil moisture values was developed. CRNS technique is used by growing number of research institutions, and it is spreading quickly. However, these techniques need refinement and improved methodology before seeing widespread use and adoption by land users and land managers, agricultural enterprises and individual farmers needs some refinement of the methodology. This is a crucial step for transforming this technique from research community to general agricultural practice. Standardised technique and interpretation methods should allow to use CRNS technique routinely for long term soil moisture monitoring programmes run by national governmental organizations, private agricultural enterprises and may be even municipal authorities, local farmer associations or individual farmers.

Refinement of CRNS methodological background and the development of agricultural applications became an objective of IAEA Coordinated Research Project D12014 “Enhancing agricultural resilience and water security using Cosmic ray Neutron Sensor” (2019–2024). The IAEA through its Soil and Water Management & Crop Nutrition (SWMCN) Subprogramme of the Joint Food and Agriculture Organization (FAO)/International Atomic Energy Agency (IAEA) Centre of Nuclear Techniques in Food and Agriculture is promoting the use of nuclear techniques in land management and soil water assessment is among its major priorities. This initiative is building on former activities of the IAEA in this field such as using water isotopes, neutron probe and cosmic ray neutron sensors. The recently running coordinated research project (CRP) is building on former achievements in promoting CRNS. This book is one of major outputs of CRP and it should complement former methodological publications of IAEA aimed on CRNS (Wahbi *et al.*, 2018; IAEA, 2017. *Cosmic Ray Neutron Sensing: Use, Calibration and Validation for Soil Moisture Estimation)*. This book provides guidelines for better CRNS data processing and several value-added products useful for agricultural applications and approach using CRNS data for remote sensing soil moisture products validation.

The presented guidelines involve (after introduction) three major chapters. The first chapter focuses on CRNS data processing to obtain soil moisture values from raw neutron counts. Two approaches

are proposed. The CRNS-PoP Spreadsheet is a simple tool based on an Excel add-in, it can be used for processing small CRNS data sets and it is suitable for beginners and CRNS users who are not familiar with computer programming. The second tool is CRSPY and it is a more sophisticated tool programmed in PYTHON programming language, which should be used by more advanced users who are familiar with computer programming and using PYTHON language and this tool is useful for quick and efficient processing of large data sets. The second chapter provides three value-added products: algorithms for smoothening neutron count signal, estimating root zone soil moisture and estimating precipitation based on soil moisture. The third chapter provides an approach using CRNS data to validate the soil moisture retrieval from C-Band of Sentinel-1 satellite image.

1 Introduction

Hami Said, Emil Fulajtár, Trenton Franz, Gabriele Baroni, Rafael Rosolem, Modou Mbaye, Gerd Dercon & Lee Heng

1.2 Importance of soil water management

As the global population marches towards 9.7 billion by 2050 (UNDESA, 2022), the demand for food production is increasing. Globally, the water withdrawal for agriculture currently represents around 70 percent (FAO, 2013). With continuing population increase and changes in dietary requirements, the competition for water use by agriculture with all other economic sectors will exacerbate the need to improve water use efficiency. Furthermore, maintaining food security for a growing population can be even more challenging under future climate change and increasing climate variability. Consequently, more crop per unit of water supply will be required to secure food availability.

Climate change will result in the increase of temperature and potential evapotranspiration, which further affect all components of the water cycle (United Nations Water, 2010). The spatiotemporal distribution of rainfall will become more unpredictable and extreme weather events such as drought periods, extreme rainfalls and floods will become more frequent. In some areas the precipitation will increase, especially in areas where the air exchange between oceans and continents is becoming more intensive due to increased heating of land masses (i.e. areas with monsoon climate such as South and East Asia, East Africa and some parts of South America). The areas with increased precipitation will be more prone to flooding. In other areas (i.e. West Asia, North and South Africa, Europe, United States of America, Australia) precipitation will be reduced (Bates *et al.*, 2008). These changes will have significant impact on agriculture productivity and water supply. More areas currently under rainfed agriculture will need to be irrigated if the same level of agricultural production is required. Water resources for irrigation will be more limited as rivers, reservoirs and groundwater recharge will be reduced (Bates *et al.*, 2008). In addition, dryland pastoral ecosystems will be under an increasing threat of land degradation (FAO, 2013). All the above-mentioned changes will require improved land and water management. A climate smart irrigation approach requires improved water allocation mechanisms, such as timely information about available soil water in addition to the reliable delivery of water. Accurate irrigation scheduling with optimised irrigation amounts is important to achieve best water practices to prevent water overuse (Howell, 2003; FAO, 2013).

Soil moisture is a key component of the surface water balance and plays a crucial role in partitioning rainfall and irrigation into evapotranspiration, surface runoff, and infiltration, for crop and forage production, flood forecasting and drought monitoring. Consequently, the characterization of soil moisture temporal dynamics and its spatial distribution is a critical observational need. Improved assessment of soil moisture is a needed first step to tackle major problems of land and water management with a changing climate: dryland management, flood forecasting and irrigation scheduling. Particularly, dryland management requires reliable and representative information on root zone soil moisture spatial distribution and its seasonal dynamics over large regions occupied mainly by pastoral ecosystems. For this task the techniques enabling a systematic monitoring of soil moisture across scales are needed. The monitoring technique should help to forecast possible drought events and their severities, provide information on medium-term and long-term soil moisture dynamics, assess the impacts of different land uses, vulnerability of ecosystems and identify the potential for implementation of remediation measures such as reforestation, green walls, etc. (FAO/NDMC, 2008).

As cultivated lands are expected to rely more on irrigation for maintaining or increasing crop yields, water withdrawals are expected to increase posing additional pressure to local and regional water resources. This scales the problem from farm- to landscape-level, hence integrated water resources management and planning will become a key challenge to secure water and food availability. Water use and the potential impacts on its quality, can affect downstream flow, reaching even multi-basin

scales across country boundaries. A combined assessment of agricultural systems and their impact on catchment water resources is necessary to evaluate changes and ensure water security. However, the lack of comprehensive soil moisture data and the limited availability of only point-scale data undermines its application to an entire landscape level and contribute to uncertainty in future predictions. For example, flood prediction is based on monitoring of water discharge in rivers and hydrological modelling. Improvement of water monitoring can be achieved through focusing more attention on conditions generating surface runoff, such as improved soil property maps and large-scale monitoring of soil moisture dynamics and its spatial distribution (Meng *et al.*, 2017; Chifflard *et al.*, 2018).

1.2 Major knowledge gaps and limits of traditional approaches

The assessment of soil moisture is a complex task despite it being perhaps the most basic soil variable. This is due to the high spatial and temporal variability of soil moisture. Significant effort has been dedicated to developing measurement methods capturing this variability. Overviews of existing soil moisture measurement methods (c.f. IAEA, 2008; Robinson *et al.*, 2008; Vereecken *et al.*, 2008; Dobriyal *et al.*, 2012) showed that all conventional methods provide point data with limited spatial representativeness, such as the gravimetric method, sensors based on the pressure of capillary suction (tensiometers), thermal sensors and electromagnetic sensors (time domain reflectometry – TDR, frequency domain reflectometry – FDR, capacitance sensors). An important problem is also that most of these methods (except for capacitance sensors using access tubes) are invasive, making it inconvenient for continuous monitoring in croplands, because sensors may need to be removed and replaced due to farm management activities (i.e. planting and harvest). Additionally, the active source soil moisture neutron probe (SMNP) measures a larger volume of soil, but it is still considered as point data. It uses access tubes similarly as capacitance sensors. The major challenge of SMNP is the radioactive neutron source which poses transportation, storage, and regulatory safety issues.

Because soil moisture dynamics are highly variable in time, it is important to establish long-term soil moisture monitoring networks to capture season to season and year to year changes and percentiles. For example, long-term records (minimum of ~ 5–8 years) can be used to assess the "soil moisture seasonal dynamics and long-term trends" of a site or an entire network. The key question of: "how severe is the current drought condition compared to historical values?" can be addressed. Understanding this has enormous benefits on our ability to predict the extent and severity of the current drought situation to mobilize an appropriate response and recovery. Second, reliable long-term soil moisture networks in agricultural systems can be used to calibrate and validate remote sensing soil moisture products for directly applied agricultural indices (e.g. linking water availability to crop yield). Establishment of point scale soil moisture networks are impractical to cover large areas. Thus, satellites have been introduced to provide global coverage and can be used in operational systems (i.e. weather prediction, regional drought monitoring, early warning systems, etc.). However, satellites have limitations, as they often trade spatial resolution with temporal sampling. For example, microwave remote sensing satellites used for soil moisture monitoring have either a good spatial resolution (tens of meters) with rather poor temporal sampling (several days to weeks) or vice versa (daily sampling at kilometre scales). Their performances are highly dependent on the type of vegetation cover, with uncertainty increasing with vegetation density. In addition, satellite remote sensing products are limited to the surface soil moisture dynamics, rarely depicting the root zone characteristics. Therefore, a clear need exists for complementing remote sensing products with ground-based root zone observations. Having ground truth standardized measurements for soil moisture in a variety of regions and land cover types is crucial for calibration and validation of satellite derived soil moisture products.

With respect to agricultural water management, reliable and representative soil moisture sensors have enormous benefits on both irrigated and rainfed systems. In irrigated settings where water delivery infrastructure exists, decisions about timing and amount of irrigation can be made to optimize water management. Likewise, in rainfed systems pre-season soil moisture can be used to optimize planting date, crop type, and fertilizer application. In agricultural systems that use heavy machinery, soil moisture is a critical factor in determining soil strength and thus optimizing the use of equipment and labour for cultivation. Despite its importance, there has been a clear spatial gap in soil moisture measurements at

scales relevant to farming. On one hand, the point measurements provide too localised information and do not represent the true heterogeneity in farm fields, whereas satellite remote sensing products are still too coarse for small farms across the globe.

1.3 The Cosmic Ray Neutron Sensor – CRNS

A promising technological advancement that fills this critical measurement gap is the cosmic ray neutron sensor (CRNS) for estimating area-average soil water content (SWC) over the top tens of centimeters of soil (reaching the root zone in some cases). The CRNS technology was first introduced by Zreda *et al.* (2008). It allows soil moisture estimation at scales of few hundred meters via interactions with naturally occurring free neutrons released by interaction of cosmic rays with atmospheric gases (Desilets *et al.*, 2010). The principle of CRNS technique is based on measuring the change in epithermal neutron intensity near the earth's surface. Following a series of known corrections for time variations in ambient pressure, air humidity, and high-energy neutrons, the corrected epithermal neutron counts are highly sensitive to changes in water content of soil. The instrument has a footprint of ~150 m radius circle and a penetration depth of ~ 70 cm in dry soil and ~ 20 cm in wet soil (Kohli, 2015). The CRNS can be used as a stationary detector or as a mobile detector carried by walking or ground and airborne vehicles to map soil moisture spatial variability. Given the spatial variability of soil moisture and measurement volume of point sensors, the scale advantage of CRNS makes it better suited for comparing against satellite soil moisture products (Döpper *et al.* 2022) and studying water circulation processes (e.g. crop evapotranspiration) (Wang *et al.*, 2018). With respect to establishing long-term monitoring networks in agricultural systems, the CRNS has many advantages over conventional point sensors. The CRNS is non-invasive (except for its initial calibration using soil samples), requires low maintenance, is not sensitive to surface roughness, soil temperature and salinity variations, and can be used in highly variable and extreme environments where in-situ sensors are impractical (e.g. sites where soils contain coarse aggregates, alpine areas).

The CRNS technology relies on the following equation to convert raw neutron counts (N_{raw}), usually expressed in counts per hour (cph), to estimated volumetric soil moisture (Θ_{vol}), usually given in cm^3/cm^3.

$$\theta_{vol} = \left[\frac{a_0}{\frac{N_{raw} \cdot f_p \cdot f_i \cdot f_h \cdot f_v}{N_0} - a_1} - a_2 - LW - WSOM \right] \frac{\rho_{bd}}{\rho_w} \tag{1.1}$$

In this equation, a_0, a_1, and a_2 are coefficients previously determined by neutron particle models (Zreda *et al.*, 2008; Desilets *et al.*, 2010) and their values are 0.0808, 0.372, and 0.115, respectively. *LW* is the lattice (chemically bounded mineral) water (g/g), *WSOM* is the water equivalent soil organic matter (g/g), ρ_{bd} is the dry soil bulk density (g/cm^3), and ρ_w is the density of liquid water taken to be constant at 1 g/cm^3. Note that *LW, WSOM*, and ρ_{bd} are site-specific parameters, which are typically provided by the user through soil sampling (Franz *et al.*, 2015; Heidbüchel *et al.*, 2016) or following the approach by Avery *et al.* (2016). *LW* can also be influenced by mineralogical composition as distinct minerals hold different amounts of lattice water. However, this may be an issue for some soils with highly specific mineral composition (e.g. tropical highly weathered soils, volcanic soils, soils with high content of swelling clays, arid soil); however, for most soils this influence can be neglected. The terms f_p, f_i, f_h and f_v correspond to the post-processing correction functions applied due to atmospheric pressure (p), incoming high-energy neutron intensity (i), atmospheric water vapor (h) variations, and aboveground biomass (v). Those correction functions are time-varying multipliers applied to the raw neutron measurements (N_{raw}) representing the site-specific corrected neutron count rate. For example, changes in atmospheric pressure (p) can impact the neutron counting rates measured by the sensor. In other words, a denser (lighter) atmospheric column can lead to relatively lower (higher) amount of neutrons reaching the sensor. Hence, it is important to monitor this variability against a reference, pre-defined, atmospheric pressure value along with information about site location (i.e. latitude),

elevation, and cut-off rigidity (Desilets 2021). The term f_i relates to the fact that solar activity and site location (due to the Earth's geomagnetic field) can impact the variability of incoming high-energy neutron reaching the surface (and ultimately contributing to the neutron counting rates) (Desilets *et al.*, 2006). This is a dynamic (time-varying) correction, which requires the user to monitor high-energy neutron variability from an external data source, for example from the Neutron Monitor Data Base (NMDB; www.nmdb.eu) following, by default, the methodology proposed by Hawdon *et al.* (2014). Alternatively, the use of muons directly measured at the site has also been shown to be a valuable approach for accounting for this effect (Stevanato *et al.*, 2022). Variability in atmospheric water vapor and aboveground biomass both follow the fact that additional sources of hydrogen (other than water in the soil) can affect the sensor measurement by incorrectly attributing the reduction of neutron counts to soil moisture changes (Rosolem *et al.*, 2013; Baatz *et al.*, 2015; Wahbi *et al.*, 2018). Such corrections are applied to effectively remove those additional sources of hydrogen before converting the neutron counts to soil moisture. Finally, N_0 is defined as the theoretical neutron count rate found in absolutely dry conditions (i.e. the maximum rate obtained at the site without any presence of hydrogen atoms). N_0 is a key parameter obtained via site-specific calibration. If not calibrated, the cosmic ray neutron sensor would only provide relative changes of soil wetness which may not be ideal for agricultural and hydrological applications. The calibration of cosmic ray neutron sensors relies on the collection of several (tens to hundreds) of soil samples within the sensor footprint (i.e. around 200 m radius). The quality of calibration is directly related to the number and quality of soil samples obtained, and the availability of information from other sources of hydrogen (e.g. atmospheric water vapor, lattice water, soil organic matter). If volumetric soil samples are available, then *in situ* dry soil bulk density (ρ_{bd}) can be estimated and the volumetric soil moisture (Θ_{vol}) is estimated; otherwise, gravimetric soil moisture ($\Theta_{grav} = \Theta_{vol} / \rho_{bd}$; in g/g) is obtained instead.

Over the past decade since its development, CRNS theory and best practices for equipment have improved including better understanding of detection area and depth, best practices for installation, calibration, and validation of stationary and mobile applications (see IAEA 2017, 2018). However, practical implementation of using the CRNS data by users requires data processing harmonization and further development of value-added products. In this book three open-source CRNS data processing tools which are targeted to both new users and dataset harmonization will be introduced (see **Chapter 2**). In addition, to maximize the relevance of CRNS, practical applications such as daily root zone soil moisture and daily landscape rainfall calculations will be outlined in the **Chapter 3**. In **Chapter 4**, an innovative approach to develop a high spatial and temporal resolution soil moisture product by combining remote sensing and CRNS technology will be presented.

References

Avery, W.A, Finkenbiner, C., Franz, T.E., Wang, T., Nguy-Robertson, A.L., Suyker, A., Arkebauer, T., & Muñoz-Arriola, F. 2016. Incorporation of Globally Available Datasets into the Roving Cosmic-Ray Neutron Probe Method for Estimating Field-Scale Soil Water Content. *Hydrol. Earth Syst. Sci.* 20 (9): 3859–72. https://doi.org/10.5194/hess-20-3859-2016

Baatz, R., Bogena, H.R., Hendricks Franssen, H.-J., Huisman, J.A., Montzka, C. & Vereecken, H. 2015. An empirical vegetation correction for soil water content quantification using cosmic ray probes, *Water Resour. Res.* 51: 2030–2046, https://doi.org/10.1002/2014WR016443.

Bates, B.C., Kundzewicz, Z.W., Wu, S. & Palutikof, J.P., eds. 2008. *Climate Change and Water. Technical Paper of the Intergovernmental Panel on Climate Change. IPCC Secretariat, Geneva.*

Bloschl, G., Blaschke, A.P., Broer, M., Bucher, C., Carr, G., Chen, X., Eder, A., Exner-Kittridge, M., Farnleitner, A., Flores-Orozco, A., Haas, P., Hogan, P., Kazemi Amiri. A., Oismuller, M., Parajka, J., Silasari, R., Stadler, P., Straub, P., Vreugdenhil, M., Wagner, W. & Zessner, M. 2016. The Hydrological Open-Air Laboratory (HOAL) in Petzenkirchen: a hypotheses-driven observatory, *Hydrol. Earth Syst. Sci.* 20: 227–255.

Chifflard, P., Kranl, J., Strassen, G., zur & Zepp, H. 2018. The significance of soil moisture in forecasting characteristics of flood events. A statistical analysis in two nested catchments. *J. Hydrol. Hydromech,* 66 (1): 1–11. https://doi.org/10.1515/johh-2017-0037

Desilets, D. 2021). *Intensity correction factors for a cosmic ray neutron sensor.* Zenodo (data set), https://doi.org/10.5281/ZENODO.4569062.

Desilets, D., Zreda, M. & Ferré, T.P.A. 2010. Nature's neutron probe: Land surface hydrology at an elusive scale with cosmic rays, *Water Resour. Res.* 46: W11505. https://doi.org/10.1029/2009WR008726.

Desilets, D., Zreda, M. & Prabu, T. 2006. Extended scaling factors for in situ cosmogenic nuclides: New measurements at low latitude, *Earth Planet. Sci. Lett.* 246 (3–4): 265–276. https://doi.org/10.1016/j.epsl.2006.03.051

Dobriyal, P., Qureshi, A., Badola, R. & Hussain, S.A. 2012. A review of the methods available for estimating soil moisture and its implications for water resource management. *J, Hydrol.* 458–459: 110–117.

FAO & National Drought Mitigation Center (NDMC). 2008. *The Near East Drought Planning Manual: Guidelines for Drought Mitigation and Preparedness Planning.* 52pp. FAO Regional Office for the Near East, and (NDMC, University of Nebraska.

FAO. 2013. *The State of Food and Agriculture 2023. Food systems for better nutrition.* Rome, Italy, 2023.

Franz, T.E., Wang, T., Avery, W., Finkenbiner, C. & Brocca., L. 2015). Combined Analysis of Soil Moisture Measurements from Roving and Fixed Cosmic Ray Neutron Probes for Multiscale Real-Time Monitoring. *Geophys. Res. Lett.* 42 (9): 3389–96. https://doi.org/10.1002/2015GL063963

Hawdon, A., McJannet, D. & Wallace, J. 2014. Calibration and correction procedures for cosmic-ray neutron soil moisture probes located across Australia. *Water Resour. Res*. 50: 5029–5043, https://doi.org/10.1002/2013WR015138

Heidbüchel, I., Güntner, A. & Blume, T. 2016. Use of Cosmic-Ray Neutron Sensors for Soil Moisture Monitoring in Forests. *Hydrol. Earth Syst. Sci.* 20 (3): 1269–1288. https://doi.org/10.5194/hess-20-1269-2016

Howell, T.A. 2003. Irrigation Efficiency. In: Howell, T.A., ed. *Encyclopedia of Water Science*, pp. 467–472. Marcel Dekker Inc., New York.

IAEA. 2008. *Field Estimation of Soil Water Content.* Training Course Series No. 30, IAEA, Vienna, 130 pp.

IAEA. 2017. *Cosmic Ray Neutron Sensing: Use, Calibration and Validation for Soil Moisture Estimation.* IAEA-TECDOC-1809. Joint FAO/IAEA Programme Nuclear Techniques in Food and Agriculture. Vienna, Austria. www pub.iaea.org/books/IAEABooks/11097/Cosmic-Ray-Neutron-Sensing-Use-Calibration-and-Validation-for-Soil-Moisture-Estimation

IAEA. 2018. Soil Moisture Mapping with a Portable Cosmic Ray Neutron Sensor. IAEA-TECDOC-1845. Joint FAO/IAEA Programme Nuclear Techniques in Food and Agriculture. Vienna, Austria. www-pub.iaea.org/books/IAEABooks/12357/Soil-Moisture-Mapping-with-a-Portable-Cosmic-Ray-Neutron-Sensor

Köhli, M., Schrön, M., Zreda, M., Schmidt, U., Dietrich, P. & Zacharias, S. 2015. Footprint characteristics revised for field-scale soil moisture monitoring with cosmic-ray neutrons, W*ater Resour. Res*. 51: 5772– 5790, https://doi.org/10.1002/2015WR017169.

McCabe, M.F., Rodell, M., Alsdorf, D.E., Miralles, D.G., Uijlenhoet, R., Wagner, W., Lucieer, A., Houborg, R., Verhoest, N.E.C., Franz, T.E., Shi, J.C., Gao, H.L. & Wood, E.F. 2017. The future of Earth observation in hydrology, *Hydrol. Earth Syst. Sci. 21* (7): 3879–3914. https://doi.org/10.5194/hess-21-3879-2017

Meng X., Wang H., Wu Y., Long A., Wang J., Shi C. & Ji X. 2017. Investigating spatiotemporal changes of the land-surface processes in Xinjiang using high-resolution CLM3. 5 and CLDAS: Soil temperature. *Sci. Rep.* 7: 1–14. 10.1038/s41598-017-10665-8

Robinson, D.A., Campbell, C.S., Hopmans, J.W., Hornbuckle, B.K., Jones, S.B., Knight, R., Ogden, F., Selker, J. & Wendroth, O. 2008. Soil Moisture Measurement for Ecological and Hydrological Watershed-Scale Observatories: A Review. *Vadose Zone J.* 7: 358–389. https://doi.org/10.2136/vzj2007.0143

Rosolem, R., Gupta, H.V., Shuttleworth, W.J., de Gonçalves, L.G.G. & Zeng, X. 2013. Towards a comprehensive approach to parameter estimation in land surface parameterization schemes. *Hydrol. Process.* 27: 2075–2097. https://doi.org/10.1002/hyp.9362

Stevanato, L., Baroni, G., Oswald, S.E., Lunardon, M., Mares, V., Marinello, F., *et al.* 2022. An alternative incoming correction for cosmic-ray neutron sensing observations using local muon measurement. *Geophys. Res. Lett.* 49: e2021GL095383. https://doi.org/10.1029/2021GL095383

United Nations Department of Economic and Social Affairs, Population Division. 2022. *World Population Prospects 2022: Summary of Results.* UN DESA/POP/2022/TR/NO. 3/

United Nations Water. 2010. *UN-Water Annual Report 2010*. 21pp

Vereecken, H., Huisman, J.A., Bogena, H., Vanderborght, J., Vrugt, J.A. & Hopmans, J.W. 2008. On the value of soil moisture measurements in vadose zone hydrology: A review, *Water Resour. Res*. 44, W00D06. https://doi.org/10.1029/2008WR006829.

Veronika, D., Thomas, J., Ann-Kathrin, H., Maik, H., Till, F., Birgit, K. & Michael, F. 2022. Following the cosmic-ray-neutron-sensing-based soil moisture under grassland and forest: Exploring the potential of optical and SAR remote sensing. *Sci. Remote Sens.* 5. https://doi.org/10.1016/j.srs.2022.100056.

Wahbi, A., Heng, L.K. & Dercon, G. 2018. *Cosmic Ray Neutron Sensing: Estimation of Agricultural Crop Biomass Water Equivalent.*

Zreda, M., Desilets, D., Ferré, T.P.A. & Scott, R.L. 2008. Measuring soil moisture content non-invasively at intermediate spatial scale using cosmic-ray neutrons, *Geophys. Res. Lett.* 35: L21402, https://doi.org/10.1029/2008GL035655.

2 Data processing: from cosmic ray neutrons to soil moisture

Gabriele Baroni & Rafael Rosolem

2.1 Data processing and sensor calibrations

Despite the continuous adoption of cosmic ray neutron sensing technology over the last decade, individual sites and even individual national networks still apply their own protocols for data collection and processing. For example, the first United States of America COSMOS network still applies the original calibration and correction procedures from Desilets *et al.* 2010 and Franz *et al.* 2012a, despite the fact that significant knowledge has been gained over the years regarding sensor calibration (Iwema *et al.* 2015; Schrön *et al.* 2017) and correction approaches to account for additional sources of hydrogen in the atmosphere (Rosolem *et al.* 2013) and biomass (Baatz *et al.* 2015). The COSMOS-UK, for example, applies all up-to-date calibration and correction steps except for the effects of biomass. These factors can play a significant role in contributing to the uncertainties associated with the CRNS technology (Iwema *et al.* 2021).

As the number of CRNS stations continue to increase globally, so does the interest in investigating the characteristics of soil moisture dynamics across different hydroclimates and continents. However, the lack of data harmonisation can undermine the quality of those findings and potentially draw incorrect conclusions about soil water process in different regions of the globe. This can be a result of the investigation to be carried out with a sub-optimal (i.e. not fully processed) CRNS database (see Dirmeyer *et al.* 2016, as an example). In addition, new end-users looking primarily to apply the sensor (and not necessarily further develop them) may still find it difficult to comply with all calibration and processing steps by following solely the vast literature available. Therefore, to mitigate these issues, recent efforts by the CRNS community have been made in the development of open-source CRNS data processing tools which are targeted to both new users and dataset harmonisation.

For easy-to-use and targeted primarily to end-users becoming familiar with the CRNS technology, two Excel spreadsheets have been developed. The first one (CRNS_SoS.xlsm) allows the user to process soil samples to calculate weighted soil moisture for the calibration of the sensor. The second spreadsheet (CRNS_PoP.xlsm) allows the user to insert raw neutrons counts and additional information to derive soil moisture based on state-of-the-art of current literature. The following sections contain the description of these spreadsheets and a step-by-step tutorial to process the data. Some datasets for both soil and CRNS data processing are also integrated in the files as an example.

Another new open-source tool available is the Cosmic Ray Sensor Python (CRSPY) initially developed by Power *et al.* 2021 and expanded here for first time users. The primary goal of CRSPY is to facilitate the harmonisation of multiple CRNS stations in a seamlessly way. Alternatively, it can be used for processing individual sites. The CRSPY tool includes all corrections steps up-to-date with current literature while also generating a comprehensive metadata with additional information from sites that are collected from publicly available global datasets. Example of additional information containing in the metadata include hydroclimate, soil and land cover properties, among others. The CRSPY code is written in Python which is a general high-level programming language widely popular in hydrological and environmental sciences. The Python language (www.python.org) has been developed with the aim to help programmers write clear and logical code for a wide range of small to large-scale projects. Python and its packages are open-source and continuously supported by the open-source community. This sub-section describes particularly the development of CRSPY in detail while also showing some examples of applications from different CRNS sites.

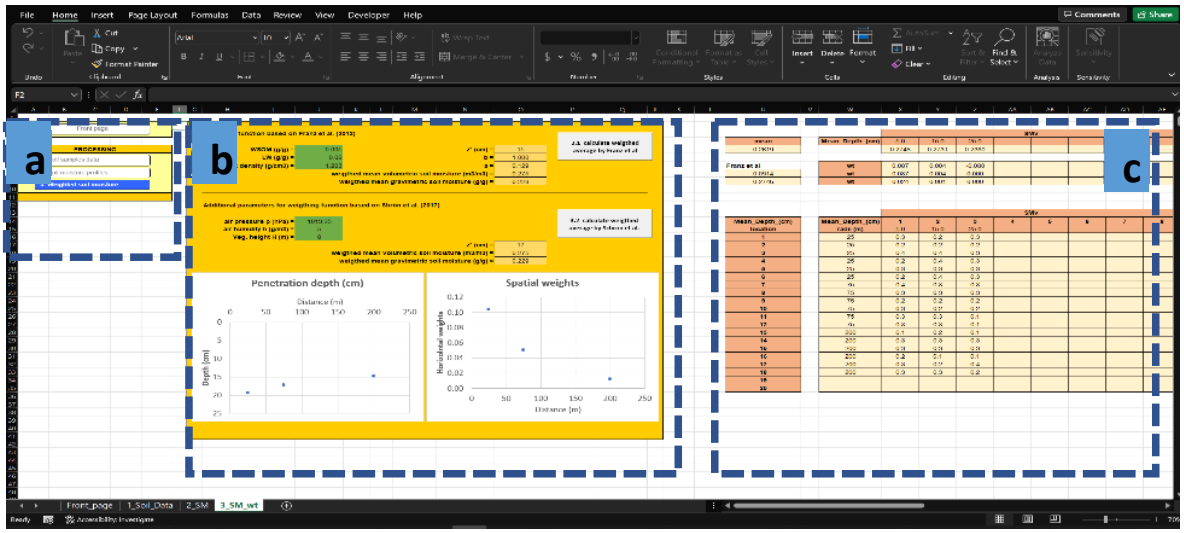

Figure 2.1. Structure of the spreadsheet CRNS soil samples data processing CRNS SoS.xlsm with: (a) table of contents (ToC); (b) data, parameters, and plots; (c) data-processing.

2.2 Soil samples data processing with the spreadsheet 'CRNS_SoS'

A relatively simple spreadsheet (CRNS_SoS.xlsm, Excel Windows) has been developed to guide the user in the analysis of the soil samples used for the calibration of a CRNS sensor. The file described here is freely available at https://zenodo.org/record/7156607. The file contains data collected at the Hydrological Open-Air Laboratory (HOAL) experiment in Petzenkirchen, Austria (Bloschl *et al.* 2016), as an example. Alternatively, the user can insert their own data and follow these guidelines for data processing. Please note that the Excel file has been coded with Macros in Visual Basic for Application (VBA). When opening the file, please enable macros: a pop-up window should appear with the request.

An overview of the structure of the file is shown in **Figure 2.1**. The file is organized in four sheets. The user can move through the file by clicking the corresponding sheet. In addition, a Table of Contents (ToC) has been integrated at the left side to help users to navigate through the file (**Figure 2.1a**). Each sheet is further structured with a window where data are summarized and plotted (**Figure 2.1b**). All the processed data are shown on the right side (**Figure 2.1c**).

The first sheet (*Front_page*) provides an overview of the file, a short description of the structure and some references. The user can select the second tab by clicking at the table of content (ToC) the button '*1. Soil samples data*'.

At the second sheet (*1_Soil_Data*), three buttons are available. The first button (*1.1 Clean and insert new data*) can be used to remove previous analysed data. Then, the user should add the sample data (from cell J51) and fill in all green cells (I5 to I13) with the following information:

- **Location**: the name of the experimental site;
- **Date**: the date when soil samples have been collected;
- **N_locations**: the number of locations where soil samples have been collected (max twenty locations);
- **N_depths**: the number of soil depths has been collected (max eight depths);
- **Ring_volume**: the volume of the soil sampler (cm^3);
- ***WSOM***: a mean value over the CRNS footprint of water equivalent soil organic matter (g/g);
- ***LW***: a mean value of lattice water over the CRNS footprint (g/g).

The sample data at cell J51 should be formatted as follow:

- **n_Sample**: the progressive number of the sample (ID);
- **n_Location**: the progressive number of the location (ID_location);
- **Degrees_(0_N)**: the direction where sample has been taken expressed by angle as the samples are distributed in circle around the CRNS (in degrees, 0 = North), (optional information);
- **Lat**: the latitude of the sample locations (optional);
- **Long**: the longitude of the sample locations (optional);
- **Distance_(m)**: the distance between the CRNS sensor and the locations;
- **Mean_Depth_(cm)**: the depth of the sample;
- **Wet_Weight_(g)**: the wet weight of the soil sample;
- **Dry_Weight_(g)**: the dry weight of the soil sample (after at least 24 h at 105 ° C in the oven);
- **Tin_Weight_(g)**: the weight of the used tin-cup (optional).

As an example, the user can click the second button (*1.2 copy example data*) and soil data collected at the Hydrological Open-Air Laboratory (HOAL) experiment in Petzenkirchen, Austria are copied at each cell.

Once all the cells have been populated with own data or from the example, the user can click on the third button (*1.3 calculate*). The cells O5-O8 are automatically filled in and four plots are visualized with calculated values of gravimetric soil moisture (SMg), bulk density (Bd), porosity and volumetric soil moisture (SMv). By a first visual interpretation the user can modify values or remove outliers from each cell.

The user can now move to the next sheet (*2_SM*) by clicking the corresponding title at the ToC (*2. Soil moisture profile*). Here one button is available (*2.1 copy data and plot*). The user can click this button and the data are further arranged to visualize the soil moisture profiles (i.e. by soil depths). Also at this sheet, the user can remove/modify any outliers that are detected by visual inspections of the results on the right side of the sheet (e.g. X9, etc.). Plots are updated automatically.

The user can move to the next sheet (*3_SM_Wt*) by clicking the correspondent title at the ToC (*3. Weighted soil moisture*). Two buttons are available in this sheet. The user can click the first button (*3.1 calculate weighted a verage by Franz et al.*). Values are weighted based on the approach proposed by Franz *et al.* (2012a). Penetration depth is also calculated (z*). In case additional information is also available on-air pressure, air humidity and vegetation height during the soil sampling campaign, the user can insert these values to the specific cells (J14, J15 and J16 respectively) and click the second button (*3.2 calculate weighted average by Schrön et al.*). Values are weighted based on the approach presented by Schrön *et al.* (2017). This approach provides a more refined estimation also considering the spatial sensitivity of the signal detected by the neutron sensor. In addition to the average penetration depth, two plots showing the spatial variability of the penetration depth and of the weights are also updated. These weighted values can be used for calibration of the parameter N_0 (see **Equation 1.1**) and for the interpretation of the CRNS signal.

2.3 CRNS data processing with the spreadsheet 'CRNS_PoP'

An additional relatively simple spreadsheet (CRNS_PoP.xlsm, Excel Windows) has also been developed to guide the user in the CRNS data processing, from measured neutrons to soil moisture estimation. The file described here is freely available at https://zenodo.org/record/7156607. The file contains data collected at the Hydrological Open-Air Laboratory (HOAL) experiment in Petzenkirchen, Austria (Bloschl *et al.* 2016), as an example. Alternatively, the user can insert their own data and follow these guidelines for data processing. Please note that the Excel file has been coded with Macros in

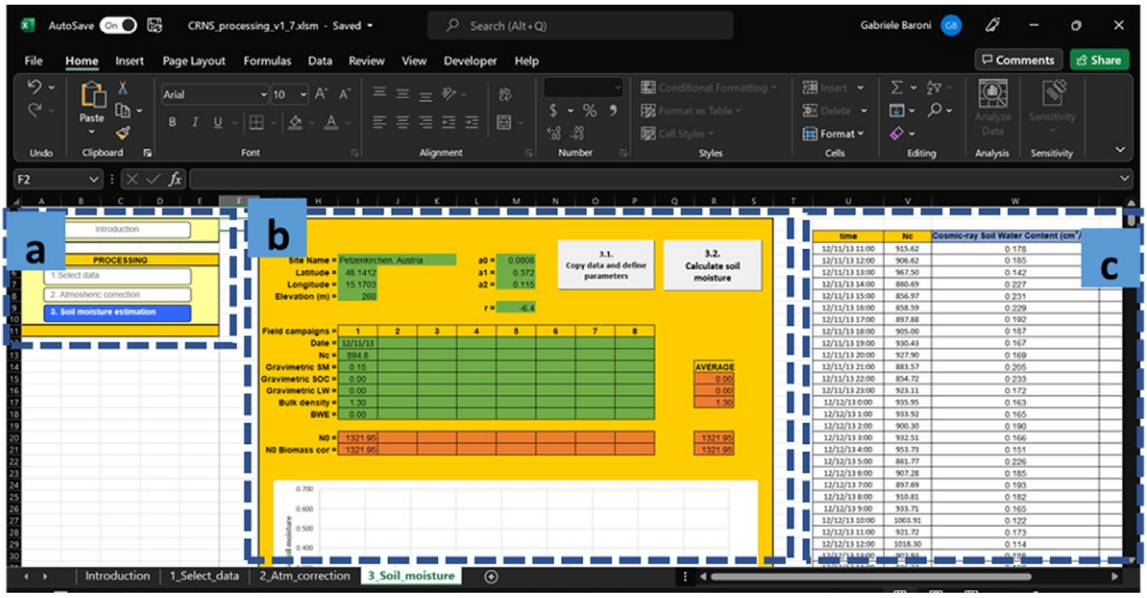

Figure 2.2. Structure of the spreadsheet CRNS-data post processing CRNS_PoP: (a) table of contents (ToC); (b) data, parameters and plots; (c) data-processing

Table 2.1. Data structure of the row data to be processed

Time	Nrow	Ninc	P (bar)	T (°)	RH (%)
12/11/2013 11:00	794.0	122.5	1002.4	4.1	87.3
12/11/2013 12:00	787.0	122.5	1002.2	4.2	87.8
12/11/2013 13:00	843.0	122.5	1001.6	4.2	88.8

Where:

Time is the interval when neutron counts have been recorded (e.g., hourly data):

Nrow is neutrons measured by the sensor;

Ninc is'measured incoming variations, e.g., from neutron data base (www.nmdb.eu/nest/) or corrected local muons

P is pressure (bar or other units can be used);

T is air temperature (degree Celsius);

RH is relative humidity (%).

Visual Basic for Application (VBA). When opening the file, please enable macros: a pop-up window should appear with the request.

An overview of the structure of the file is shown in **Figure 2.2**. The file is organized in four sheets. The user can move through the file by clicking the correspondent sheets. In addition, ToC has been integrated at the left side to help users navigate through the file (**Figure 2.2a**). Each sheet is further broken down into sub-windows (a,b,c) as shown in **Figure 2.2**. All processed data are shown as in **Figure 2.2c**.

The first sheet (*Introduction*) provides an overview of the file, a short description of the structure and some references. The user can select the second sheet by clicking at ToC the button *1. Select data*.

At this second sheet, two buttons are available. The first button (*1.1 Data from Petzenkirchen, Austria*) can be used to copy the data that are further processed. Alternatively, the user can click the second button (*1.2 New data at cell J50*). In this second case, the user should fill in all the green cells (I5 to I8) with general information about the experimental sites: Site name, Latitude, Longitude, Elevation. Row data should be copied at line J50 based on the following structure (**Table 2.1**).

When data has been copied, the user can move to the next sheet (*2_atm_corrections*) by clicking the corresponding button in ToC (2. Atmospheric correction). Two buttons are available in this sheet. The user can click the first button (*2.1 copy data and define parameters*) to copy the data that are further processed. In addition to the general information provided before, in this sheet three additional parameters should be defined:

- Cell I11: reference value for incoming correction (see TECDOC 1809);
- Cell M11: reference value for pressure correction (i.e. long term average);
- Cell M12: parameter for pressure correction (i.e. high energy attenuation length).

By default, the program suggests the long-term average pressure over the time series as a reference condition and uses a value of 130 g/cm^2 for the high energy attenuation length (see details in Zreda *et al.* 2012). Users can change these values directly by editing the cells. Once the parameters have been defined, the user can press the second button (*2.2 Calculate corrected neutrons*). This automatically implements the equations for calculating the corrected neutron counts (see Zreda *et al.* 2012 for details). Time series of correction factors and corrected neutrons are plotted in the main central window (**Figure 2.3a**). All the processed data can be explored in the right-side window (**Figure 2.3b**).

The user can move to the next sheet (*3_Soil_moisture*) by clicking the correspondent button in ToC (*Soil moisture estimation*). Two buttons are available in this sheet. The user can click the first button (*3.1 copy data and define parameters*) to copy the data that are further processed. In addition to the general information provided before, in this sheet some additional parameters should be defined:

- Cells M5 to MM7: the parameters of the Desilets's equations (a0, a1, and a2) are reported (see **Equation 1.1**);
- Cell M9: parameter for biomass correction has been reported (see Franz *et al.* 2015);
- The user can modify these values but for standard processing the default values should be used.

Data for the CRNS calibration should be reported in the table (cells from I12 to P18). It is assumed that calibration is performed based on soil samples collected at the experimental site in one day. See also the companion spreadsheet described in the **Section 2.3** for details. The following parameters should be specified:

- Cell I12: date when soil samples have been collected;
- Cell I13: average neutron counts during the sampling campaign;
- Cell I14: gravimetric soil moisture (possibly weighted average, see also the companion spreadsheet described in the previous section for details);
- Cell I15: average water equivalent soil organic matter (WSOM);
- Cell I16: average lattice water (*LW*);
- Cell I17: average bulk density (*BD*);
- Cell I18: average biomass water equivalent (BWE).

By default, the spreadsheet suggests some values for the first campaign that can be modified by the user editing the cells.

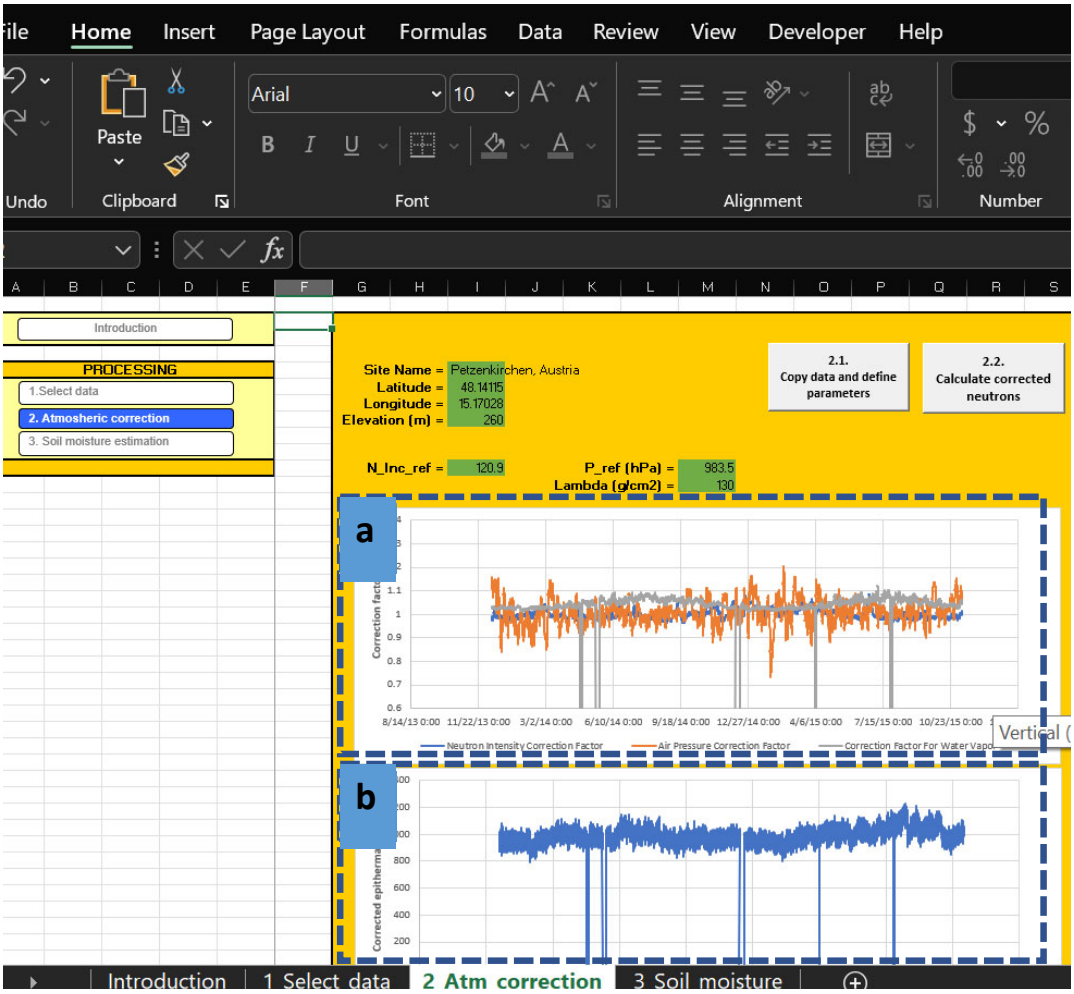

Figure 2.3. Examples of the results of the CRNS data-processing collected at Petzenkirchen, Austria: (a) correction factors; (b) corrected neutron counts

A maximum of eight campaigns can be processed. As soon as these cells are populated, the spreadsheet automatically calculates the value of N_0 parameter (cell I20), N_0 corrected for biomass (cell I21) for each campaign, and average over the campaigns (cells R20 and R21).

Once all the soil sample data have been copied, the user can click the second button (*3.2 Calculate soil moisture*). Volumetric soil moisture based on CRNS data are then estimated. Penetration depth is also estimated based on the simplified approach presented by Franz *et al.* (2012a). The results are visualised in the main central window. All the processed data can be explored on the right-side windows. These values could be copied in a new file for further analyses. The results of data collected at Petzenkirchen (Austria) are shown in **Figure 2.4**, as an example.

2.4 CRNS data processing with Cosmic Ray Sensor Python tool (CRSPY)

2.4.1 Description of the tool

The Cosmic Ray Sensor Python tool (CRSPY; pronounced 'crispy') is an open-source Python package designed to process raw measurements from the Cosmic Ray Neutron Sensor (CRNS) to derive soil moisture (Power *et al.* 2021). The version of the code described here is freely available at https://zenodo.org/record/5543669#.YZ-EcS-l1pQ. Data processing in CRSPY follows the most up-to-date correction and sensor calibration steps (Franz *et al.* 2012a; Rosolem *et al.* 2013; Hawdon *et al.* 2014;

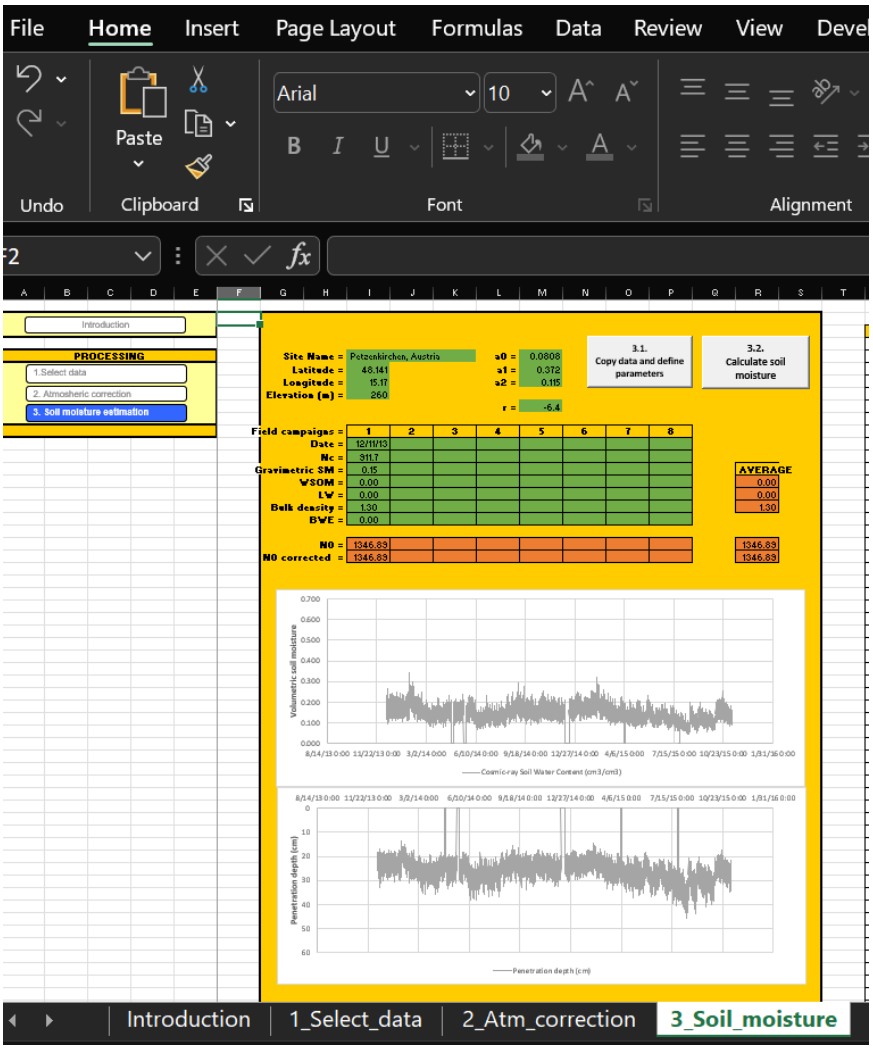

Figure 2.4. Estimation of CRNS soil moisture and pentration depth based on data from Petzenkirchen (Austria)

Baatz *et al.* 2015; Schrön *et al.* 2017). Since the initial development of cosmic ray neutron sensing for soil moisture monitoring (Zreda *et al.* 2008; Desilets *et al.* 2010), the adoption of this technology is increasing globally, particularly with the establishment of national scale networks such as the first Cosmic Ray Soil Moisture Observing System (COSMOS) in the United States of America (Zreda *et al.* 2012); the Australian CosmOz network (Hawdon *et al.* 2014; McJannet *et al.* 2021); in Germany, supported by the TERENO and, more recently, the COSMIC-SENSE initiatives (Bogena *et al.* 2016); and the COSMOS-UK in the United Kingdom of Great Britain and Northern Ireland: (Evans *et al.* 2016; Cooper *et al.* 2021, Stanley *et al.* 2021). Each of those national networks operates independently following their own set of protocols. The primarily development of CRSPY was motivated by the need to process multiple sites simultaneously to bring the information from those national networks together in a harmonized way for regional to global scale analysis. However, the CRSPY tool is versatile enough that users can also set up and take advantage of CRSPY for single-site applications.

The scheme shown in **Figure 2.5** summarizes the main steps in CRSPY. The procedure starts by the user entering pre-defined information about their site (or sites) as well as providing a time-series of the raw neutron count measurements and any available ancillary data. All this information is provided following standard formatting as required by CRSPY (please, refer to the Appendix section in Power *et al.* (2021) for detailed information on requirements and formatting standards supported by CRSPY). CRSPY employs equation 1 to convert measured raw neutron counts into estimated volumetric soil moisture using up-to-date corrections and processing steps. For example, CRSPY allows users to specify *LW*, *WSOM* and ρ_{bd} as site-specific parameters. However, should those parameters be unavailable locally,

CRSPY makes use of external global dataset products, such as the SoilGridv2 (Poggio *et al.* 2021), to estimate *WSOM* and ρ_{bd}. In addition, *LW* has shown direct relationship with clay content in soils and could be obtained indirectly from SoilGridv2 dataset, to estimate it (see Avery *et al.* (2016) for United States of America data). However, it should be advised to obtain those quantities directly at the site whenever possible for better performance of the cosmic ray neutron sensor. In CRSPY, the N_0 parameter is obtained via site-specific calibration by analysing the collection of several (e.g. hundreds) of soil samples within the sensor footprint (i.e. around 200 m radius). In this case, the user provides this information following a standard formatting. CRSPY then applies the most recent spatial weighting approach proposed by Schrön *et al.* (2017) to calculate an independent weighted-average soil moisture within the sensor footprint at the time of calibration campaign. The N_0 parameter is then estimated by rearranging the terms in equation 1, so that N_0 is the dependent variable (i.e. isolated in the left-hand side of the equation). In CRSPY, if the N_0 parameter has been calibrated elsewhere, the user has the option to bypass the calibration step and provide N_0 manually.

Another novel aspect of CRSPY is the use of external data sources to facilitate the corrections described above. Should the site present with data gaps or additional *in situ* measurements are not available, CRSPY takes advantage of state-of-the-art global databases to replace meteorological (e.g. temperature and humidity estimates for atmospheric water vapor estimation) and site characteristics data (e.g. soil characteristics or aboveground biomass). In the case of meteorological data, CRSPY obtains information from the ERA5-Land product (Muñoz Sabater, 2021). The ERA5-Land product combines modelled data with real world observations, and it is available in a gridded, global hourly product at 9 km spatial resolution. For soil characteristics, CRSPY uses information available publicly from the SoilGridv2 database provided by the International Soil Reference and Information Centre (ISRIC). The SoilGridv2 is a global data product providing soil properties estimates at approximately 250 m resolution grid from soil sample collections compiled by the World Soil Information Service (WoSIS) (Batjes *et al.* 2020). CRSPY uses information of dry aboveground biomass obtained from the European Space Agency (ESA) Climate Change Initiative (CCI) database. The ESA-CCI aboveground biomass estimates global gridded data product at 100 m spatial resolution (Santoro and Cartus, 2019).

In addition to the steps described above, CRSPY implements a few quality-control steps. First, CRSPY removes doubtful data points by applying the quality flags to neutron counts. The adopted quality flags in CRSPY are consistent with the similar procedures found in other national cosmic ray neutron sensor networks. Neutron counting rates are removed if:

- Counts differ by 20 percent from the previous time step;
- Counts are below 30 percent of N_0 ;
- Counts are above N_0 ;
- 4 Battery voltages are below 10 V.

As an intermediate step, CRSPY produces diagnostic time-series plots of all variables to help identifying potential issues with the data that might require manual correction as a final step. **Figure 2.6** shows examples of two diagnostic time-series plots produced for the grass site at the Sheepdrove Organic Farm in the United Kingdom of Great Britain and Northern Ireland (Schrön *et al.* 2017; Iwema *et al.* 2021). For instance, the user can track moisture build up in the enclosure box affecting the sensor electronics to decide to control humidity by adding desiccant bags inside the enclosure box (highlighted by the black arrows in **Figure 2.6a**). In addition, the user can track the battery voltage powering up the datalogger throughout the seasons, noticing how much more variable (i.e. unstable) the voltage output can become during winter periods with low solar input (highlighted by the black ovals in **Figure 2.6b**). CRSPY's diagnostic plots are aimed to provide the user with an intermediate check to identify sensor or data inconsistencies.

Finally, if the estimated volumetric soil moisture (Θ_{vol}) exceeds the maximum allowed value (i.e. soil moisture at saturation; Θ_{sat}), the value is capped accordingly (i.e. $\Theta_{vol} \leq \Theta_{sat}$). This flag is applied using dry soil bulk density (ρ_{bd}), hence a more accurate estimation of Θ_{sat} is achieved if ρ_{bd} is obtained at the site directly (as opposed to indirectly via SoilGridv2 database). Θ_{sat} is defined in CRSPY as follows:

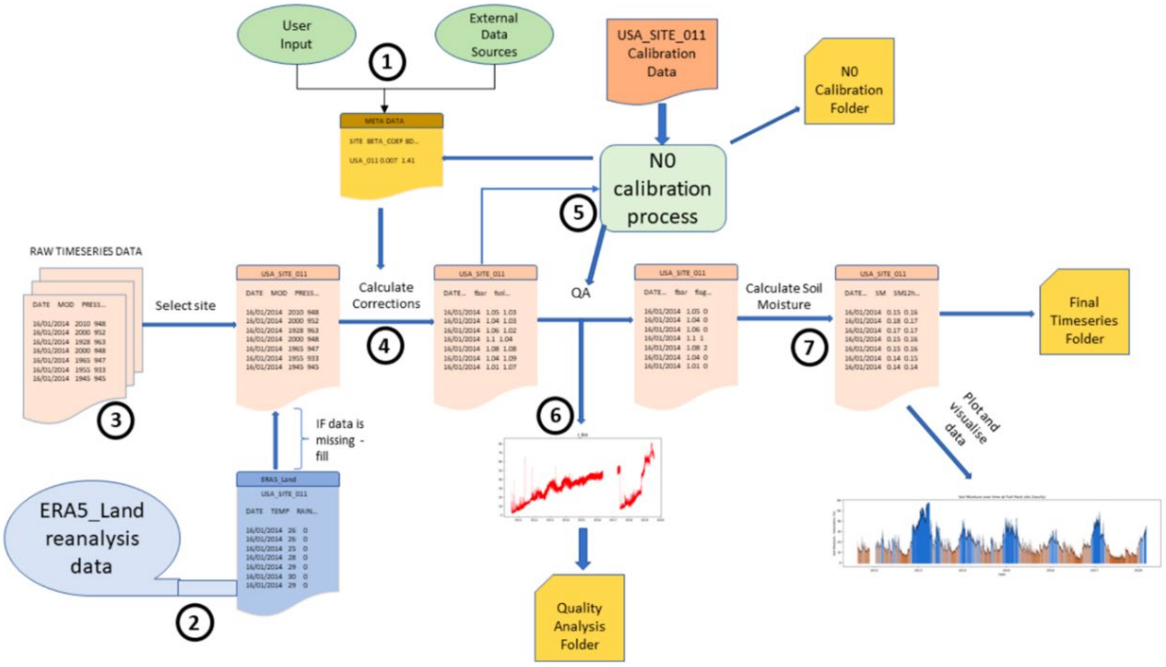

Figure 2.5. Scheme of CRNS data processing by CRSPY: (1) user input information from the site and the use of stationary external data sources for metadata production; (2) use of external dynamic global products for gap-filling and correction procedures; (3) raw measurements from cosmic ray neutron sensor, (4) correction procedures applied to raw measurements; (5) sensor calibration (i.e. the N0 parameter in Equation 1), (6) quality control and diagnostic plots, (7) final soil moisture estimates and output plots. Please, refer to the text for detailed information about each step. Source: Power, D., Rico-Ramirez, M. A., Desilets, S., Desilets, D. & Rosolem, R. Cosmic-Ray neutron Sensor PYthon tool (crspy 1.2.1): An open-source tool for the processing of cosmic-ray neutron and soil moisture data, Geosci. Model Dev., 14, 7287–7307. https://doi.org/10.5194/gmd-14-7287-2021, 2021

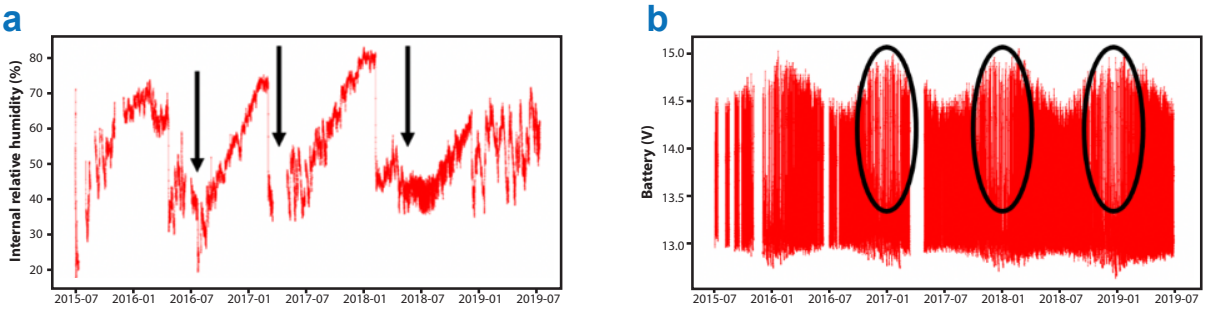

Figure 2.6. Example of diagnostic time-series plots produced by CRSPY from the Sheepdrove Organic Farm site in the United Kingdom of Great Britain and Northern Ireland: (a) internal relative humidity with arrows highlighting periods after desiccant bags are added inside the enclosure box; and (b) battery voltage with ovals highlighting winter periods where periods of alternating high and low voltages are more frequently observed due to lack of solar radiation

$$\theta_{sat} = 1 - \frac{\rho_{bd}}{\rho_{particle}} \tag{2.1}$$

where $\rho_{particle}$ is the density of ground material (assumed to be the density of quartz at 2.65 g/cm^3).

2.4.2 Examples of processed data

In order to show some examples of fully processed data, measurements from two distinct sites from the COSMOS network in the United States of America were chosen: the Santa Rita Creosote site in

southwestern United States of America (**Figure 2.7**), characterized by a hot semi-arid climate with mean annual temperature and precipitation of 18.7 °C and 335 mm, respectively; and the Harvard Forest Site in northeastern United States of America (**Figure 2.8**), characterized by a humid continental climate, with colder temperatures (mean annual temperature = 9.0 °C) and higher rainfall rates (mean annual precipitation = 1.131 mm) in comparison to the Santa Rita Creosote site. According to the Ameriflux network (https://ameriflux.lbl.gov), which describes both sites' characteristics, the vegetation cover at the Santa Rita site[1] is defined by sparse shrubs with woody vegetation less than 2 m tall with canopy cover varying between 10 and 60 percent (**Figure 2.7 a,b**), while the Harvard Forest[2] site cover is dominated by deciduous broadleaf forest with a canopy cover significantly exceeding 60 percent (**Figure 2.8 a,b**).

The top panels (**Figures 2.7c and 2.8c**) show the individual correction factors (i.e. the individual 'f' terms described in **Equation 2.1**). However, their numerical values were plotted here in terms of percent deviation (rather than the 'f' term directly). For example, a percent deviation of +10 percent corresponds to a correction factor of 1.10 applied as the 'f' term in **Equation 2.1**. Alternatively, a percent deviation of –10 percent corresponds to an 'f' term of 0.90. All 'f' terms [i.e. correction functions due to atmospheric pressure (p), incoming high-energy neutron intensity (i), atmospheric water vapor (h), and aboveground biomass (v)] are presented together for each site to allow for direct comparison among different correction steps.

For the Santa Rita Creosote site a few features are easily observed regarding the correction factors. Current version of CRSPY only applies static correction to aboveground biomass signal (f_v) shown in black, and that according to the ESA CCI database, the amount of aboveground biomass within the sensor average footprint (**Figure 2.7b**) is negligible. In addition, the correction due to incoming high-energy neutron intensity (f_i), shown in magenta, varies between –5 percent and 5 percent with a slightly tendency towards negative percent impacts (i.e. $f_i < 1$). Both corrections for atmospheric pressure (f_p in cyan) and water vapor (f_h in blue) variabilities show stronger dynamics and seasonal patterns. In the case of atmospheric water vapor correction, the effect of increased humidity due to the summer monsoon in southwest United States of America is clearly observed. Once these corrections are applied, an updated series of now corrected neutron counts is generated from the original raw neutron counts. Both raw (black) and corrected (red) neutron counting rates are shown in **Figure 2.7d.** Notice the dynamics of the signal are retained but the corrected neutron counting rates tend to be slightly shifted upwards (i.e. relatively higher neutron counts), especially after atmospheric pressure variability is considered and the unwanted contribution of atmospheric water is completely removed. Ultimately, with the appropriate corrections and additional information obtained at the site, a time-series of derived soil moisture is produced by **Equation 2.1** (**Figure 2.7e**). Notice that CRSPY computes not only the hourly estimated volumetric water content (black) but also its uncertainty bound (light gray shading) which is directly related to the coefficient of variation of the observed neutron counts (Zreda *et al.* 2012). However, due to the relatively high neutron counts observed at the Santa Rita Creosote, the uncertainty of the estimated soil moisture is considerably small in this case. Observed soil moisture at this semi-arid site is relatively low. Most of the time, soil moisture ranges between 0 and 0.15 m^3/m^3 with some wet periods observed exceeding 0.20 or 0.30 m^3/m^3 as a result of heavy rainfall in both winter and summer seasons. Another important feature observed at the Santa Rita site is the behaviour of quick dry-down events right after a sudden increase in soil moisture due to high intensity rainfall pulses. Due to high neutron counting rates, the uncertainty propagate to soil moisture is considered to be practically negligible except during high soil moisture peaks (i.e. the uncertainty increases in relation to soil moisture).

Comparing the correction factors obtained at the more humid and relatively colder Harvard Forest site, a few key features were observed. The magnitudes for both high-energy neutron intensity f_i (in magenta) and atmospheric water vapor f_h (in blue) (**Figure 2.8c**) are comparable with those values observed at the Santa Rita site (**Figure 2.7c**). Despite of similar magnitude, the seasonal dynamics of the atmospheric water vapor correction at the Harvard site appears to have larger spread within the years and to be less

1 Site information from Santa Rita Creosote is available at https://ameriflux.lbl.gov/sites/siteinfo/US-SRC.
2 Site information from Harvard Forest https://ameriflux.lbl.gov/sites/siteinfo/US-Ha1

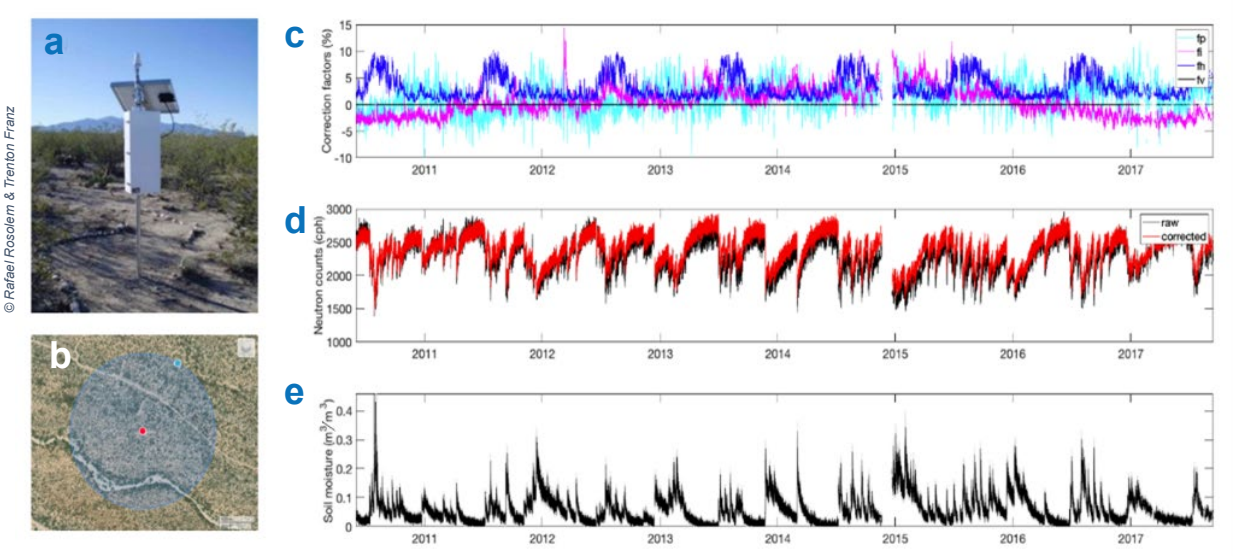

Figure 2.7 (a) CRNS at the Santa Rita Creosote study site; (b) Position and footprint of CRNS on map; (c) Time-series of correction factors (as percent deviation on neutron counting rates); (d) Raw and corrected neutron counts (cph); and (e) Derived volumetric soil moisture m^3/m^3)

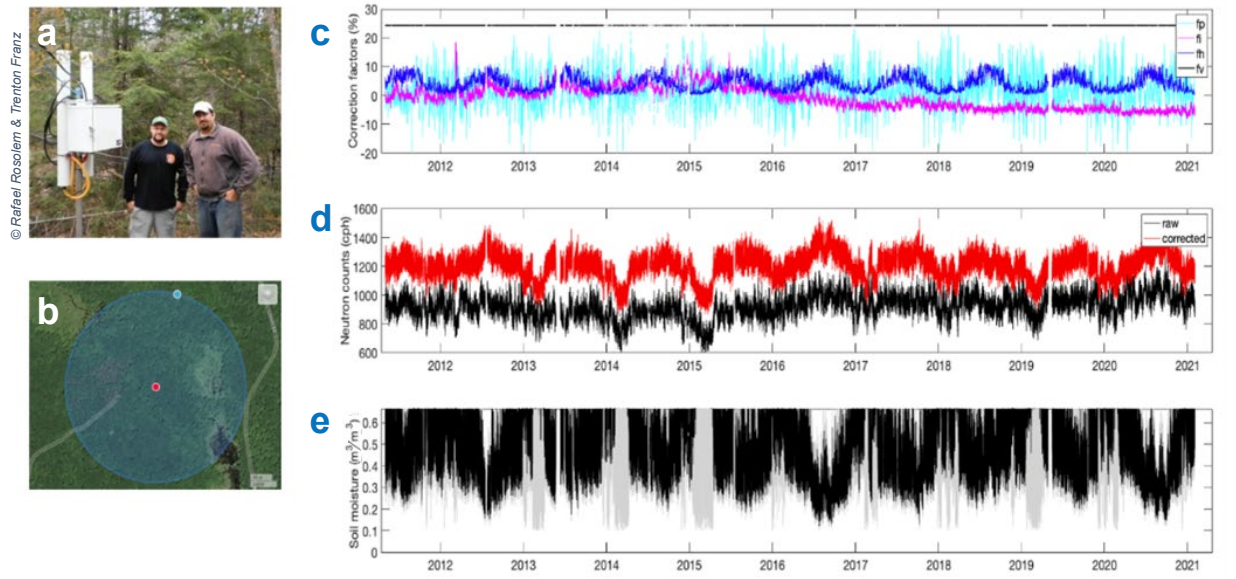

Figure 2.8. (a) CRNS at the Harvard Forest study site; (b) Position and footprint of CRNS on map; (c) Time-series of correction factors (as percent deviation on neutron counting rates); (d) Raw and corrected neutron counts (cph); and (e) Derived volumetric soil moisture (m^3/m^3)

peaky than the same factor obtained at the Santa Rita. The correction factor for atmospheric pressure f_p (in cyan) at the Harvard Forest shows higher overall range (between –20 percent to 20 percent) when compared to the Santa Rita site. Also, there is the higher impact of aboveground biomass from the forest-covered site shown as f_v (in black). As a result, the corrected neutron counts, shown in red in **Figure 2.8d**, are systematically higher than the original raw neutron counting rates (black). However, despite the overall impact of the aboveground biomass on the neutron counts, its impact on the soil moisture is cancelled out because the N_0 parameter is also computed from the same corrected neutron counts time series. The reason of aboveground biomass correction currently introduced in CRSPY allows only for static signal from the ESA CCI database to be accounted for, but future versions are

planned for dynamic aboveground biomass data to be incorporated. This would make the correction procedure even more accurate for croplands where biomass closely follows a seasonal pattern, for example, to better account for uncertainties in crops. The derived volumetric soil moisture is shown as black line in **Figure 2.8e**. Here, because neutron counting rates are lower then those observed at the Santa Rita, the uncertainty on estimated soil moisture (gray shading) is higher and easily observed. In addition, at the Harvard site, the application of a maximum soil moisture cap (Θ_{vsat} as shown in **Equation 2.1**) at the time-series is also observed. This prevents unrealistically high soil moisture values to be incorrectly derived at the site. Periods with saturated soil moisture with very high uncertainties occur mainly in the wintertime. These are periods with the lowest raw neutron counting rates and once propagated to soil moisture, they predict unrealistically high soil moisture values (e.g. exceeding 0.80 $m^3\ m^{-3}$). The uncertainty bound is originally obtained with the original raw neutron counts, hence it is high magnitude, however since the final soil moisture is capped at the saturated soil moisture value, this obtained uncertainty is retained to ensure robustness of the approach. The seasonal pattern observed in **Figure 2.8a** (bottom panel) suggests very wet conditions (i.e. soil moisture above 0.40 m^3m^3) for most of the year (from autumn until spring) with reduced soil moisture (i.e. below 0.40 m^3/m^3) observed in the summer. Also notice the hourly soil moisture from Harvard Forest tends to be noisier and show higher variability range withi n each season as a result of the lower counting statistics. For example, wintertime neutron counts range approximately from 0.40 to 0.65 m^3/m^3 while summertime ranges from 0.20 to 0.40 m^3/m^3.

2.4.3 New metadata feature

In addition to processing the CRNS data at selected sites, CRSPY contains a new feature that facilitates metadata analysis. A comprehensive metadata from multiple CRNS stations can provide additional characteristics beyond the observed soil moisture dynamics. This integration of knowledge has not yet been effectively explored (Wagener *et al.* 2021) and can lead to development of more accurate perceptual and conceptual models to tackle future hydrologic and environmental stresses in densely populated and intensively exploited watersheds. Improved models would contribute to better land and water management especially in vulnerable agroecosystems. **Figure 2.9** shows an example of part of the metadata file assembling metadata collected by CRSPY from 166 publicly available cosmic ray neutron sensing stations worldwide. For the metadata, CRSPY combines information obtained from *in situ* measurements at the site as well as from the global database products highlighted in **Section 2.4.1.** This will enable a much more comprehensive way characterizing the multiple CRNS stations and performing comparisons of selected sites. More detailed information about the metadata table can be found at https://github.com/danpower101/CRSPY/wiki/Metadata and in **Table A3** in Power *et al.* (2021).

An example of metadata analysis facilitated by the CRSPY tool is provided on **Figure 2.9**. Among the 166 sites analyzed, most of the land cover type are classified, by the ESA CCI Land Cover product, as forest, grasslands, or croplands with similar contribution despite slightly higher occurrence of cropland (**Figure 2.10a**). Cosmic ray neutron sensing stations have also been reported at shrubland sites with very few stations deployed at bare soils. Similar analysis can be carried out for different soil texture classes as shown on **Figure 2.10b**. Despite most of the sites are classified by the SoilGridv2 product as sandy loam, loam, or clay loam, the results from the metadata analysis show a desirable spread of CRNS sites across a wide range of soil texture types. In addition, **Figure 2.11** demonstrates another potential use of the metadata generated by CRSPY. In this case, the estimates of dry soil bulk density collected from the SoilGridv2 global product are compared against the estimates from site-specific soil samples. Surprisingly, and despite their similar spatial resolution (both on the order of 250 m), the results show quite different estimates for dry soil bulk density compared to local estimates. These highlights potential limitations of global dataset in determining the local characteristics accurately.

2.4.4 Setting up and running CRSPY

The information below is provided to help new users run CRSPY for the first time with an example set of data. The guide below is based on an example workbook (run_crspy_workthrough.ipynb) in Python available at https://github.com/danpower101/crspy_example/. The user is expected to have some

COUNTRY	SITENUM	SITE_NAME	INSTALL_DATE	LATITUDE	LONGITUDE	ELEV	TIMEZONE	GV	LW	SOC	BD	N0	AGBIWEIGHT	RAIN_DATA_SOURCE	TEM_DATA_SOURCE	RH_DATA_SOURCE	BETA_COEFF
USA	1	Mount Lemmon	27/10/2007	32.4418	-110.7822	2747	-7	5.08	0.04	0.016			5.4				0.007357765
USA	3	Biosphere 2	28/04/2008	32.5795	-110.851	1180	-7	5.02	0.04	0.016			0				0.007379807
USA	4	Manitou Forest Tower	24/10/2009	39.101	-105.102	2411	-6	2.93	0.028	0.005	1.4	10190	5.7	ERA5_land	ERA5_land	None	0.00752316
USA	5	Santa Fe Watershed-SF2	24/10/2009	35.683	-105.8225	2427	-7	3.72	0.04	0.016			5.2	ERA5_land	ERA5_land		0.007468456
USA	6	Marshall Colorado	24/10/2009	39.9495	-105.1955	1756	-6	2.74	0.04	0.016		6958	3.4	ERA5_land	ERA5_land	None	0.007519225
USA	7	Manitou Forest Ground	24/10/2009	39.1006	-105.1025	2391	-6	2.93	0.028	0.005	1.4		6.3	ERA5_land	ERA5_land	None	0.007523116
USA	8	Santa Fe Watershed-SF1	23/12/2009	35.6792	-105.8269	2482	-7	3.68	0.04	0.016			5.3	ERA5_land	ERA5_land	None	0.007470286
USA	9	Rancho No Tengo	06/02/2010	31.7438	-110.0219	1401	-7	5.08	0.0317	0.016	1.4	3794	0	ERA5_land	ERA5_land	None	0.007384998
USA	10	Kendall	06/02/2010	31.7368	-109.9418	1548	-7	5.26	0.024	0.008	1.23	4279	0	ERA5_land	ERA5_land	None	0.00737799
USA	11	Santa Rita Creosote	06/02/2010	31.9085	-110.8394	989	-7	5.21	0.01	0.003	1.43	2740	0	ERA5_land	ERA5_land	None	0.007359102
USA	12	Silver Sword	15/06/2010	19.765	-155.4234	2868	-10	12.87	0.0957	0.0181	0.78		1.2	ERA5_land	ERA5_land	None	0.006895236
USA	13	Island Dairy	16/06/2010	19.998	-155.2859	381	-10	12.82	0.2093	0.0325	1.01		2	ERA5_land	ERA5_land	None	0.006584091
USA	14	SMAP-OK	21/07/2010	36.0635	-97.217	326	-6	3.27	0.0517	0.0065	1.42	1607	0.1	ERA5_land	ERA5_land	None	0.007356186
USA	15	AMM-1	21/07/2010	36.6054	-97.4878	322	-6	3.14	0.0537	0.0059	1.4	1575	0.5	ERA5_land	ERA5_land	None	0.007357994
USA	16	Iowa Validation Site	09/05/2010	41.9832	-93.6837	316	-6	1.93	0.045	0.0159	1.43	1672	1.6	ERA5_land	ERA5_land	None	0.007364034
USA	17	Sterling	09/10/2010	38.9739	-77.4852	95	-4	2.49	0.0637	0.0045	1.32		0				0.007319544
AUT	18	Rietholzbach	16/12/2010	47.3805	8.9934	755	1	4.34	0.0518	0.0308	0.97		1.4				0.007380412
USA	19	VCNP CZO	15/12/2010	35.8896	-106.5328	3037	-6	3.79	0.04	0.016			2.1				0.007443943
USA	20	San Pedro 2	19/01/2011	31.5615	-110.1404	1233	-7	5.3	0.016	0.005	1.42	3038	0.2	ERA5_land	ERA5_land	None	0.007367546
GER	21	Juelich		50.503	6.3314	588	1	3.16	0.04	0.016			13.6				0.007399953
FRA	22	Toulouse	23/02/2011	43.3848	1.2922	188	1	5.34	0.03	0.0076	1.34		0				0.007258533
USA	23	Desert Chaparral UCI	03/08/2011	33.6094	-116.4506	1292	-8	4.96	0.0179	0.0017	1.58	4255	0	ERA5_land	ERA5_land	None	0.007387804
USA	24	Coastal Sage UCI	03/09/2011	33.7342	-117.6961	320	-8	5	0.0398	0.0121	1.16	2166	1.5	ERA5_land	ERA5_land	None	0.007296504
USA	25	Chestnut Ridge NOAA	21/03/2011	35.9311	-84.3324	370	-6	2.98	0.026	0.01	1.41	2226	16.7	ERA5_land	ERA5_land	None	0.00736887
USA	26	Bondville	23/03/2011	40.0062	-88.2904	219	-6	2.19	0.0373	0.0157	1.45	2039	1.9	ERA5_land	ERA5_land	None	0.007345227
USA	27	Morgan Monroe	24/03/2011	39.3232	-86.4131	275	-6	2.33	0.0325	0.0121	1.38	2098	22.9	ERA5_land	ERA5_land	None	0.007357006
USA	28	Mozark	18/04/2011	38.7441	-92.2	219	-6	2.48	0.036	0.0145	1.43	1996	18.3	ERA5_land	ERA5_land	None	0.007345555
USA	29	Neb Field 3	20/04/2011	41.179859	-96.441235	363	-6	2.17	0.0375	0.0126	1.42	2157	0.6	ERA5_land	ERA5_land	None	0.007374453
USA	30	Harvard Forest	05/02/2011	42.5378	-72.1715	350	-4	1.93	0.052	0.0605	0.89	2531	21.7	ERA5_land	ERA5_land	None	0.007371093
USA	31	Howland	05/04/2011	45.2041	-68.7402	124	-5	1.52	0.034	0.0815	1.23	1768	15.1	ERA5_land	ERA5_land	None	0.007313336
USA	32	Tonzi Ranch	05/11/2011	38.4316	-120.9659	177	-8	3.97	0.0605	0.0055	1.49	1795	5.1	ERA5_land	ERA5_land	None	0.007313069
USA	33	Soaproot	06/09/2011	37.031	-119.2564	1160	-8	4.26	0.0478	0.0325	1.02	2638	19.4	ERA5_land	ERA5_land	None	0.007415997
USA	34	P301	06/10/2011	37.0678	-119.1944	2014	-7	4.26	0.0448	0.0236	1.05	4573	16.2	ERA5_land	ERA5_land	None	0.007437696
USA	35	Wind River	13/06/2011	45.8205	-121.9519	371	-8	2.22	0.0628	0.038	0.88	2293	46.6	ERA5_land	ERA5_land	None	0.007376341
USA	36	Hauser Farm North	06/05/2011	34.5798	-111.8627	942	-7	4.57	0.024	0.006	1.36		2.2	ERA5_land	ERA5_land	None	0.007386662

S	T	U	V	W	X	Y	Z	AA	AB	AC	AD	AE	AF	AG	AH	AI
REFERENCE_PRESS	BD_ISRIC	BD_ISRIC_UC	SOC_ISRIC	SOC_ISRIC_UC	pH_H20_ISRIC	pH_H20_ISRIC_UC	CEC_ISRIC	CEC_ISRIC_UC	CFVO_ISRIC	CFVO_ISRIC_UC	NITROGEN_ISRIC	NITROGEN_ISRIC_UC	SAND_ISRIC	SAND_ISRIC_UC	SILT_ISRIC	SILT_ISRIC_UC
723.9370415	1.26	0.052	0.2936	0.0434	5.44	0.62	227	31	20.88	3.52	3.698	0.536	0.6048	0.007	0.274	0.0174
879.2955978	1.512	0.04	0.0838	0.024	7.12	0.36	246.6	15.8	18.02	5.6	0.866	0.274	0.3074	0.0268	0.4012	0.0218
755.2144076	1.488	0.038	0.201	0.0328	6.32	0.56	113.4	36.6	15.22	3.14	1.502	0.378	0.6516	0.0052	0.1952	0.0194
753.7006227	1.352	0.062	0.2842	0.0406	6.46	0.38	209	19.6	18.46	6.18	2.112	0.318	0.4526	0.0148	0.3058	0.0258
819.3327571	1.5	0.042	0.1292	0.0248	7.16	0.44	161.8	22	10.08	22.82	1.276	0.23	0.3874	0.0186	0.3788	0.0266
757.1100999	1.488	0.038	0.201	0.0328	6.32	0.56	113.4	36.6	15.22	3.14	1.502	0.378	0.6516	0.0052	0.1952	0.0194
748.5157147	1.36	0.062	0.251	0.0338	6.46	0.4	206.2	20.2	17.46	6.58	1.86	0.334	0.5088	0.0136	0.2758	0.0348
855.8828937	1.52	0.03	0.0696	0.0146	7.56	0.24	157	15	24.88	2.76	0.81	0.192	0.5926	0.0062	0.16	0.021
840.5912415	1.558	0.036	0.0774	0.0172	7.46	0.3	182	21.4	31.4	1.68	0.898	0.202	0.5846	0.0072	0.2036	0.0172
899.9454163	1.528	0.038	0.0554	0.026	7.64	0.3	151.8	23.8	20.16	4.9	0.64	0.264	0.5444	0.0096	0.2638	0.0242
712.9338435	1.236	0.08	0.3064	0.0624	6.8	0.56	300.2	29.6	27	3.76	2.478	0.614	0.4046	0.0184	0.2686	0.033
968.3092002	1.306	0.072	0.341	0.066	5.66	0.66	202.8	40.2	13.88	43.02	2.336	0.448	0.3272	0.0254	0.338	0.0306
974.6951017	1.608	0.026	0.1506	0.0624	6.38	0.5	132.8	24.2	3.6	25.76	1.482	0.284	0.5202	0.0154	0.2312	0.0414
975.1608578	1.674	0.03	0.115	0.019	6.66	0.44	212.2	13.4	3.64	34.44	1.134	0.174	0.1082	0.0156	0.5436	0.0112
975.8598298	1.59	0.024	0.1316	0.0242	6.96	0.3	174.4	17	3.34	2.16	1.342	0.24	0.5064	0.009	0.2808	0.013
1001.88943	1.518	0.042	0.1504	0.028	5.86	0.46	129.2	32.4	6	12.66	1.544	0.24	0.2748	0.0216	0.4912	0.0178
925.777588	1.246	0.09	0.4052	0.05	6	0.52	256.2	33.8	19	2.4	3.682	0.388	0.4162	0.0084	0.3092	0.0124
697.7927687	1.234	0.056	0.2756	0.0428	5.92	0.36	315.8	15.2	27.32	3.72	1.49	0.342	0.4068	0.012	0.414	0.0132
873.6340825	1.51	0.036	0.061	0.022	8	0.34	156.8	23.2	17.46	6	0.834	0.26	0.477	0.0128	0.2346	0.0272
944.5779237	1.194	0.096	0.7736	0.0862	4.42	0.66	236.8	29.8	20.72	2.9	4.022	0.916	0.1978	0.0186	0.5562	0.011
990.8681543	1.446	0.062	0.2196	0.0506	6.66	0.44	228.2	31.4	11.22	5.84	2.018	0.36	0.2418	0.0208	0.4572	0.0154
867.3663968	1.446	0.048	0.0684	0.0302	6.94	0.34	156.8	24.8	13.76	11.78	0.784	0.304	0.6342	0.009	0.2482	0.029
975.3938034	1.528	0.05	0.1058	0.0316	7	0.4	201	18.8	9.86	43.8	1.37	0.362	0.4742	0.0116	0.2938	0.0244
969.5836624	1.456	0.048	0.2046	0.0362	5.34	0.58	108	20.8	10.96	7.32	1.358	0.264	0.2842	0.0144	0.3762	0.02
987.2162909	1.542	0.038	0.1796	0.021	6.3	0.44	228	11	1.34	7.44	1.758	0.304	0.0758	0.0348	0.561	0.0136
980.6470044	1.516	0.038	0.127	0.0142	4.82	0.32	165.6	15.4	3.58	14.18	2.244	0.27	0.093	0.0478	0.6468	0.0116
987.2162909	1.54	0.036	0.1504	0.0284	5.58	0.56	227.8	14.2	7.52	42.06	1.394	0.266	0.0854	0.0356	0.5678	0.0134
970.3953908	1.558	0.036	0.1298	0.0196	6.58	0.44	210.4	11	0.2	1.2	1.35	0.156	0.1162	0.0502	0.5184	0.0158
971.9043462	1.322	0.052	0.7096	0.0434	4.9	0.44	163.2	30.6	13.46	6.16	4.534	0.932	0.6214	0.0088	0.2894	0.024
998.4420917	1.384	0.066	0.7182	0.0974	5.16	0.56	197	28.4	18.52	4.8	3.674	0.382	0.4416	0.0136	0.4278	0.018
992.166603	1.466	0.054	0.1114	0.026	6.08	0.42	208.2	17.4	5.7	24.88	0.972	0.212	0.39	0.0114	0.3694	0.0168
881.4397234	1.394	0.06	0.2524	0.0274	5.94	0.2	164.8	14	9.68	21.78	1.404	0.276	0.5544	0.008	0.249	0.0206
793.5711048	1.258	0.054	0.3458	0.0346	5.86	0.3	148.2	22.6	18.06	4.22	1.55	0.334	0.6956	0.0048	0.1896	0.017
969.4677461	1.146	0.074	0.5998	0.0394	5.48	0.3	282	21.8	11.32	9.28	3.282	0.308	0.3908	0.017	0.4524	0.017
905.086505	1.534	0.034	0.0706	0.0276	7.88	0.26	183.4	19.4	9.04	24.26	0.694	0.246	0.4476	0.0152	0.3022	0.0374

AJ	AK	AL	Formula Bar	AN	AO	AP	AQ	AR	AS	AT	AU
CLAY_ISRIC	CLAY_ISRIC_UC	SOIL_TEXTURE	WRB_ISRIC	LAND_COVER	KG_CLIMATE	MEAN_ANNUAL_PRECIP	MEAN_ANNUAL_TEMP	SM_MAX	MEAN_ANNUAL_PET	MEAN_ANNUAL_VPD	MEAN_ANNUAL_RH
0.1214	0.065	sandy_loam	Luvisols	tree_needleleaved_evergreen_closed_to_open	BSk	411.4116211	16.6818161		1580.401537	1481.468161	34.10335123
0.2918	0.0364	clay_loam	Luvisols	shrubland	BSh	383.2165833	19.44105339		1845.199642	1835.074464	32.08014309
0.1528	0.0298	sandy_loam	Luvisols	tree_needleleaved_evergreen_closed_to_open	Dwb	661.7086182	3.310071707	0.471698113	778.7189467	482.3245908	54.68511968
0.2416	0.0462	loam	Cambisols	tree_needleleaved_evergreen_closed_to_open	Dwb	576.5680542	7.656064034		967.5519313	715.2918518	45.49390206
0.234	0.039	loam	Kastanozems	mosaic_cropland	Dfb	662.2278442	7.138348579		943.913937	592.3738464	54.66136547
0.1528	0.0298	sandy_loam	Luvisols	tree_needleleaved_evergreen_closed_to_open	Dwb	661.7086182	3.310071707	0.471698113	778.7189467	482.3245908	54.68511968
0.2156	0.0644	sandy_clay_loam	Luvisols	tree_needleleaved_evergreen_closed_to_open	Dwb	576.5680542	7.656064034		967.5519313	715.2918518	45.49390206
0.2474	0.0186	sandy_clay_loam	Calcisols	shrubland	BWk	223.3825226	16.92350578	0.471698113	1584.328271	1513.872123	32.26533978
0.2118	0.0266	sandy_clay_loam	Luvisols	shrubland	BWk	226.1120148	16.92362976	0.535849057	1586.424985	1520.715485	32.12788904
0.1924	0.0326	sandy_loam	Calcisols	shrubland	BSh	321.8552246	18.77453232	0.460377358	1759.010752	1704.535052	32.1423287
0.3266	0.0376	clay_loam	Andosols	shrubland				0.705660377			
0.335	0.036	clay_loam	Andosols	cropland_rainfed_herbaceous_cover				0.618867925			
0.2484	0.0524	sandy_clay_loam	Cambisols	grassland	Cwa	868.571228	16.68259239	0.464150943	1552.569829	790.9729699	62.94339106
0.3484	0.0208	silty_clay_loam	Kastanozems	cropland_rainfed_herbaceous_cover	Cwa	816.4761963	16.26268196	0.471698113	1530.57383	820.6398025	61.17334697
0.2128	0.0376	loam	Phaeozems	cropland_rainfed_herbaceous_cover	Dwa	1022.089111	9.925845146	0.460377358	1148.874583	503.6270733	67.10828055
0.2344	0.0454	loam	Luvisols	cropland_rainfed	Dfa	1147.733521	13.53659058	0.501886792	1354.706395	573.4999772	67.68651428
0.2748	0.0168	clay_loam	Cambisols	grassland				0.633962264			
0.1794	0.0338	loam	Luvisols	tree_needleleaved_evergreen_closed_to_open	Dwb	602.4647217	6.094103813		887.5740047	625.1241813	48.18855207
0.2886	0.0278	sandy_clay_loam	Fluvisols	shrubland	BWh	227.5814819	18.28193855	0.464150943	1705.050338	1635.766863	32.44758442
0.246	0.0226	silt_loam	Cambisols	tree_needleleaved_evergreen_closed_to_open							
0.301	0.0284	clay_loam	Cambisols	cropland_rainfed_herbaceous_cover				0.494339623			
0.1176	0.044	sandy_loam	Calcisols	shrubland	BSk	296.645874	16.09002557	0.403773585	1498.675874	1399.85263	34.63370599
0.2322	0.0494	loam	Kastanozems	shrubland	BSk	346.5385132	17.16669083	0.562264151	1529.39024	732.255607	64.99820741
0.3396	0.0228	clay_loam	Acrisols	tree_broadleaved_deciduous_closed_to_open	Cfa	1383.141602	15.5839901	0.467924528	1490.946154	593.0261411	70.67916432
0.3632	0.0252	silty_clay_loam	Phaeozems	cropland_rainfed_herbaceous_cover	Dfa	1060.915527	12.06075096	0.452830189	1254.184049	552.5072571	66.7718652
0.26	0.0462	silt_loam	Luvisols	tree_broadleaved_deciduous_closed_to_open	Dfa	1205.265503	12.60216713	0.479245283	1284.578122	531.3881642	68.99324085
0.3468	0.028	silty_clay_loam	Luvisols	tree_broadleaved_deciduous_closed_to_open	Dfa	1066.956787	13.61904049	0.460377358	1343.045538	554.8552845	68.51088276
0.3656	0.0268	silty_clay_loam	Phaeozems	cropland_rainfed_herbaceous_cover	Dwa	919.4439697	11.33444118	0.464150943	1226.170967	578.2322745	64.25713763
0.0894	0.0828	sandy_loam	Cambisols	tree_mixed	Dfa	1125.707886	9.082471848	0.664150943	1075.315599	461.0352365	67.67984716
0.1304	0.055	sandy_loam	Cambisols	tree_cover_flooded_fresh_or_brakish_water	Dfb	1190.168457	7.115363598	0.535849057	970.4563777	391.2939838	69.49755259
0.2406	0.0232	loam	Luvisols	shrubland	Csa	772.661377	16.48259544	0.437735849	1539.029339	1010.716334	56.47886968
0.1966	0.0202	sandy_loam	Luvisols	tree_needleleaved_evergreen_closed_to_open	Csa	898.5559082	14.16964149	0.61509434	1359.107131	999.053497	51.6038756
0.115	0.025	sandy_loam	Cambisols	tree_needleleaved_evergreen_closed_to_open	Dwb	976.5604858	8.1801157	0.603773585	976.9762897	665.2862038	52.93190303
0.1564	0.0698	loam	Cambisols	tree_needleleaved_evergreen_closed_to_open	Csb	2194.604492	8.467631 34	0.667924528	972.3330446	357.5425139	75.48771525
0.25	0.0414	loam	Calcisols	cropland_rainfed_herbaceous_cover	BSk	423.8950195	17.02587891	0.486792453	1642.28575	1617.247882	33.51856642

Figure 2.9. Subset of current metadata file generated by CRSPY

basic knowledge of Python and it is recommended to install CRSPY in a new Python environment to ensure the required packages have the correct interdependencies. In order to follow along with this walkthrough a user should clone the crspy_example repository, copy run_crspy_workthrough.ipynb into a new working directory and follow the instructions.

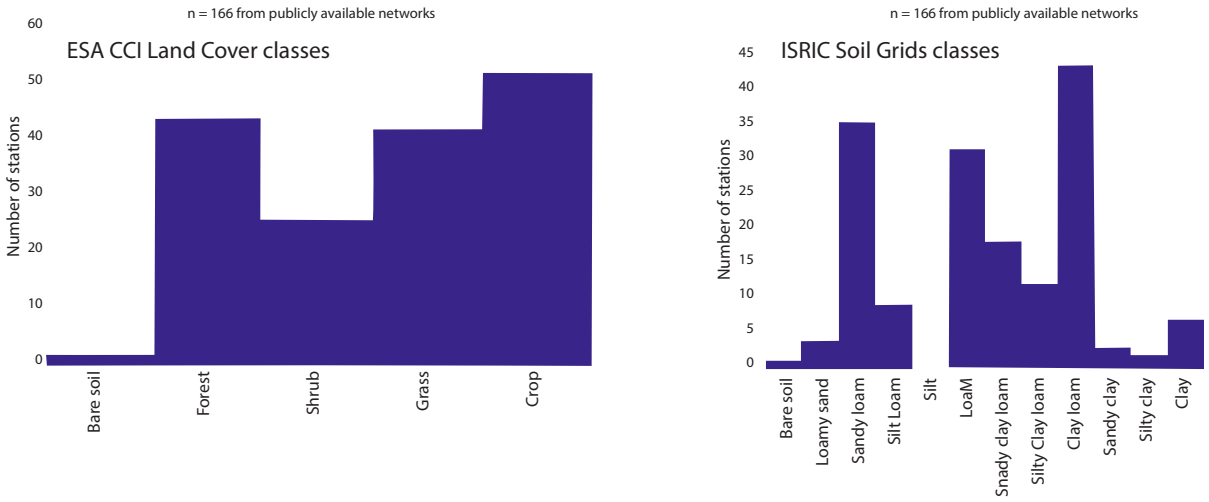

Figure 2.10. Distribution of (a) main land cover and (b) soil texture classes from 166 publicly available cosmic ray neutron sensors stations

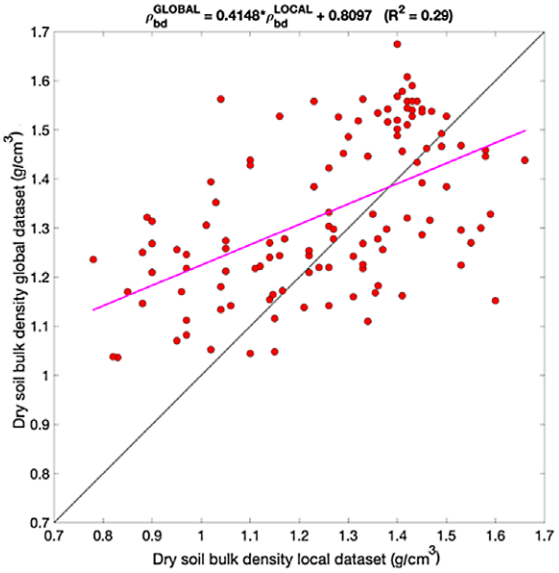

Figure 2.11. Correlation between the dry soil bulk density (g/ cm ^{3}) values obtained with the SoilGridv2 global product and those measured directly at CRNS sites

Step 1. Installing CRSPY to the user's Python environment

Run the command pip install CRSPY to install CRSPY into your Python environment. There are some operational system requirements that may be needed first, namely HDF5 headers and NetCDF4 system files. If errors occur during installation, install these libraries first. Alternatively, Python Anaconda distributions (https://www.anaconda.com/) of Python should have all these libraries pre-installed.

Step 2. Setting up the working directory

The working directory has a specific folder structure which is used to store the inputs required to run CRSPY, as well as the outputs produced from CRSPY. In order to build it, run the command lines shown in **Figure 2.12**. This will create the directory structure along with base *config.ini* file.

Step 3. Adjust the config.ini file

The next step is to update the *config.ini* file. First, run the command line shown in **Figure 2.13** to obtain the path to the current working directory. Next, replace *defaultdir* in the ***config.ini*** file with this new

```
import crspy
import os

crspy.initial(os.getcwd()) # This should only be run once as it will overwrite your config.ini file if you do it a second time.
```

Figure 2.12. Command lines for Step 2 (Setting up the working directory)

```
os.getcwd()
```

Figure 2.13. Command line for Step 3 (Adjust the config.ini file

```
import crspy
import os

from configparser import RawConfigParser
nld = RawConfigParser()
nld.read('config.ini')
```

Figure 2.14. Command lines for Step 4 (Read in the config.ini file)

```
# UNCOMMENT BELOW IF YOU WISH TO RUN THIS STEP - this requires preparing your computer for the CDS database
#crspy.dl_land_cover() # about 2GB
#crspy.dl_agb() # about 25GB
```

Figure 2.15. Command lines for Step 5 (Adding data)

path. The next step is to change the *era5_filename* variable with the name of the variable from the file in the /data/era5land directory. In this example case, the variable is changed to *example_era5land*.

Step 4. Read in the config.ini file

Once the *config.ini* file has been updated accordingly, the next step is to read it into the working environment. The command lines shown in **Figure 2.14** below read the *config.ini* file and store it as name list directory (nld). The variable nld is used throughout CRSPY as a lookup for universal values. When running certain functions in CRSPY, CRSPY will now read in the nld file automatically. It is important to restart the Python kernel here, then run the command lines shown in **Figure 2.14**. If changes are made to the *config.ini* file, it is best practice to restart the Python kernel here, then import the CRSPY and os packages, and import the nld variable again, as shown with the command lines in **Figure 2.14**. This is to ensure the updated version of the *config.ini* file is used when running CRSPY.

Step 5. Adding data

Looking to the working directory, the directory structure should now be ready. There are some files, such as the *metadata.csv* file. For more information on this metada file can be found at https://github.com/danpower101/crspy/wiki/Metadata. To demonstrate CRSPY's functions first, there are some example files at https://github.com/danpower101/crspy/tree/master/data, which allow the user to run CRSPY for the first time. Then, the user needs to replace the skeleton *metadata.csv* (created when running the crspy.initial() function shown in **Figure 2.12**) with the one from the example files folder discussed just above. The user also needs to copy over the *nmdb_stations.csv* file to the same folder location.

There are a few other steps needed here, particularly with regards to the example files:

- Place the calibration data (Calib_USA_SITE_011.csv) into the data/calibration_data/ directory;
- Place the raw data (*USA_SITE_011.txt*) into the data/crns_data/raw/ directory;
- Place the era5land data (*example_era5land.nc)* into the data/era5land/ directory. (Generated using Copernicus Climate Change Service Information; Muñoz Sabater, 2019). Note: The example era5land data is pre-extracted using the *era5land* functions (more information on this process is available at https://github.com/danpower101/crspy/wiki/ERA5-Land-Data). When building your own era5land file you can change its name, but this name then needs to be also changed in the *config.ini* file to match.

```
import pandas as pd # pandas is needed to read in the csv

# Read in the metadata.csv file using pandas
meta = pd.read_csv(os.getcwd()+"/data/metadata.csv")

# Run the function
meta = crspy.fill_metadata(meta)
```

Figure 2.16. Command lines for Step 6 (Fill the metadata)

```
# Use the getlistoffiles function to get a list of file paths for time series data
fileslist = crspy.getlistoffiles(os.getcwd()+"/data/crns_data/raw/")

# Run the process with the following - outputs are the dataframe and metadata file - args are first file in list, and whether calibration
df, meta = crspy.process_raw_data(fileslist[0], calibrate=True)
```

Figure 2.17. Command lines for Step 7 (Process CRNS data)

There are two more external sources required which can be collected by running the command line functions shown in **Figure 2.15**. These commands download the land cover and the aboveground biomass data from the European Space Agency Climate Change Initiative (ESA CCI). This involves first setting up the user's computer to interact with the CDS database (https://cds.climate.copernicus.eu/cdsapp#!/home) with further instructions available at https://github.com/danpower101/crspy/wiki/ERA5-Land-Data. These files are large and they can be skipped when running CRSPY for the first time with the example files. As a result, this will remove the aboveground biomass correction from the calculations.

Step 6. Fill the metadata

The commands shown in **Figure 2.16** are used to fill the metadata table (more information on what is collected is available at https://github.com/danpower101/crspy/wiki/Metadata). In addition, it will also generate a unique beta coefficient (required for pressure corrections to the neutron signal) and reference pressure for each site following the approach by Desilets (2021).

Step 7. Process CRNS data

Now with the metadata filled correctly, the measured data can be processed properly. This is done with a simple function call shown in **Figure 2.17**. The *files list* function will provide a list of all the raw datasets currently in the raw folder. This is particularly helpful when processing many sites at once. For now, however, the example files only contain a single site.

Step 8. Check the outputs

Once the previous step has been completed, the user can check the directories to see the saved outputs. Key directories are:

- /data/crns_data/final/ which will contain the final output file including soil moisture estimates as well as variables that have been calculated along the data processing steps;
- /data/qa/ which will contain a folder with Quality Assurance (QA) graphs. These are time series that are useful in identifying possible issues with the data;
- /data/n0_calibration/ which will contain numerous files related to the N_0 calibration process. The report should be checked by the user to ensure that reasonable values have been obtained (these values are collected automatically). For further details on the N_0 calibration process, please refer to Schron *et al.* 2017.

2.5 Temporal filtering of Cosmic Ray Neutron Sensor data

As described in detail in IAEA-TECDOC-1809, the neutron count rate follows Poisson counting statistics. As a result, the total counts per interval is also equal to the variance or the standard deviation is equal to the square root of the total counts. Using this principle, it is possible to propagate count rate

uncertainty into soil water content (SWC) uncertainty. This allows us to design experiments considering the instrument and site-specific count rates (i.e. site conditions are primarily affected by elevation and latitude). IAEA-TECDOC-1845 goes into detail about the pros and cons of different CRNS detectors and how to design robust experiment given the acceptable count rate and SWC uncertainty. In addition to designing robust experiments statistical techniques may be used to help further reduce noise and uncertainty in the neutron count rate. In **Chapter 3.2** a detailed example of different time series filters comparing the raw 1-hour count rates against the common Moving Average (MA) filter and Savitzky-Golay (SG) filter will be described. In **Chapter 3**, an example from Austria will be provided to show some practical hydrological applications using Cosmic Ray Neutron Sensor.

2.6 Conclusion

The cosmic ray neutron sensing technology is used to estimate root zone soil moisture at sub-kilometer scales. The technology has been firstly introduced in 2008 followed by the establishment of the first national COSMOS network in the United States of America. New national networks have been established in Australia, Germany, India, and the United Kingdom of Great Britain and Northern Ireland: along with many sites maintained by individual users. Over the years and with a growing number of users, our understanding of this technology has increased, particularly regarding its spatial footprint of the measurement as well as on how to better quantify the uncertainties from measured cosmic ray neutrons and improve converting neutron data to soil moisture. Despite of such effort, new end-users still lack access to common data processing steps, which results in individual sites or national networks employing their own individual database protocols. As a result, worldwide CRNS stations still lack harmonization, hindering a more comprehensive and broader understanding of soil moisture dynamics at continental and global scales. With that challenge in mind, one of the major contributions of this guideline is to provide information on newly developed open-source CRNS data processing tools and guidance on their use to facilitate the adoption of the CRNS technology by new users and to help with data harmonisation of multiple sites worldwide.

The first tool please give name of tool (available at https://zenodo.org/record/7156607) based on the EXCEL spreadsheets provides an easy and simple approach suitable for processing limited amounts of the data (time series representing few years from few CRNS sites) and this tool is very suitable also for beginners starting to use the CRNS technique who want to learn the basic principles of CRNS data processing. This tool comprises of two spreadsheets, one for processing the soil samples that can be used for sensor calibration and the second for processing the neutron counting rates.

The second tool CRSPY (available at https://zenodo.org/record/5543669#.YZ-EcS-l1pQ) is for processing of large quantities of data representing many years of data series from a great number of monitoring sites and this tool is good especially for advanced users familiar with CRNS technique and having sufficient experience with data processing. It was developed to address the needs for efficient and standardised CRNS data processing and is based on python computer language. The CRSPY tool allows users to process CRNS data from single or multiple sites seamlessly by applying all necessary signal correction and calibration steps while integrating local collected data with publicly available global data products to help with harmonization steps. A new metadata feature is also introduced in CRSPY to help users easily access ancillary site information from the public domain regarding, for example, hydroclimate, soil and land cover properties.

Both tools presented here are flexible enough for any user to incorporate changes and further updates regarding processing neutron counts. Ultimately, it can be expected that with both tools (and future ones to come), the CRNS technology and its data will become more accessible to new users including interdisciplinary research communities working on various research fields (e.g. hydrological modelling, remote sensing, land management, environmental studies, etc.)

References

Avery, W.A., Finkenbiner, C., Franz, T.E., Wang, T., Nguy-Robertson, A.L., Suyker, A., Arkebauer, T. & Muñoz-Arriola, F. 2016. Incorporation of Globally Available Datasets into the

Roving Cosmic-Ray Neutron Probe Method for Estimating Field-Scale Soil Water Content. *Hydrol. Earth Sys. Sci.* 20(9): 3859–3872. https://doi.org/10.5194/hess-20-3859-2016

Baatz, R., Bogena, H.R., Hendricks Franssen, H.J., Huisman, J.A., Montzka, C. & Vereecken, H. 2015. An empirical vegetation correction for soil water content quantification using cosmic ray probes. *Water Resour. Res.* 51: 2030–2046. https://doi.org/10.1002/2014WR016443

Batjes, N.H., Ribeiro, E. & van Oostrum, A. 2019. Standardised soil profile data to support global mapping and modelling (WoSIS snapshot 2019). *Earth Syst. Sci. Data* 12: 299–320. https://doi.org/10.5194/essd-12-299-2020, 2020

Blöschl, G., Blaschke, A.P., Broer, M., Bucher, C., Carr, G., Chen, X., Eder, A., Exner-Kittridge, M., Farnleitner, A., Flores-Orozco, A., Haas, P., Hogan, P., Kazemi Amiri, A., Oismüller, M., Parajka, J., Silasari, R., Stadler, P., Strauss, P., Vreugdenhil, M., Wagner, W. & Zessner, M. 2016. The Hydrological Open Air Laboratory (HOAL) in Petzenkirchen: a hypothesis-driven observatory, *Hydrol. Earth Syst. Sci*. 20: 227–255. https://doi.org/10.5194/hess-20-227-2016

Bogena, H.R. 2016. TERENO: German network of terrestrial environmental observatories, *JLSRF* 2: A52, https://doi.org/10.17815/jlsrf-2-98

Cooper, H.M., Bennett, E., Blake, J., Blyth, E., Boorman, D., Cooper, E., Evans, J., Fry, M., Jenkins, A., Morrison, R., Rylett, D., Stanley, S., Szczykulska, M., Trill, E., Antoniou, V., Askquith-Ellis, A., Ball, L., Brooks, M., Clarke, M.A., Cowan, N., Cumming, A., Farrand, P., Hitt, O., Lord, W., Scarlett, P., Swain, O., Thornton, J., Warwick, A. & Winterbourn, B. 2021. COSMOS-UK: national soil moisture and hydrometeorology data for environmental science research. *Earth Syst. Sci. Data* 13: 1737–1757. https://doi.org/10.5194/essd-13-1737- 2021

Desilets, D., Zreda, M. & Prabu, T. 2006. Extended scaling factors for in situ cosmogenic nuclides: New measurements at low latitude, *Earth Planet. Sc. Lett*. 246: 265–276.

Desilets, D., Zreda, M. & Ferré, T.P.A. 2010. Nature's neutron probe: Land surface hydrology at an elusive scale with cosmic rays. W*ater Resour. Res*. 46: W11505. https://doi.org/10.1029/2009WR008726

Desilets, D. 2021. *Intensity correction factors for a cosmic ray neutron sensor*. Zenodo [data set]. https://doi.org/10.5281/ZENODO.4569062

Dirmeyer, P.A., Wu, J., Norton, H.E., Dorigo, W.A., Quiring, S.M., Ford, T.W., Santanello, J.A., Bosilovich, M.G., Ek, M.B., Koster, R.D., Balsamo, G. & Lawrence, D.M. 2016. Confronting weather and climate models with observational data from soil moisture networks over the United States. *J. Hydrometeorol.* 17: 1049–1067, https://doi.org/10.1175/JHM-D-15-0196.1

Evans, J.G., Ward, H.C., Blake, J.R., Hewitt, E.J., Morrison, R., Fry, M., Ball, L.A., Doughty, L.C., Libre, J.W., Hitt, O.E., Rylett, D., Ellis, R.J., Warwick, A.C., Brooks, M., Parkes, M.A., Wright, G.M.H., Singer, A.C., Boorman, D.B., Jenkins, A., Evans, J.G., Libre, J.W., Jenkins, A., Rylett, D., Singer, A.C., Warwick, A.C., Morrison, R., Ward, H.C., Ellis, R.J., Ball, L.A., Hewitt, E.J., Fry, M., Parkes, M.A., Boorman, D.B., Hitt, O.E., Brooks, M., Wright, G.M.H. & Doughty, L.C. 2016. Soil water content in southern England derived from a cosmic-ray soil 100 moisture observing system – COSMOS-UK, *Hydrol. Process.* 30: 4987–4999. https://doi.org/10.1002/hyp.10929

Franz, T.E., Zreda, M., Ferre, T.P.A., Rosolem, R., Zweck, C., Stillman, S., Zeng, X. & Shuttleworth, W.J. 2012a. Measurement depth of the cosmic-ray soil moisture probe affected by hydrogen from various sources. *Water Resour. Res.* 48: W08515, https://doi.org/10.1029/2012WR011871

Franz, T.E., Zreda, M., Rosolem, R. & Ferre, T.P.A. 2012b. Field Validation of a Cosmic-Ray Neutron Sensor Using a Distributed Sensor Network. *Vadose Zone J.* 11, vzj2012.0046. https://doi.org/10.2136/vzj2012.0046

Franz, T.E., Tiejun W., William A., Finkenbiner, C. & Brocca, L. 2015. Combined Analysis of Soil Moisture Measurements from Roving and F ixed Cosmic Ray Neutron Probes for Multiscale Real-Time Monitoring. *Geophys. Res. Lett.* 42(9): 3389–96. https://doi.org/10.1002/2015GL063963

Hawdon, A., McJannet, D. & Wallace, J. 2014. Calibration and correction procedures for cosmic-ray neutron soil moisture probes located across Australia. *Water Resour. Res.* 50: 5029–5043. https://doi.org/10.1002/2013WR015138

IAEA. 2017. *Cosmic Ray Neutron Sensing: Use, Calibration and Validation for Soil Moisture Estimation*. IAEA-TECDOC-1809. Joint FAO/IAEA Programme Nuclear Techniques in Food and Agriculture. Vienna, www.pub.iaea.org/books/IAEABooks/11097/Cosmic-Ray-Neutron-Sensing-Use-Calibration-and-Validation-for-Soil-Moisture-Estimation

IAEA. 2018. *Soil Moisture Mapping with a Portable Cosmic Ray Neutron Sensor.* IAEA-TECDOC-1845. Joint FAO/IAEA Programme Nuclear Techniques in Food and Agriculture. Vienna, Austria. www-pub.iaea.org/books/IAEABooks/12357/Soil-Moisture-Mapping-with-a-Portable-Cosmic-Ray-Neutron-Sensor

Kohli, M., Schron, M., Zreda, M., Schmidt, U., Dietrich, P. & Zacharias, S. 2015. Footprint characteristics revised for field-scale soil moisture monitoring with cosmic-ray neutrons. Water Resour. Res. 51(7): 5772–5790. https://doi.org/10.1002/2015wr017169

Iwema, J., Rosolem, R., Baatz, R., Wagener, T. & Bogena, H.R. 2015. Investigating temporal field sampling strategies for site-specific calibration of three soil moisture–neutron intensity parameterisation methods. *Hydrol. Earth Syst. Sci*. 19: 3203–3216. https://doi.org/10.5194/hess-19-3203-2015

Iwema, J., Schrön, M., Da Silva, J.K., De Paiva Lopes, R.S., Rosolem, R. 2021. Accuracy and precision of the cosmic-ray neutron sensor for soil moisture estimation at humid environments, *Hydrol. Proces*. https://doi.org/10.1002/hyp.14419

McJannet, D., Stenson, M., Sommer, A. & Hawdon, A. 2021. *CosmOz – The Australian Cosmic-ray Soil Moisture Sensor Network, Version 1.0.0*. Terrestrial Ecosystem Research Network (TERN) [data set]. https://doi.org/10.25901/5e7ab81af0394

Muñoz Sabater, J. 2021. *ERA5-Land hourly data from 1950 to 1980.* Copernicus Climate Change Service (C3S), Climate Data Store (CDS) [data set]. https://doi.org/10.24381/cds.e2161bac

Poggio, L., Sousa, L.M. de, Batjes, N.H., Heuvelink, G.B.M., Kempen, B., Ribeiro, E. & Rossiter, D. 2021. SoilGrids 2.0: producing soil information for the globe with quantified spatial uncertainty. *Soil* 7: 217–240. https://doi.org/10.5194/soil-7-217-2021. https://soilgrids.org (accessed 11 November 2021.)

Power, D., Rico-Ramirez, M.A., Desilets, S., Desilets, D. & Rosolem, R. 2021. Cosmic-Ray neutron Sensor Python tool (CRSPY): An open-source tool for the processing of cosmic-ray neutron and soil moisture data, *Geosci. Model Dev. Discuss* (preprint). https://doi.org/10.5194/gmd-2021-77 (in review).

Rosolem, R., Shuttleworth, W.J., Zreda, M., Franz, T.E., Zeng, X. & Kurc, S.A. 2013. The effect of atmospheric water vapor on neutron count in the cosmic-ray soil moisture observing system. *J. Hydrometeorol.* 14: 1659–1671.

Santoro, M. & Cartus, O. 2019. *ESA Biomass Climate Change Initiative (Biomass_cci): Global datasets of forest aboveground biomass for the year 2017*. Vol. 1. Centre for Environmental Data Analysis [data set]. https://doi.org/ 10.5285/BEDC59F37C9545C981A839EB552E4084

Schrön, M., Köhli, M., Scheiffele, L., Iwema, J., Bogena, H.R., Lv, L., Martini, E., Baroni, G., Rosolem, R., Weimar, J., Mai, J., Cuntz, M., Rebmann, C., Oswald, S.E., Dietrich, P., Schmidt, U. & Zacharias, S. 2017. Improving calibration and validation of cosmic-ray neutron sensors in the light of spatial sensitivity. *Hydrol. Earth Syst. Sci*. 21: 5009–5030. https://doi.org/10.5194/hess-21-5009–2017

Stanley, S., Antoniou, V., Askquith-Ellis, A., Ball, L.A., Bennett, E.S., Blake, J.R., Boorman, D.B., Brooks, M., Clarke, M., Cooper, H.M., Cowan, N., Cumming, A., Evans, J.G., Farrand, P., Fry, M., Hitt, O.E., Lord, W.D., Morrison, R., Nash, G.V., Rylett, D., Scarlett, P.M., Swain, O.D., Szczykulska, M., Thornton, J.L., Trill, E J., Warwick, A.C. & Winterbourn, B. 2021. *Daily and sub-daily hydrometeorological and soil data (2013–2019)*. [COSMOS-UK], NERC Environmental Information Data Centre [data set]. https://doi.org/10.5285/b5c190e4-e35d-40ea-8fbe- 598da03a1185

Wagener, T., Gleeson, T., Coxon, G., Hartmann, A., Howden, N., Pianosi, F., Rahman, M., Rosolem, R., Stein, L. & Woods, R. 2021. On doing hydrology with dragons: Realizing the value of perceptual models and knowledge accumulation. *WIREs Water* 8: e1550. https://doi.org/10.1002/wat2.1550

Zreda, M., Desilets, D., Ferré, T.P.A. & Scott, R.L. 2008. Measuring 105 soil moisture content non-invasively at intermediate spatial scale using cosmic-ray neutrons. *Geophys. Res. Lett.* 35: L21402, https://doi.org/10.1029/2008GL035655

Zreda, M., Shuttleworth, W.J., Zeng, X., Zweck, C., Desilets, D., Franz, T. & Rosolem, R. 2012. COSMOS: the COsmic-ray Soil 110 Moisture Observing System. *Hydrol. Earth Syst. Sci.* 16, 4079– 4099. https://doi.org/10.5194/hess-16-4079-2012

3. Practical hydrological applications using Cosmic Ray Neutron Sensor

Trenton Franz

3.1 Introduction

To maximise the societal relevance of Cosmic Ray Neutron Sensor (CRNS) soil water content (SWC) data, practical value-added products need to be developed that can estimate both water fluxes (i.e. rainfall, deep percolation, evapotranspiration) and water pools (especially those most relevant for agriculture, such as root zone water storage and its spatial heterogeneity and temporal dynamics). In particular, simple methods that can be used to estimate daily values at area-average scales are needed by decision makers, researchers and other users interested in utilising this technique. Developing such methods of CRNS data processing and approaches for creating value added products relevant for agriculture water management and environmental assessment is a new task for present time and near future. This effort is starting only recently as during the earlier period since introducing CRNS method in 2008, the research was focused on developing, testing, verifying, and refining the CRNS technique as such and the monitoring activities were established in various countries representing a wide range of geographical conditions, climates, and land managements. In recent years the development of CRNS value-added products started, and this chapter is aimed on presenting the first results achieved in this field. Three tools to produce value-added products are presented below: (a) temporal filtering the CRNS signal to reduce noise of the neutron count signal; (b) estimating rainfall from the CRNS data, and (c) estimating root zone soil moisture. These approaches were tested on dataset collected at CRNS monitoring site installed at the Hydrological Open-Air Laboratory (HOAL) in Petzenkirchen, Austria, operating by the Joint FAO/IAEA Centre since 2013. Firstly, the corrected neutron counts were filtered to reduce noise. For this purpose, two different filters (moving average and Savitzky-Golay filter) were tested. Both these filters can be used with different temporal windows and Savitzky-Golay filter can be used with different ordered polynomials so in total 23 different versions of filters were tested. The daily rainfall was estimated with the Soil Moisture 2 Rain (SM2RAIN) algorithm and the root zone SWC using the exponential filter algorithm and it was evaluated how the different neutron filter methods translate into hourly SWC, daily rainfall estimates and root zone soil moisture estimates.

These advanced CRNS data processing methods and resulting value-added products are very useful for agricultural water management and environmental studies such as improved soil moisture management under rainfed agriculture, irrigation scheduling, drought management, hydrological modelling, flood prediction, surface runoff management and land conservation. Moreover, the CRNS data can be used also for estimating area-average soil moisture values, which are needed for validating remote sensing soil moisture products and developing better algorithms for their further refinement.

Figure 3.1 provides the reader with a clear framework outlining this chapter. It describes the processes, data sources, algorithms, and value-added products covered in this chapter. **Appendices I–III** provide the main computer program and subroutines using the software Matlab R2020a. In the following chapter, each technique will be introduced and applied at the CRNS site established in 2013 in Petzenkirchen, Austria. The CRNS data are supported by observations of rainfall and SWC point measurements using Time-Domain Transmissivity (TDT) at HOAL to calibrate and validate the algorithms. This chapter is based on the work provided in Franz *et al.* (2020).

3.2 Description of study area

A CRNS (Model # CRS 1000/B, HydroInnova LLC, Albuquerque, NM, United States of America) was installed at the study area in the northeast of Austria (**Figure 3.2**) on 11 December 2013. The HOAL (Bloschl *et al.* 2016) site located in Petzenkirchen, is a cooperation project between the Austrian Federal

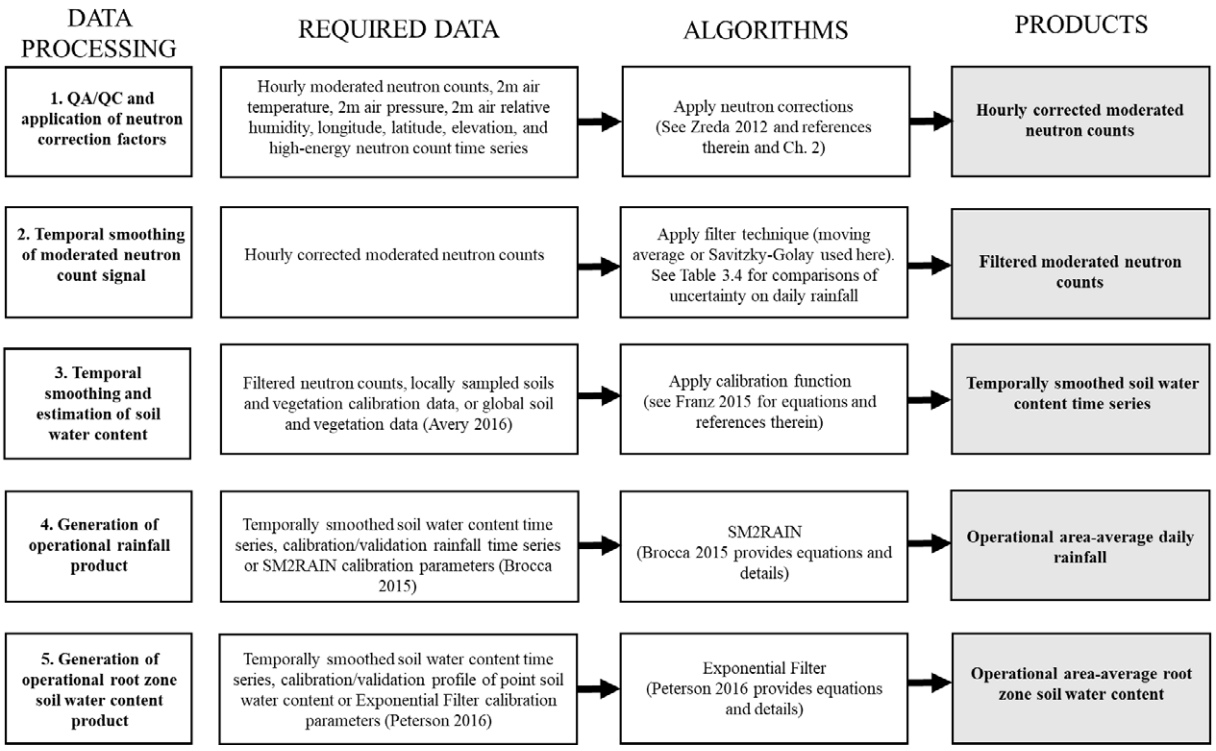

Figure 3.1. Scheme of processing the CRNS data and developing hydrologic products

Table 3.1. Summary of site and soil properties for Petzenkirchen

Latitude	48.15
Longitude	15.15
Elevation (m)	278.0
Reference air temperature (°C)	25.0
Reference air pressure (hPa)	980.2
Scaling factor	1.174
Lattice water (g/g) please use g/g throughout	0.039
Soil organic carbon water equivalent (g/g)	0.0044
Avg. Soil bulk density (g/cm^3)	1.41
Standard Deviation of soil bulk density (g/cm^3)	0.130

Source: Franz, T.E., Wahbi, A., Vreugdenhil, M., Weltin, G., Heng, L., Oismueller, M., Strauss, P., Dercon, G. & Desilets, D. 2016. Using Cosmic-ray Neutron Probes to Monitor Landscape Scale Soil Water Content in Mixed Land Use Agricultural Systems. *Appl. Environ. Soil Sci.* 2016. https://doi.org/10.1155/2016/432374.

Agency for Water Management (BAW) and the Technical University Vienna (TU Vienna). It is about 100 km west of Vienna (48.15°N, 15.15°E). The research station is located in an undulating agricultural landscape (elevation 277 m). The average annual temperature is 9.5 ˚C and the annual average reaches 823 mm, mostly between April and September. The soilscape is dominated by Cambisols (56 percent) Planosols (21 percent) and Anthrosols (17 percent) and smaller portion of the area occupied by Gleysols (6 percent) and Histosols (< 1 percent). Infiltration capacity tends to be medium to low, water storage capacity tends to be high, and shrinking cracking may occur in summer due to the high clay content (Bloschl *et al.* 2016). The land use is almost entirely dominated by cultivated land, apart from one small strip of forest (see **Figure 3.3** for map). The main crops are winter wheat, barley, maize and

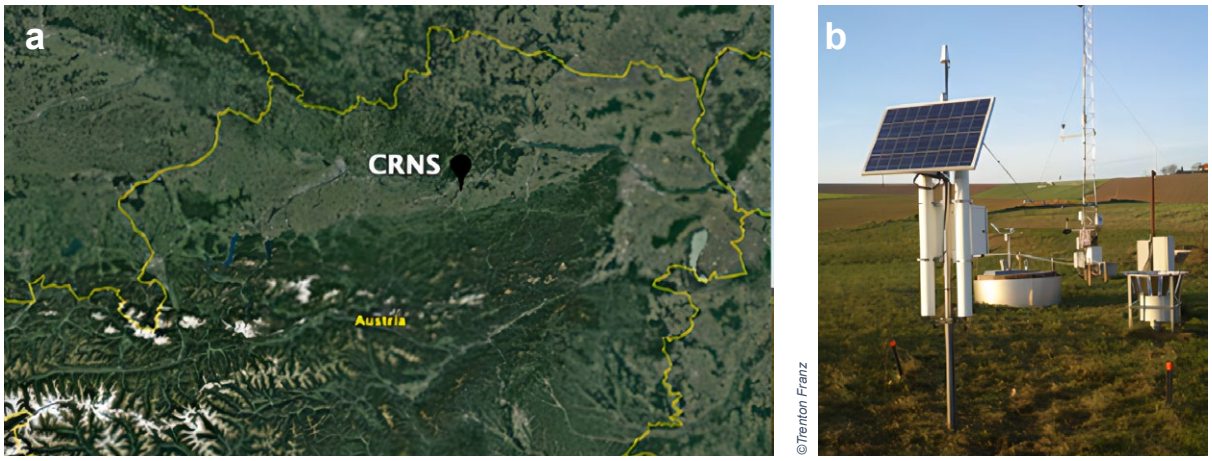

Figure 3.2. (a) Location of the CRNS (48.15°N, 15.15°E) in an agricultural area in northeast Austria; (b) CRNS located at study site with weather station and eddy covariance tower. See Figure 3.5 for raw and processed neutron counts. Source: Franz, T.E., Wahbi, A., Vreugdenhil, M., Weltin, G., Heng, L., Oismueller, M., Strauss, P., Dercon, G. & Desilets, D. 2016. Using Cosmic-ray Neutron Probes to Monitor Landscape Scale Soil Water Content in Mixed Land Use Agricultural Systems. *Appl. Environ. Soil Sci.* 2016. https://doi.org/10.1155/2016/432374.

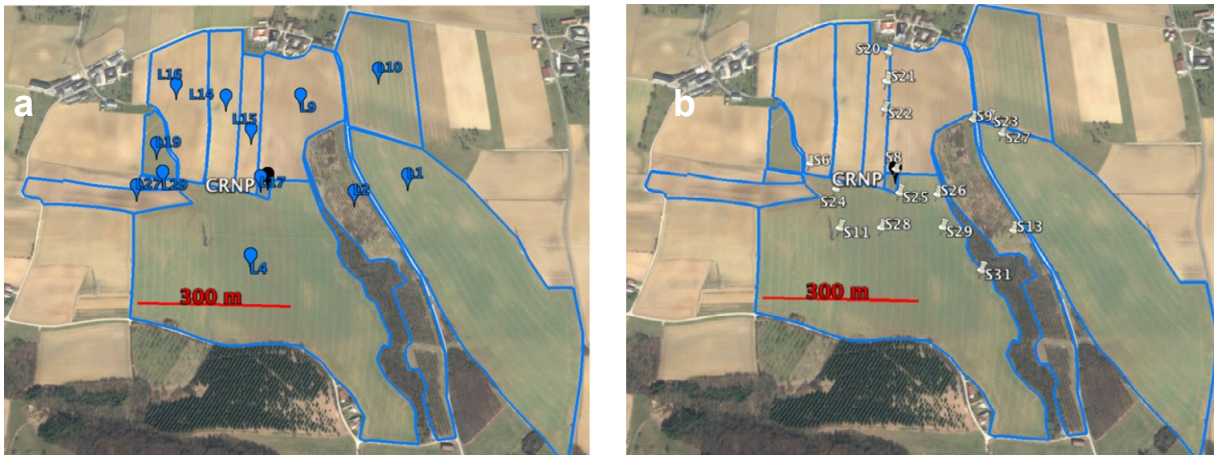

Figure 3.3. (a) Location of 16 land use plots within the ~200 m radial CRNS footprint (see **Table 2.1** for planting, soil cultivation, and harvest information); (b) Location of 16 TDT site profiles (probe measurement depths at 0-5 cm, 5-10 cm, 15–20 cm, and 45–50 cm) within the ~200 m radial CRNS footprint that were operational during the first half of 2014. Source: Franz, T.E., Wahbi, A., Vreugdenhil, M., Weltin, G., Heng, L., Oismueller, M., Strauss, P., Dercon, G. & Desilets, D. 2016. Using Cosmic-ray Neutron Probes to Monitor Landscape Scale Soil Water Content in Mixed Land Use Agricultural Systems. *Appl. Environ. Soil Sci.* 2016. https://doi.org/10.1155/2016/432374.

rape (see **Table 3.2** for 2014 cropping information). **Figure 3.3** illustrates the location of the CRNS, the eddy covariance tower, rain gauge, the various land use plots within the CRNS's measurement area (~13 ha) of a ~200 m radius circle, and the location of the TDT sensors that were used in the first half of 2014. A network of TDT sensors (31 sensors, SPADE, Julich, Germany) were installed in the second half of 2013 and they were distributed all over the HOAL area). They recorded hourly SWC. **Figure 3.3** illustrates the 16 TDT sensor locations within the CRNS footprint, see Bloschl *et al.* (2016) for full details. At each location four TDT sensors were installed vertically at four depths (representing soil layers of ~ 0–5 cm, 5–10 cm, 15–20 cm, and 45–50 cm, see **Figure 3.4)**. Depending on routine agricultural operations and location of the stations, the TDT sensors were removed at various times throughout the year. Here the data record from Dec 2013 through April 2014 (before the sensors were removed for spring and summer field operations) will be used. For full details of the study site, available datasets, overarching research questions, and specific hypotheses, see Bloschl *et al.* (2016).

Gravimetric soil samples were collected from 18 locations to calibrate the CRNS. A total of five calibrations were completed in 2016 and 2017 (see **Table 3.1**). Samples were taken every 60 degrees

Table 3.2. Summary of planting, soil cultivation and harvest dates for each land use plot. Note, no data was available for land use in plot 1 (see Figure 3.2 for locations).

Field	TDT Location	Date of Activity	Activity	Activity Description	Amount of Activity	Units of Activity
1	27	NA	NA	NA	NA	NA
2	9, 13	7/30/14	Harvest	Straw mulch)	3500	kg/ha
2		7/30/14	Harvest	Winter Wheat	7400	kg/ha
2		8/8/14	Tillage	Chisel (20 cm)	NA	NA
2		9/11/14	Tillage	Plow (25–30 cm)	NA	NA
2		9/24/14	Planting	Winter Barley	160	kg/ha
4	11, 24, 25, 26, 28, 29, 31	7/30/14	Harvest	Straw (mulch)	3500	kg/ha
4		7/30/14	Harvest	Winter Wheat	7600	kg/ha
4		8/7/14	Tillage	Chisel (20 cm)	NA	NA
4		9/17/14	Tillage	Plow (25–30 cm)	NA	NA
4		9/21/14	Planting	Winter Barley	160	kg/ha
9		11/18/13	Tillage	Plow (25–30 cm)	NA	NA
9		3/21/14	Tillage	Harrow	NA	NA
9		4/4/14	Planting	Maize	85000	seeds/ha
9		9/5/14	Harvest	Maize	16900	kg/ha
9		10/5/14	Tillage	Mulch application	NA	NA
9		10/16/14	Tillage	Plow (25–30 cm)	NA	NA
10	23	7/20/14	Harvest	Wheat	10.1	t/ha
10		7/30/14	Planting	Kress	2	kg/ha
10		7/30/14	Planting	Phacelia	3	kg/ha
10		7/30/14	Planting	Clover	5	kg/ha
10		7/30/14	Planting	Buckwheat	15	kg/ha
10		11/17/14	Tillage	Plow (25–30 cm)	NA	NA
14		7/28/14	Harvest	Winter Wheat	6300	kg/ha
14		7/28/14	Harvest	Straw (mulch)	NA	NA
14		8/2/14	Tillage	Grubber plow (15cm)	NA	NA
14		8/14/14	Planting	Phacelia	15	kg/ha
14		11/18/14	Tillage	Chisel (25–30 cm)	NA	NA
15	20, 21, 22	3/7/14	Tillage	Harrow	NA	NA
15		4/1/14	Tillage	Harrow	NA	NA
15		4/15/14	Planting	Maize	90000	seeds/ha
15		10/10/14	Harvest	Maize	12380	kg/ha
15		10/13/14	Tillage	Plow (25–30 cm)	NA	NA
15		10/14/14	Tillage	Harrow	NA	NA
15		10/20/14	Planting	Winter Wheat	180	kg/ha
16	6	7/28/14	Harvest	Wheat	6300	kg/ha
16		8/2/14	Tillage	Harrow	NA	NA
16		8/14/14	Planting	Phacelia	15	kg/ha
16		11/19/14	Tillage	Plow (25–30 cm)	NA	NA
17	8	3/13/14	Tillage	Harrow	NA	NA
17		5/21/14	Harvest	Meadow	NA	NA
17		8/6/14	Harvest	Meadow	NA	NA
19		7/1/14	Harvest	Rapeseed	4600	kg/ha
19		8/10/14	Planting	Phacelia	25	kg/ha
27		7/7/14	Harvest	Rapeseed	4500	kg/ha
29		7/7/14	Harvest	Rapeseed	4500	kg/ha

Source: Franz, T.E., **Wahbi, A., Vreugdenhil, M., Weltin, G., Heng, L., Oismueller, M., Strauss, P., Dercon, G. & Desilets, D.** 2016. Using Cosmic-ray Neutron Probes to Monitor Landscape Scale Soil Water Content in Mixed Land Use Agricultural Systems. *Appl. Environ. Soil Sci.* 2016. https://doi.org/10.1155/2016/432374.

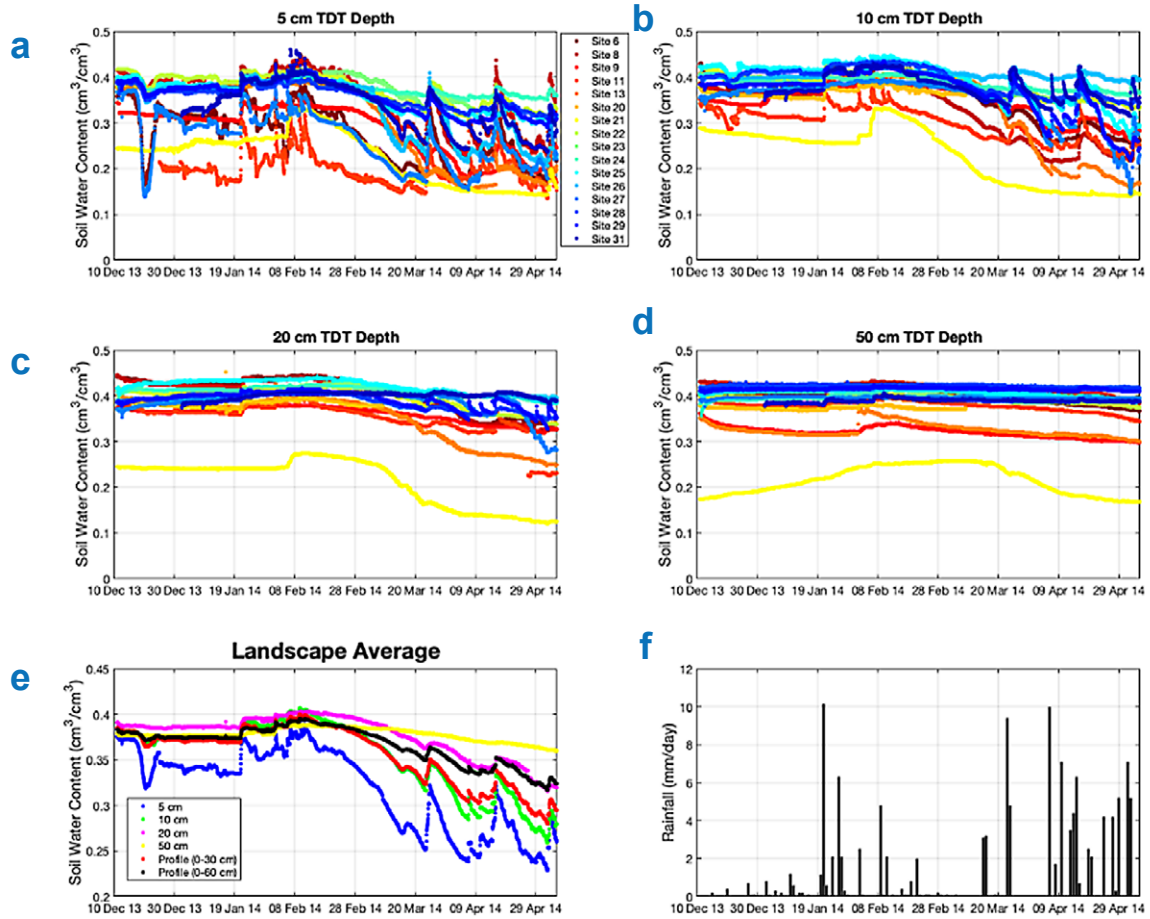

Figure 3.4. Time series of TDT probes organized by depth (a–d) and by site location illustrating the wide range of SWC encountered. All TDT sensors were installed in the second half of 2013 but were removed over time on different dates due to the various soil cultivation and harvest times of each of the land use plots. See **Figure 2a** in Franz *et al.* (2016) for spatial locations; (e) Time series of landscape average SWC by TDT depth and profile weighted averages of 0–30 cm and 0–60 cm; (f) Time series of daily rainfall data. Adapted from Franz, T., Wahbi, A., Zhang, J., Vreugdenhil, M., Heng, L., Dercon, G., Strauss, P., Brocca, L. & Wagner, W. 2020. Practical Data Products From Cosmic-Ray Neutron Sensing for Hydrological Applications Front. Water. 2. https://doi.org/10.3389/frwa.2020.00009

and at radii of 25, 75, and 200 m. At each location, samples were collected every 5 cm down to 30 cm for a total of 108 samples per calibration. The ~200 gm samples were placed in a soil can and weighed to obtain a wet weight. The samples were then placed in an oven for 24 hours at a temperature of 105 deg. C and reweighed to obtain a dry weight and calculate gravimetric water content. On one sampling date undisturbed soil cores were collected from 3 locations to determine soil bulk density. In addition, on that date, ~1 gm from each sample location was used to make a composite sample. The composite sample was used to determine lattice water and soil organic carbon (see **Table 3.1**).

3.3 Temporal filtering of CRNS data to reduce noise of the neutron count signal

As outlined in **Chapter 2.5**, it is important to apply a time series filter to further reduce noise in the neutron count data and thus SWC. The detector gas type, volume, site elevation and latitude determine the observed neutron count rates. Here the 1-hour count rates are compared against 2 types of filters, a Moving Average (MA) filter and Savitzky-Golay (SG) filter (see Savitzky and Golay, 1964 and Orfanidis, 1996 for full details). These two filters were selected because an MA is a common and simple filter and SG is a common filter that will better preserve sharp troughs in the neutron count time series due to rain events. The MA filter will smooth out these troughs leading to errors in the SWC time

series. The software package Matlab 2020a was used to perform filters on the neutron count time series (see **Appendices I–III**). Other packages like R studio or Python will have similar subroutines to run the calculations.

The CRNS technique works by counting low-energy neutrons (~0.5 to 1000 eV) from a moderated detector over a certain time interval (typically 1 hour for stationary sensors) (see Zreda *et al.* 2008, Desilets *et al.* 2010, Zreda *et al.* 2012, and Andresen *et al.* 2017 for details). Because of the inherent counting statistics, plots of hourly neutron counts and SWC appear noisy with random fluctuations around a mean value. The uncertainty of CRNS neutron count rates follows Poisson statistics (Knoll 2000, Zreda *et al.* 2012), where the standard deviation is equal to the square root of the total counts. For example, 1000 counts per hour (cph) would have an uncertainty of 31.6 cph or 3.16 percent. To get more precise SWC data, it is needed to filter the raw neutron counts (to reduce the noise). To produce a smoothed SWC time series, a temporal filter should be applied to the corrected neutron data. Following the standard set of corrections for time-varying barometric pressure, high-energy incoming neutron intensity, and atmospheric water vapor (Zreda *et al.* 2012, Rosolem *et al.* 2013), two different time series filters (SG and MA) were applied to the example CRNS data from Austria described above. The MA filter is also known to over smooth sharp changes in the input time series. The SG filter is less common but still a widely used filter in many fields (i.e. electrical engineering). It was selected because it is known to better preserve sharp changes in the input time series.

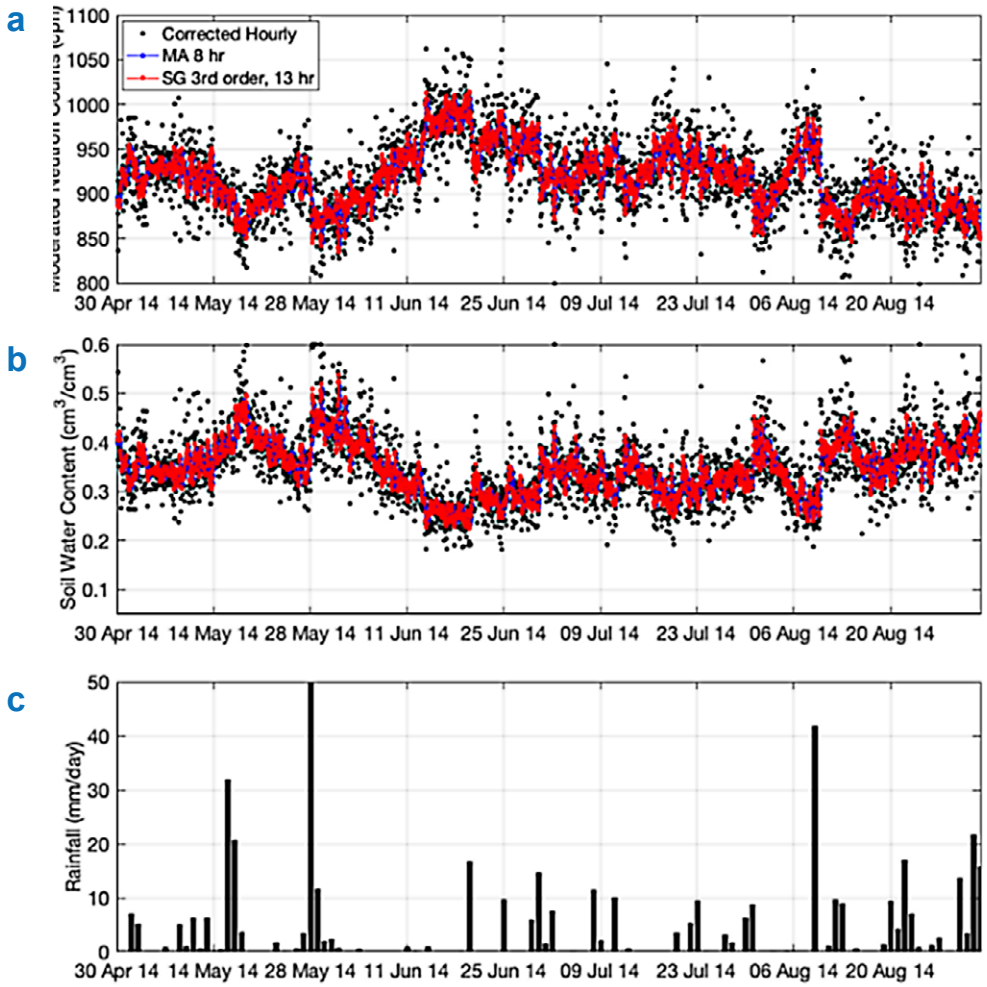

Figure 3.5. Time series of (a) hourly corrected neutron counts (black dots), MA (blue dots with line) and SG filtered neutrons (red dots with line); (b) hourly SWC using the Desilets *et al.* (2010) equation and (c) daily rainfall observed study site for the same time period as TDT observations. Adapted from Franz, T., Wahbi, A., Zhang, J., Vreugdenhil, M., Heng, L., Dercon, G., Strauss, P., Brocca, L. & Wagner, W. 2020. Practical Data Products From Cosmic-Ray Neutron Sensing for Hydrological Applications Front. Water. 2. https://doi.org/10.3389/frwa.2020.00009

At this site, the 1-hour corrected neutron count data contained large fluctuations due to the low counting rate (~1000 cph ± 31 cph). Several different window sizes were used for MA and SG filters to investigate the degree of smoothing the neutron counts. MA filter was used with 3, 6, 8, 10, 12 and 24-hours temporal windows and SG filter with 3, 7, 9, 11, 13, 25 hours because the SG filter requires an odd number of input data points. Moreover, the SG filter can be used with different ordered polynomials (1st to 3rd order), so each of temporal windows mentioned above was used with 1st, 2nd and 3rd ordered polynomials (Savitzky and Golay, 1964 and Orfanidis, 1996). In total 23 versions of filters were investigated.

When using a number of different approaches such as 23 filters used in this case, it is an important task to find out which approach has better results. To identify the best approach, it is necessary to compare the results with some measured data. In this case it was possible to use the rainfall data available from Petzenkirchen site, because the second topic of this research is the rainfall estimation from CRNS data (**Chapter 3.4**). To estimate the rainfall the SM2RAIN algorithm was used. For details of this approach, see **Chapter 3.4**. The soil water contents were calculated from neutron counts filtered by all 23 versions of filters, and they were used for calculating daily rainfall values with SM2RAIN algorithm. The calculated rainfall values were compared with rainfall values measured in field and it was assumed that those versions of the filters are best which resulted in best rainfall estimates closest to measured rainfall.

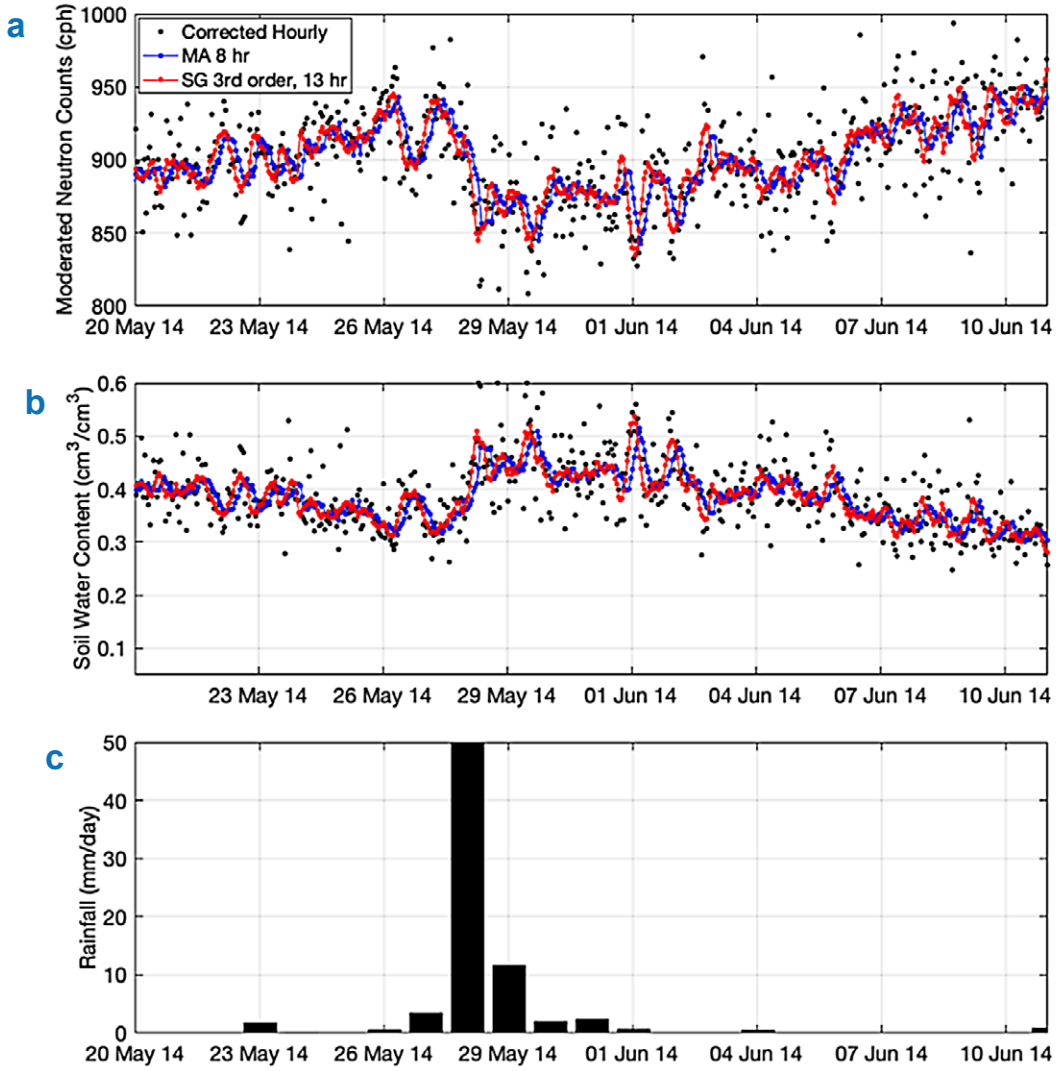

Figure 3.6. Zoomed in times series of Figure 3.5 better illustrating the 2 to 4 hr shift in the timing of rainfall using the MA filter./ Adapted from Franz, T., Wahbi, A., Zhang, J., Vreugdenhil, M., Heng, L., Dercon, G., Strauss, P., Brocca, L. & Wagner, W. 2020. Practical Data Products From Cosmic-Ray Neutron Sensing for Hydrological Applications Front. Water. 2. https://doi.org/10.3389/frwa.2020.00009

Table 3.3 in **Chapter 3.4** provides a comparison of the 23 different neutron filters propagated through the SM2RAIN algorithm for estimating daily rainfall (**Figure 3.5**). Using the cumulative sum percent error and the Kling-Gupta-Efficiency (KGE) index (Gupta *et al.* 2009) as criteria, the best MA (8 h) and SG (3rd order, 13 h) filters were selected. These two filters and the 1 h data will be used for visual purposes for the remainder of analyses. **Figure 3.6a** illustrates the 1 h corrected neutron counts (black dots), the MA 8 h (blue dots and line) and SG 3rd order, 13 h filtered neutrons counts (red dots and line) for the Petzenkirchen site from 2013 to mid-2014, corresponding to the available TDT data. Following the neutron count filtering, the standard calibration function of Desilets *et al.* (2010) was applied to all datasets and SWC is then estimated (**Figure 3.5b**, See Franz *et al.* 2016 for on-site parameters and supplemental data). **Figure 3.5c** illustrates the observed rainfall time series. A porosity upper bound (= 0.6 cm^3/cm^3 based on the soil bulk density value, see Franz *et al.* 2016) was also applied to the SWC data. Neutron counts that result in SWC of the above porosity are due to the presence of water on the surface. Given the closeness of the SG and MA time series results, **Figure 3.7** provides a zoomed-in view between May and June 2014. From **Figures 3.6 and 3.7a** the connection between rainfall events and sharp decrease in neutron count rates is evident. Also note that for periods between rainfall events a steady increase in neutron counts is observed as more water is being transported to the atmosphere and soil via evapotranspiration (soil evaporation and plant transpiration). From **Figures 3.5 and 3.6** it is evident that both the MA and SG filter time series follow the central tendency of the black dot data cloud. However, **Figure 3.7**b illustrates that the MA filter changes the SWC peak by 2 to 4 h and slightly decreases the amplitude compared to the SG filter. The change in amplitude and timing of the SWC peak will affect surface runoff generation and connections to the watershed discharge (Dingman, 2002). This chapter is focused only on the connection of CRNS data to daily rainfall and root zone SWC, but future work should also investigate the connections to surface runoff and discharge (Dimitrova-Petrova *et al.* 2020).

3.4 Estimation of landscape average rainfall using SM2RAIN algorithm

Given the challenge of estimating landscape average rainfall from ground-based observations and space-based approaches using satellites, additional sources of rainfall data are greatly needed (McCabe *et al.* 2017). One recently proposed approach is the Soil Moisture 2 Rain (SM2RAIN) algorithm (http://hydrology.irpi.cnr.it/research/sm2rain/ and Brocca *et al.* 2014, Chiaravalloti *et al.* 2018). SM2RAIN assumes that the soil acts like a bucket and that measurements of SWC can be inverted to estimate rainfall from a ground-based approach (Brocca *et al.* 2014). Following the bucket analogy, the following equations can be used to describe the mass balance:

$$Z^* \frac{ds(t)}{dt} = p(t) - r(t) - e(t) - g(t) \tag{3.1}$$

where

Z^*	is the soil water capacity equal to soil depth times porosity
$s(t)$	is relative soil moisture (= SWC/porosity) as a function of time t
$p(t)$	is precipitation
$r(t)$	is surface runoff
$e(t)$	is evaporation
$g(t) = a \times s(t)^b$	is deep drainage and a and b are calibration coefficients.

During rainfall, surface runoff and evapotranspiration are assumed to be negligible at the daily timescale. This assumption is most appropriate on flat areas, or smooth slopes and land with rough surfaces where runoff does not occur during rainfall. Runoff is likely to occur for areas with: (a) steep slopes, (b) during high intensity rainfall, (c) during mild but long-lasting rainfall, and (d) after earlier rain periods when soil is already saturated. If this assumption is applied, precipitation can be estimated as:

$$p(t) = Z^* \frac{ds(t)}{dt} + a \times s(t)^b \tag{3.2}$$

thereby leaving three parameters to calibrate (Z^*, a, b) using of observations of SWC and rainfall.

Given the wide array of SWC products at different scales, the SM2RAIN algorithm has been applied and validated across time and space. By using the European Space Agency Climate Change Initiative (ESA CCI) soil moisture product, Ciabatta *et al.* (2018) developed a global scale SM2RAIN-CCI rainfall product that has been compared with 5 different global rainfall products showing good correlation at 1-degree spatial resolution and 5-day accumulated totals against gridded rain gauge-based rainfall observations (assumed to be the actual true rainfall). Spatial correlations range from 0.3 to 0.8 across a wide portion of the global land surface. At finer spatial (12.5 km) and temporal (1-day) resolutions, the SM2RAIN algorithm has been recently applied to the EUMETSAT Satellite Application Facility on Support to Operational Hydrology and Water Management (HSAF) soil moisture product (Brocca *et al.* 2019) showing better performance than a state-of-the-art satellite rainfall product (i.e. Global Precipitation Measurement, GPM) over Africa and South America. From a study in Italy, Chiaravalloti

Table 3.3. Summary of daily rainfall error analysis using different filtering techniques on moderated neutron counts and propagating calculated SWC data through SM2RAIN algorithm. MA stands for moving average and SG for Savitzky-Golay.

Neutron Filter Method	SM2Rain Estimated Rainfall (mm)	Rainfall difference, SM2RAIN-Observed rain (mm)	% Error	R Value	RMSE (mm/day)	Bias (mm/day)	KGE	Z*	a	b
1 h raw neutron counts	3104.7	876.7	39.4	0.598	4.20	0.79	0.481	20.00	3.81	49.92
MA 3 h	2225.2	-2.8	0.1	0.694	3.57	0.00	0.559	31.43	5.37	29.71
MA 6 h	2239.5	11.5	0.5	0.738	3.34	0.01	0.623	56.98	6.97	50.00
MA 8 h*	2144.2	-83.8	3.8	0.743	3.32	-0.08	0.615	69.65	3.32	46.85
MA 10 h	2090.0	-138.0	6.2	0.721	3.44	-0.12	0.609	81.58	0.00	50.00
MA 12 h	2051.8	-176.2	7.9	0.736	3.36	-0.16	0.629	91.43	0.00	50.00
MA 24 h	1919.5	-308.5	13.8	0.753	3.27	-0.28	0.641	139.02	0.00	50.00
SG 1st order, 3 h	2062.9	-165.2	7.4	0.686	3.62	-0.15	0.518	30.28	8.54	47.32
SG 2nd order, 3 h	3104.7	876.7	39.4	0.598	4.20	0.79	0.410	20.00	3.81	49.93
SG 1st order, 7 h	2140.4	-87.6	3.9	0.731	3.38	-0.08	0.601	63.28	7.94	49.97
SG 2nd order, 7 h	2162.8	-65.2	2.9	0.701	3.54	-0.06	0.555	32.35	4.97	49.70
SG 3rd order, 7 h	2162.8	-65.2	2.9	0.701	3.54	-0.06	0.555	32.35	4.97	49.70
SG 1st order, 9 h	2148.5	-79.5	3.6	0.728	3.40	-0.07	0.619	77.32	1.04	46.90
SG 2nd order, 9 h	2023.8	-204.2	9.2	0.713	3.49	-0.18	0.536	39.60	4.24	49.93
SG 3rd order, 9 h	2064.1	-163.9	7.4	0.711	3.50	-0.15	0.547	40.23	4.27	49.93
SG 1st order, 11 h	2094.8	-133.2	6.0	0.719	3.45	-0.12	0.606	86.95	2.85	49.96
SG 2nd order, 11 h	2116.2	-111.8	5.0	0.704	3.52	-0.10	0.577	46.68	3.40	10.36
SG 3rd order, 11 h	2116.2	-111.8	5.0	0.704	3.52	-0.10	0.577	46.68	3.40	10.36
SG 1st order, 13 h	2051.8	-176.2	7.9	0.710	3.50	-0.16	0.593	97.39	0.41	49.98
SG 2nd order, 13 h	2193.9	-34.1	1.5	0.733	3.37	-0.03	0.631	53.17	2.20	5.62
SG 3rd order, 13 h*	2193.7	-34.3	1.5	0.733	3.37	-0.03	0.631	53.17	2.20	5.62
SG 1st order, 25 h	1895.8	-332.3	14.9	0.693	3.60	-0.30	0.583	139.97	0.07	50.00
SG 2nd order, 25 h	1965.4	-262.6	11.8	0.702	3.54	-0.24	0.579	97.91	0.00	49.99
SG 3rd order, 25 h	1965.4	-262.6	11.8	0.702	3.54	-0.24	0.579	97.91	0.00	49.99

Record Period 12/13/2013 to 12/31/2016, 2228.0 mm of observed rainfall

*Denotes selected method for each filtering technique

Adapted from Franz, T., Wahbi, A., Zhang, J., Vreugdenhil, M., Heng, L., Dercon, G., Strauss, P., Brocca, L. & Wagner, W. 2020. Practical Data Products From Cosmic-Ray Neutron Sensing for Hydrological Applications Front. Water. 2. https://doi.org/10.3389/frwa.2020.00009

et al. (2018) compared in-situ rain gauges vs. satellite remote sensing products obtaining a correlation of around 0.7 for 24-hour periods. Brocca *et al.* (2015) applied the SM2RAIN algorithm to in situ soil moisture observations across Europe. The above algorithm has never been applied to or compared with CRNS. Therefore, the potential of the method to obtain landscape average rainfall estimates at field scale is tested here for the first time.

Using the CRNS and rainfall data from Petezenkirchen, the SM2RAIN algorithm was run for all 23 different time series filters investigated in section 3.2. Each time series used the observed rainfall data to calibrate the SM2RAIN algorithm. The three parameters Z^*, a, b were selected by using the KGE and root mean square error criterion. By looking at all 23 different filter options it was identified which filter is optimal for connecting the SWC time series with the best performing rainfall estimate with SM2RAIN (**Table 3.3**). Accurately connecting SWC and water fluxes (i.e. rainfall) is a challenging

Table 3.4. Summary of SM2RAIN algorithm statistical performance at Petzenkirchen for different integration periods

Neutron Filter Method	Integration Period	R	RMSE (mm/day)	KGE	SM2RAIN Estimated Rainfall (mm)	Rainfall Difference (SM2RAIN-Observed Rain) (mm)	%Error
1 h raw data	1 day	0.598	4.20	0.41	3104.74	876.74	39.4
MA8 h	1 day	0.743	3.32	0.62	2144.23	-83.77	3.8
SG 3rd order, 13 h	1 day	0.733	3.37	0.63	2193.72	-34.28	1.5
1 h raw data	3 days	0.635	2.72	0.45	3085.45	857.44	38.5
MA 8 h	3 days	0.788	2.00	0.68	2299.48	71.48	3.2
SG 3rd order, 13 h	3 days	0.788	1.99	0.68	2238.16	10.15	0.5
1 h raw data	5 days	0.652	2.15	0.48	3062.31	834.31	37.4
MA 8 h	5 days	0.791	1.55	0.69	2274.14	46.14	2.1
SG 3rd order, 13 h	5 days	0.753	1.67	0.65	2158.14	-69.86	3.1

Note: MA – moving average, SG - Savitzky-Golay filter, RMSE – root mean square error, KGE - Kling-Gupta-Efficiency
Adapted from F**ranz**, T., Wahbi, A., Zhang, J., Vreugdenhil, M., Heng, L., Dercon, G., Strauss, P., Brocca, L. & Wagner, W. 2020. Practical Data Products From Cosmic-Ray Neutron Sensing for Hydrological Applications Front. Water. 2. https://doi.org/10.3389/frwa.2020.00009

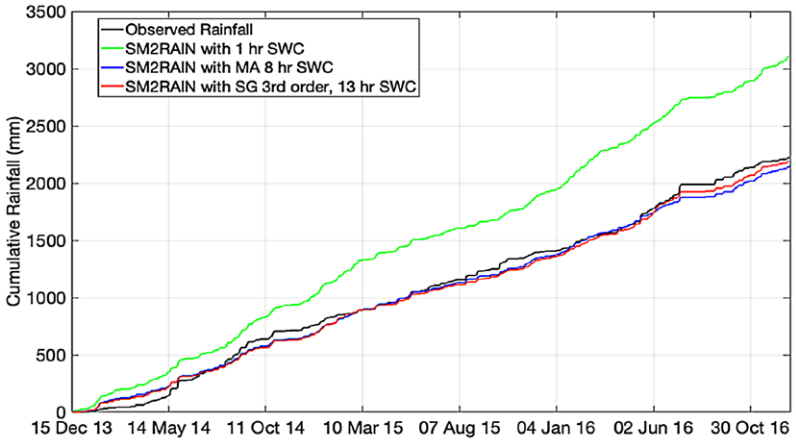

Figure 3.7. Cumulative sums of observed rainfall and SM2RAIN estimates using three neutron filters (1 hour neutron data, MA and SG filters). The neutrons were then used to estimate SWC and then used in the SM2RAIN algorithm. See **Table 3.4** for full summary. Adapted from F**ranz, T., Wahbi, A., Zhang, J., Vreugdenhil, M., Heng, L., Dercon, G., Strauss, P., Brocca, L. & Wagner, W.** 2020. Practical Data Products From Cosmic-Ray Neutron Sensing for Hydrological Applications Front. Water. 2. https://doi.org/10.3389/frwa.2020.00009

problem in hydrology particularly when the observations occur at different spatial resolutions (Peters-Lidard *et al.* 2017). From the results in **Table 3.3**, the 1 h data results in a poor comparison with the observed data as the cumulative sum is 39.4 percent larger than the observations (3105 vs 2228 mm over the 3-year period from 2013 to 2016). The MA filter with a temporal window of 3-12 hours resulted in small cumulative error (< 8 percent). The SG filter with 1st to 3rd order polynomials and temporal windows of 7 to 13 hours also had small cumulative error (< 9 percent). The other statistical metrics (Pearson correlation (R), KGE, Bias) were also comparable for these neutron filters.

Comparing the three parameters with Brocca *et al.* (2015), different values were found. This is expected as the CRNS depth and remote sensing depths are different (~20 cm vs 3 cm). At the daily level, an R-value of 0.74 and 0.73 is found for the study site for the optimal MA and SG filters, which is comparable with the results obtained with satellite soil moisture products (e.g., Chiaravalloti *et al.* (2018); Brocca *et al.* (2019)). **Figure 3.7** illustrates the daily cumulative sum of the three selected filters vs. the observed rainfall, again showing excellent agreement for the SG and MA filters. The green line is the 1-hour data and leads to large cumulative errors due to the hourly neutron fluctuations inherent in the CRNS. There are a few periods early in the record that showed small deviations. If compared with the results obtained with classical in situ measurements shown in Brocca *et al.* (2015), in which the range of R-values is between 0.75 and 0.95, the performance with CRNS SWC is in the lower range but with the significant added value to provide landscape average rainfall estimates. Table 3.4 includes summary statistics for rainfall accumulations of 1, 3, and 5 days. For increasing integration time, the statistical metrics improve to the levels reported by Brocca *et al.* (2015) and Chiaravalloti *et al.* (2018). With respect to error, the World Meteorological Organization (Di Valle *et al.* 2007 and_https://www.wmo-sat.info/oscar/variables/view/1) reports rain gage error around 1 mm/day and 2–4 mm/day for satellite estimates, however each method has different spatial resolution and coverage. The CRNS derived rainfall provides a missing and critical gap at the ca 10 ha resolution.

3.5 Estimation of root zone soil water content using an exponential filter

A major problem with remotely sensed SWC data is that only the near surface (~0–3 cm) is directly observed using microwave wavelengths (Jackson *et al.* 1997). For these satellite products to be useful, SWC storage should be extrapolated across a plant root zone. This extrapolation can be accomplished in a number of ways using simple linear interpolation to a full data assimilation approach using a physically based water and energy balance model. However, given the computational demands, lack of boundary and initial conditions, and model parameters this approach can be challenging. A fairly simple method to do root zone SWC extrapolation uses the idea of an exponential filter to solve the time delay between surface soil response and deeper soils (Wagner *et al.* 1999). The exponential filter has been used with great success for remote sensing products, in-situ point scale networks (Paulik *et al.* 2014, Wang *et al.* 2017), and recently CRNS (Peterson *et al.* 2016).

In this chapter, the continuous CRNS SWC data was utilized, and assumed a CRNS depth penetration of ~0–20 cm based on expected effective depth at the site (see Franz *et al.* 2012 and Kohli *et al.* 2015 for details on effective depth calculation). In addition, by using the seasonal TDT data from 2014 at Petzenkirchen, the exponential filter approach was parametrised, thus being able to produce an operational root zone storage product from the CRNS data henceforth. The exponential filter model considers the water balance model of a two-layer soil profile. Layer one has traditionally been set to the depth of the remote sensing product (0–3 cm), but 0–20 cm (CRNS penetration depth) will be used here for CRNS applications. Layer two has been set to a root zone depth around ~1 m depending on vegetation type and local soil depths. The exponential filter approach is flexible enough to allow user to specify a desired depth, given the stated assumptions about the method. Here, it should be assumed that layer one is the surface layer (provided by the continuous CRNS SWC data ~0–20 cm, denoted by SWC_1), and layer two is the lower soil layer of interest (here an integrated root zone storage estimate constrained by the depth of the TDT sensors to calibrate the exponential filter approach). For demonstration purposes, the calculations for layer two were done for a shallow root zone (0–30 cm) and a deeper root zone (0–60). Having two different root zone depths may be important to relate

the available SWC with different growth stages of crop over the growing season. SWC of layer two (denoted by SWC_2) is described as:

$$L\frac{dSWC_2}{dt} = C(SWC_1 - SWC_2) \quad (3.3)$$

where

t	is time,
L	is the depth of layer two
C	is an area-representative pseudo-diffusivity constant.

This approach assumes that plant transpiration and drainage losses from the lower layer are negligible, and that hydraulic diffusivity between the soil layers is constant (Wagner *et al.* 1999). This assumption is more applicable for arid environments. **Equation 3.3** can be solved using a recursive formulation following (Albergel *et al.* 2008):

$$SWI_{2(t)} = SWI_{2(t-1)} \times (1 - K_t) + SWI_{1(t)} \times K_t \quad (3.4)$$

where

$SWI_{2(t)}$ and $SWI_{1(t)}$	are the Soil Water Index (SWI) of layer 2 and layer 1, respectively
t	is a time index, and
K_t	is the gain.

Soil water index is the *SWC* scaled between 0 and 1 using assumed minimum and maximum values, $\mathrm{SWI}=\left(\frac{SWC-SWC_{min}}{SWC_{max}-SWC_{min}}\right)$.

For layer one, the *SWC* is bounded by the minimum and maximum of the hourly CRNS observations. The lower bound is dependent on the length of CRNS record and drier periods may be experienced in future drought periods. For layer two, previous work has bounded SWC by the wilting point as the minimum value, and the mid-point between field capacity and porosity as the maximum value. Soil data or calibration of the model is thus required. The gain K_t ranges from 0 to 1 and is calculated as:

$$K_t = \frac{K_{t-1}}{K_{t-1}+exp(-\Delta t/T)} \quad (3.5)$$

where

K_{t-1} is the gain of the previous time step,
Δt is the time step (here one day)
T is a characteristic time period (equal to L/C from **Equation 3.3**).

The filter is initialized by setting $K_t = 1$ and $SWI_{2(1)} = SWI_{1(1)}$. The characteristic time length (T) is dependent on a variety of factors, including thickness of layer two, topographic complexity (Paulik *et al.* 2014), and soil properties that may influence water movement (flux) rates (Albergel *et al.* 2008) thus requiring local calibration. Here the same methodology was used as in Peterson *et al.* (2016), which calibrated three parameters: T and the layer two minimum and maximum *SWC* (T, SWA_{2min}, SWC_{2max}). In order to perform the calibration, the in-situ TDT data and a Monte Carlo approach were used. The three parameters varied over their expected range (from 0.01 to 0.25 every 0.005 cm^3/cm^3, SWC_{2max} from 0.36 to 0.75 every 0.005 cm^3/cm^3, and T from 10 to 70 every two days). The three optimal model parameters were selected based on the objective function of maximizing the Kling-Gupta-Efficiency (KGE) criteria (Gupta *et al.* 2009), where a perfect fit would be KGE equal to 1. KGE has been shown to be a superior metric in hydrologic model calibration (Gupta *et al.* 2009) as it is based on weighting the correlation, the mean, and standard deviation between the observed and predicted time series.

Figure 3.4e illustrates the time series of landscape average TDT sensors by depth that were available at the HOAL from 2013 to 2014. Due to various land management operations the sensors were removed from different land uses at different times. To calibrate the exponential filter model to a root zone product a profile SWC was estimated from a weighted average of TDT sensors within those 0–30 cm and 0–60 cm profiles. Using the CRNS SWC data as layer one and the SWC profile 0–30 cm and 0–60 cm data as

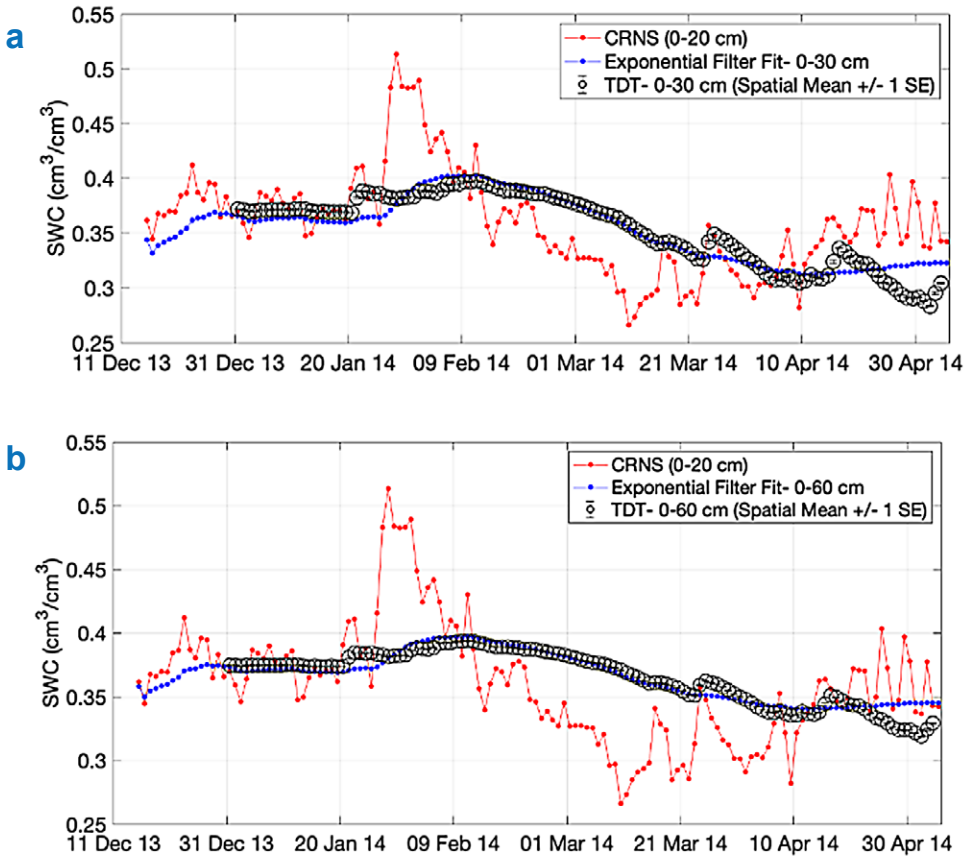

Figure 3.8. Comparison of SWC for the CRNS (neutron filter SG 3rd order, 13 h), fitted exponential model, and observed landscape average TDT data for the (a) 0–30 cm and (b) 0–60 cm products. Adapted from Franz, T., Wahbi, A., Zhang, J., Vreugdenhil, M., Heng, L., Dercon, G., Strauss, P., Brocca, L. & Wagner, W. 2020. Practical Data Products From Cosmic-Ray Neutron Sensing for Hydrological Applications Front. Water. 2. https://doi.org/10.3389/frwa.2020.00009

Table 3.5. Summary of calibration fit, and three parameter estimates for the 0–30 cm and 0–60 cm exponential filter models for different neutron filters. MA stands for moving average and SG for Savitzky-Golay.

Calibration of CRNS vs. TDT					
Neutron Filter Method	Depth (cm)	KGE	SWC_{2min} (cm^3/cm^3)	SWC_{2max} (cm^3/cm^3)	T (Days)
Daily SWC, 1 h data	30	0.911	0.01	0.675	50
Daily SWC, MA 8 h	30	0.909	0.045	0.68	48
Daily SWC, SG 3rd order, 13 h	30	0.908	0.035	0.68	50
Daily SWC, 1 h data	60	0.914	0.125	0.585	64
Daily SWC, MA 8 h	60	0.913	0.15	0.59	62
Daily SWC, SG 3rd order, 13 h	60	0.912	0.145	0.59	64

Adapted from F**ranz, T., Wahbi, A., Zhang, J., Vreugdenhil, M., Heng, L., Dercon, G., Strauss, P., Brocca, L. & Wagner, W.** 2020. Practical Data Products From Cosmic-Ray Neutron Sensing for Hydrological Applications Front. Water. 2. https://doi.org/10.3389/frwa.2020.00009

layer two, the three free parameters (T, SWA_{2min}, SWC_{2max}) for the exponential filter model (**Equations 3.3 and 3.4**) were estimated using a Monte Carlo approach. The objective function was maximizing KGE between the observed and modelled SWC time series. **Table 3.5** provides the summary results illustrating that all three methods (1hr SWC, 8hr MA SWC and 13hr SG 3rd order SWC) had large

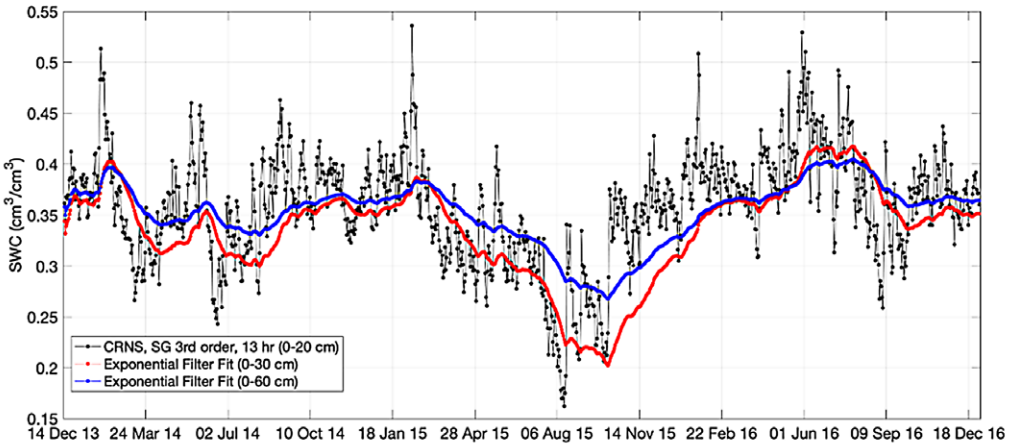

Figure 3.9. Time series of SWC for CRNS, 0–30 cm exponential filter product, and 0-60 cm exponential filter product for the 3-year period. Adapted from Franz, T., Wahbi, A., Zhang, J., Vreugdenhil, M., Heng, L., Dercon, G., Strauss, P., Brocca, L. & Wagner, W. 2020. Practical Data Products From Cosmic-Ray Neutron Sensing for Hydrological Applications Front. Water. 2. https://doi.org/10.3389/frwa.2020.00009

KGE values of greater than 0.9. Estimates of SWC_{2max} and T were very similar for all methods. SWC_{1min} was lower for the 1 h neutron data due to the higher random fluctuations. As expected, T was larger for the 0–60 cm layer. Following calibration **Figure 3.8a and b** illustrate the comparison of SWC between the exponential filter fit and the TDT landscape averages for both depths. With respect to estimating the critical parameter T, Paulik *et al.* (2014) used the International Soil Moisture Network (Dorigo *et al.* 2013) data to compare T vs. different environmental covariates. Paulik *et al.* (2014) found depth and topographic complexity to be most correlated to T. In contrast, Wang *et al.* (2017) used the Nebraska Mesonet sites (same sensor type) and found that T was strongly correlated to depth and soil texture (percent sand and clay). A relatively new commercial product exists that uses the exponential filter in a combination with passive microwave sensors to produce an operational daily 100 m resolution SWC product at 10, 20 and 40 cm (/www.vandersat.com/soil-moisture-monitoring).

Using the CNRS SWC data and the exponential model (**Table 3.3**), an operational daily SWC products for 0–30 cm and 0-60 cm were produced. **Figure 3.9** illustrates the CRNS SWC, 0–30 cm SWC, and 0–60 cm SWC products. By tracking changes in SWC over these depths in real-time, users will be able to make more informed decisions about irrigation, fertilization rates, and other management operations.

3.6 Conclusion

This chapter provides the background, equations, and example calculations from the Petzenkirchen CRNS study site using three well established algorithms summarized in the framework in **Figure 3.1** and is available for general use. **Figure 3.1** and the Appendices 1,2 and 3 provide a step-by-step process. The algorithms make the essential step of enhancing the CRNS SWC data for providing users with the value-added products of a smoothed SWC time series, root zone SWC data, and landscape average rainfall in order to make decisions. While the provided examples are written in the computer program MATLAB R2020a mostly used by engineers and academics, next steps require the data and value-added products and code be made available on web-based data portals, code sharing environments and smartphone applications for users. Future work with CRNS and available in situ SWC data should further validate these approaches and their use in complex environments.

References

Andreasen, M., Jensen, K.H., Desilets, D., Franz, T.E., Zreda, M., Bogena, H.R. & Looms, M.C. 2017). Status and Perspectives on the Cosmic-Ray Neutron Method for Soil Moisture Estimation and Other Environmental Science Applications. *Vadose Zone J. 16*(8):11. https://doi.org/10.2136/vzj2017.04.0086

Albergel, C., Rudiger, C., Pellarin, T., Calvet, J.C., Fritz, N., Froissard, F., Suquia, D., Petitpa, A., Piguet, B., & Martin, E. 2008). From near-surface to root-zone soil moisture using an exponential filter: an assessment of the method based on in-situ observations and model simulations. *Hydrol. Earth Sys. Sci*. 12(6): 1323–1337. https://doi.org/10.5194/hess-12-1323-2008

Avery, W., Finkenbiner, C., Franz, T.E., Wang, T., Nguy-Roberston, A.L., Suyker, A., Arkebauer, T. & Munoz-Arriola, F. (2016. Incorporation of globally available datasets into the roving cosmic-ray neutron probe method for estimating field-scale soil water content. *HESS* 20: 3859–3872. https://doi.org/10.5194/hess-20-3859-2016

Baatz, R., Franssen, H.J.H., Han, X.J., Hoar, T., Bogena, H.R. & Vereecken, H. 2017. Evaluation of a cosmic-ray neutron sensor network for improved land surface model prediction, *Hydrol. Earth Sys. Sci. 21*(5): 2509–2530. https://doi.org/10.5194/hess-21-2509-2017

Bauer-Marschallingere, B., Freeman, V., Cao, S., Paulik, C., Schaufler, S., Stachl, T., Modanesi, S., Massario, C., Ciabatta, L., Brocca, L. & Wagner, W. 2019. Toward Global Soil Moisture Monitoring with Sentinel-1: Harnessing Assets and Overcoming Obstacles. IEEE Trans. Geosci. Remote Sens. 57(1): 520–539. https://doi.org/10.1109/tgrs.2018.2858004

Blöschl, G., Blaschke, A.P., Broer, M., Bucher, C., Carr, G., Chen, X., Eder, A., Exner-Kittridge, M., Farnleitner, A., Flores-Orozco, A., Haas, P., Hogan, P., A. Kazemi Amiri, Oismuller, M., Parajka, J., Silasari, R., Stadler, P., Strauss, P., Vreugdenhil, M., Wagner, W. & Zessner, M. 2016). The Hydrological Open-Air Laboratory (HOAL) in Petzenkirchen: a hypotheses-driven observatory. *HESS* 20: 227–255.

Bogena, H.R., Huisman, J.A., Baatz, R., Franssen, H.J.H. & Vereecken, H. 2013. Accuracy of the cosmic-ray soil water content probe in humid forest ecosystems: The worst-case scenario. *Water Resour. Res. 49*(9): 5778–5791. https://doi.org/10.1002/wrcr.20463

Brocca, L., Ciabatta, L., Massari, C., Moramarco, T., Hahn, S., Hasenauer, S., Kidd, R., Dorigo, W., Wagner, W. & Levizzani, V. 2014. Soil as a natural rain gauge: Estimating global rainfall from satellite soil moisture data, *J. Geophys. Res.-Atmos.* 119(9): 5128–5141. https://doi.org/10.1002/2014jd021489

Brocca, L., Massari, C., Ciabatta, L., Moramarco, T., Penna, D., Zuecco, G., Pianezzola, L., Borga, M., Matgen, P. & Martínez-Fernández, J. 2015. Rainfall estimation from in situ soil moisture observations at several sites in Europe: an evaluation of SM2RAIN algorithm. J. Hydrol. Hydromech. 63(3): 201–209, https://doi.org/10.1515/johh-2015-0016

Brocca, L., Filippucci, P., Hahn, S., Ciabatta, L., Massari, C., Camici, S., Schüller, L., Bojkov, B. & Wagner, W. 2019). SM2RAIN-ASCAT (2007–2018): global daily satellite rainfall from ASCAT soil moisture. *Earth Sys. Sci. Data* (in press).

Chiaravalloti, F., Brocca, L., Procopio, A., Massari, C. & Gabriele, S. 2018. Assessment of GPM and SM2RAIN-ASCAT rainfall products over complex terrain in southern Italy. *Atmos. Res.* 206: 64–74. https://doi.org/ 10.1016/j.atmosres.2018.02.019

Ciabatta, L., Massari, C., Brocca, L., Gruber, A., Reimer, C., Hahn, S., Paulik, C., Dorigo, W., Kidd, R. & Wagner, W. 2018. SM2RAIN-CCI: a new global long-term rainfall data set derived from ESA CCI soil moistur. *Earth Sys. Sci. Data* 10(1): 267–280. https://doi.org/10.5194/essd-10-267-2018

Desilets, D., Zreda, M. & Ferre, T.P.A. 2010. Nature's neutron probe: Land surface hydrology at an elusive scale with cosmic rays. *Water Resour. Res.* 46. https://doi.org/10.1029/2009wr008726

Di Valle, V., Vuerich, E., Monesi, C., Lanza, L.G., Stagi, L. & Lanzinger, E. 2008. Instruments and Observing Methods (IOM) Report No. 99. WMO Field Intercomparison of Rainfall Intensity Gauges. WMO, Geneva.

Dimitrova-Petrova, K., Geris, J., Wilkinson, M.E., Rosolem, R., Verrot, L., Lilly, A. & Soulsby, C. 2020). Opportunities and challenges in using catchment-scale storage estimates from cosmic ray neutron sensors for rainfall-runoff modelling. *J. Hydrol. 586*. https://doi.org/ 10.1016/j.jhydrol.2020.124878

Dingman, L.S. 2002. *Physical Hydrology: Second Edition*, 646 pp. Prentice-Hall Inc., Upper Saddle River.

Dorigo, W.A., Xaver, A., Vreugdenhil, M., Gruber, A., Hegyiova, A., Sanchis-Dufau, A.D., Zamojski, D., Cordes, C., Wagner, W. & Drusch, M. 2013. Global Automated Quality Control of In Situ Soil Moisture Data from the International Soil Moisture Network. *Vadose Zone J. 12*(3): 21. https://doi.org/10.2136/vzj2012.0097

Fersch, B., Jagdhuber, T., Schron, M., Volksch, I. & Jage, M. 2018. Synergies for Soil Moisture Retrieval Across Scales from Airborne Polarimetric SAR, Cosmic Ray Neutron Roving, and an In Situ Sensor Network. *Water Resour. Res. 54*(11): 9364–9383. https://doi.org/10.1029/2018wr023337

Finkenbiner, C.E., Franz, T.E., Gibson, J., Heeren, D.M. & Luck, J. 2019. Integration of hydrogeophysical datasets and empirical orthogonal functions for improved irrigation water management, *Precis. Agric.* 20(1): 78–100. https://doi.org/10.1007/s11119-018-9582-5

Franz, T.E., Zreda, M., Ferre, P.A., Rosolem, R., Zweck, C., Stillman, S., Zeng, X. & Shuttleworth, W.J. 2012a. Measurement depth of the cosmic-ray soil moisture probe affected by hydrogen from various sources. *Water Resour. Res. 48*. https://doi.org/10.1029/2012WR011871

Franz, T.E., Zreda, M., Rosolem, R. & Ferre, P.A. 2012b. Field validation of cosmic-ray soil moisture sensor using a distributed sensor network. *Vadose Zone J.* 11(4). https://doi.org/10.2136/vzj2012.0046

Franz, T.E., Zreda, M., Rosolem, R., Hornbuckle, B., Irvin, S., Adams, H., Kolb, T., Zweck, C. & Shuttleworth, W.J. 2013. Ecosystem scale measurements of biomass water using cosmic-ray neutrons. *Geophys.Res. Lett.* 40: 3929–3933. https://doi.org/10.1002/grl.50791

Franz, T.E., Wang, T., Avery, W., Finkenbiner, C. & Brocca, L. 2015. Combined analysis of soil moisture measurements from roving and fixed cosmic ray neutron probes for multiscale real-time monitoring. *Geophys. Res. Lett.* 42: 3389–3396. https://doi.org/10.1002/2015GL063963

Franz, T.E., Wahbi, A., Vreugdenhil, M., Weltin, G., Heng, L., Oismueller, M., Strauss, P., Dercon, G. & Desilets, D. 2016. Using Cosmic-ray Neutron Probes to Monitor Landscape Scale Soil Water Content in Mixed Land Use Agricultural Systems. *Appl. Environ. Soil Sci*. 2016. https://doi.org/10.1155/2016/4323742

Franz, T., Wahbi, A., Zhang, J., Vreugdenhil, M., Heng, L., Dercon, G., Strauss, P., Brocca, L. & Wagner, W. 2020. Practical Data Products From Cosmic-Ray Neutron Sensing for Hydrological Applications *Front. Water.* 2. https://doi.org/10.3389/frwa.2020.00009

Jackson, T.J., Oneill, P.E. & Swift, C.T. 1997. Passive microwave observation of diurnal surface soil moisture. *IEEE Trans. Geosci. Remote Sens.* 35(5): 1210–1222. https://doi.org/10.1109/36.628788

Gupta, H.V., Kling, H., Yilmaz, K.K. & Martinez, G.F. 2009. Decomposition of the mean squared error and NSE performance criteria: Implications for improving hydrological modelling. *J. Hydrol.* 377(1–2): 80–91. https://doi.org/10.1016/j.jhydrol.2009.08.003

Knoll, G.F. 2000. *Radiation Detection and Measurement*, John Wiley & Sons, Inc., Hoboken, NJ.

Kohli, M., Schron, M., Zreda, M., Schmidt, U., Dietrich, P. & Zacharias, S. 2015. Footprint characteristics revised for field-scale soil moisture monitoring with cosmic-ray neutrons. W*ater Resour. Res.* 51(7): 5772–5790. https://doi.org/10.1002/2015wr017169

Lawston, P.M., Santanello, J.A., Franz, T.E. & Rodell, M. 2017. Assessment of irrigation physics in a land surface modeling framework using non-traditional and human-practice datasets. *Hydrol. Earth Sys. Sci.* 21(6), 2953–2966. https://doi.org/10.5194/hess-21-2953-2017

Lv, L., Franz, T.E., Robinson, D.A. & Jones, S.B. 2014. Measured and Modeled Soil Moisture Compared with Cosmic-Ray Neutron Probe Estimates in a Mixed Forest. *Vadose Zone J.* 13(12): 13. https://doi.org/10.2136/vzj2014.06.007.

McCabe, M.F., Rodell, M., Alsdorf, D.E., Miralles, D.G., Uijlenhoet, R., Wagner, W., Lucieer, A., Houborg, R., Verhoest, N.E.C., Franz, T.E., Shi, J.C., Gao, H.L. & Wood, E.F. 2017. The future of Earth observation in hydrology. *Hydrol. Earth Sys. Sci*. 21(7): 3879–3914. https://doi.org/10.5194/hess-21-3879-2017

Montzka, C., Bogena, H.R., Zreda, M., Monerris, A., Morrison, R., Muddu, S. & Vereecken, H. 2017. Validation of Spaceborne and Modelled Surface Soil Moisture Products with Cosmic-Ray Neutron Probes, *Remote Sens.* 9(2). https://doi.org/10.3390/rs902010.

Orfanidis, S.J. 1996. *Introduction to Signal Processing*. Englewood Cliffs, NJ. Prentice-Hall.

Paulik, C.; Melzer, T., Hahn, S., Bartsch, A., Heim, B., Elger, K., Wagner, W. 2014. *Circumpolar surface soil moisture and freeze/thaw surface status remote sensing products (version 4) with links to geotiff images and NetCDF files (2007–01 to 2013–12).* Department of Geodesy and Geoinformatics, TU Vienna, PANGAEA. https://doi.org/10.1594/PANGAEA.832153

Peterson, A.M., Helgason, W.D. & Ireson, A.M. 2016. Estimating field-scale root zone soil moisture using the cosmic-ray neutron probe. *Hydrol. Earth Sys. Sci*. 20(4): 1373–1385. https://doi.org/10.5194/hess-20-1373-2016

Peters-Lidard, C.D., Clark, M., Samaniego, L., Verhoest, N.E.C., van Emmerik, T., Uijlenhoet, R., Achieng, K., Franz, T.E. & Woods, R. 2017. Scaling, similarity, and the fourth paradigm for hydrology. *Hydrol. Earth Sys. Sci.* 21(7): 3701–3713. https://doi.org/10.5194/hess-21-3701-2017

Rosolem, R., Shuttleworth, W.J., Zreda, M., Franz, T.E., Zeng, X. & Kurc, S.A. 2013. The Effect of Atmospheric Water Vapor on the Cosmic-ray Soil Moisture Signal, *J. Hydrometeorol.* https://doi.org/10.1175/JHM-D-12-0120.1.

Rosolem, R., Hoar, T., Arellano, A., Anderson, J.L., Shuttleworth, W.J., Zeng, X. & Franz, T.E. 2014. Translating aboveground cosmic-ray neutron intensity to high-frequency soil moisture profiles at sub-kilometer scale. *Hydrol. Earth Sys. Sci.* 18(11): 4363–4379. https://doi.org/10.5194/hess-18-4363-2014

Savitzky, A. & Golay, M.J.E. 1964. Smoothing and differentiation of data by simplified least squares procedures. *Anal. Chem.* 36(8): 1627-1639. https://doi.org/10.1021/ac60214a047

Schattan, P., Baroni, G., Oswald, S.E., Schober, J., Fey, C., Kormann, C., Huttenlau, M. & Achleitner, S. 2017. Continuous monitoring of snowpack dynamics in alpine terrain by aboveground neutron sensing. *Water Resour. Res.* 53(5): 3615–3634. https://doi.org/10.1002/2016wr020234

FAO. 2007. *World Reference Base for Soil Resources 2006*. First update 2007, IUSS Working Group WRB. World Soil Resources Reports No. 103. FAO, Rome. www.fao.org/fileadmin/templates/nr/images/resources/pdf_documents/wrb2007_red.pdf

Vereecken, H., Huisman, J.A., Bogena, H., Vanderborght, J., Vrugt, J.A. & Hopmans, J.W. 2008. On the value of soil moisture measurements in vadose zone hydrology: A review. *Water Resour. Res.* 44. https://doi.org/ W00d0610.1029/2008wr006829

Wagner, W., Lemoine, G. & Rott, H. 1999. A method for estimating soil moisture from ERS scatterometer and soil data. *Remote Sens. Environ.* 70(2): 191–207. https://doi.org/10.1016/s0034-4257(99)00036-x

Wang, T. J., Franz, T.E., You, J.S., Shulski, M.D. & Ray, C. 2017. Evaluating controls of soil properties and climatic conditions on the use of an exponential filter for converting near surface to root zone soil moisture contents. *J. Hydrol.* 548: 683–696. https://doi.org/ 10.1016/j.jhydrol.2017.03.055

Zreda, M., Desilets, D., Ferre, T.P.A. & Scott, R.L. 2008. Measuring soil moisture content non-invasively at intermediate spatial scale using cosmic-ray neutrons. *Geophys. Res. Lett.* 35(21). https://doi.org/ L21402 10.1029/2008gl035655

Zreda, M., Shuttleworth, W.J., Xeng, X., Zweck, C., Desilets, D., Franz, T.E. & Rosolem, R. 2012. COSMOS: The COsmic-ray Soil Moisture Observing System, *Hydrol. Earth Sys. Sci.* 16: 4079–4099. https://doi.org/10.5194/hess-16-1-2012

4. High-resolution soil moisture retrieval using C-band radar Sentinel-1 and Cosmic Ray Neutron Sensor data

Modou Mbaye & Hami Said

4.1 Introduction

Soil moisture retrieval at a global or regional scale can only be achieved by employing satellite remote sensing. However, the limiting factor is the calibration and validation of remote sensing soil moisture products. The CRNS technique has great potential to be used for calibration and validation of remote sensing soil moisture products. The large CRNS soil moisture footprint makes it more suitable for remote sensing soil moisture product validation (Montzka *et al.* 2017) than point sensor data (such as electromagnetic sensors, gravimetric method, etc.). Improved confidence in remote sensing soil moisture will significantly increase its applicability for assessment and monitoring for regional, national, and global applications.

While remote sensing has made significant progress in recent years (**Figure 4.1** and McCabe *et al.* 2017), significant observational gaps in space and time still exist (**Table 4.1**). Of particular note for this work, estimates of daily rainfall and root zone soil moisture at the critical field scale (~1 to 10 ha) remain elusive and impractical with current and planned satellite missions. With the limitation of satellites to directly estimate root zone water storage, indirect methods using a combination of satellites, ground sensors, and models are needed for the practical use of their data products.

There are still considerable limitations in high-resolution soil moisture retrieval. For example, the latest NASA mission called Soil Moisture Active Passive (SMAP, launched in 2015) collects surface soil moisture (0–5 cm) ever 2–3 days at a spatial resolution of 36 km. Unfortunately, this scale is insufficient for many practical agricultural applications. More recently, active microwave remote sensing, Synthetic Aperture Radar (SAR) imaging has emerged as an effective tool to estimate surface soil moisture because of its sensitivity toward the dielectric and geometric properties of the target (Behari, 2005). The Sentinel-1 C-band SAR satellite shows great potential for high spatial resolution soil monitoring. For example, Bhogapurapu *et al.* (2022) proposed an extended change detection methodology for soil moisture retrieval of croplands using the Dual-pol SAR vegetation Index with the RMSE values for estimated volumetric soil moisture within the range of 0.048 to 0.055 m^3/m^3. Chung *et al.* (2022) used an artificial neural network (ANN) over 40 × 50 km^2 and with Sentinel-1A/B SAR images to estimate soil water content (SWC) with an RMSE of 0.045 m^3/m^3. Ma *et al.* (2020) presented an algorithm that retrieves soil moisture, surface roughness, and vegetation water content simultaneously using high-resolution Sentinel-1 SAR and Sentinel-2 multispectral images together. The proposed single-channel dual-polarisation VV algorithm approach can provide reasonable soil moisture retrievals, with RMSE ranging from 0.039 to 0.078 m^3/m^3.

Sentinel-1 C-band SAR satellite imagery can be the basis for producing global soil moisture maps. However, these maps can be only used once they are calibrated and validated. Such calibration can be done through traditional but time-consuming point soil sampling. CRNS technology provides an opportunity for more rapid calibration at the landscape scale level over various land uses.

The primary objective of this study is to present a method for estimating soil moisture on a large scale by combining satellite and field data obtained by CRNS. The second objective is to show the potential of using satellite data for a holistic analysis of agricultural systems by integrating into a platform, agricultural and climatic data (rainfall, evapotranspiration, crop calendar) with soil moisture. The

Figure 4.1. Diagram of various satellite, airborne, and ground-based observations for collecting data on hydrological cycle. Source:McCabe, M.F., Rodell, M., Alsdorf, D.E., Miralles, D.G., Uijlenhoet, R., Wagner, W., Lucieer, A., Houborg, R., Verhoest, N.E.C., Franz, T.E., Shi, J.C., Gao, H.L. & Wood, E.F. 2017. The future of Earth observation in hydrology. *Hydrol. Earth Sys. Sci.* 21(7): 3879–3914. https://doi.org/10.5194/hess-21-3879-2017

platform is fully automated and data is available at various scales in a quasi-real-time web-application. Such an approach is possible with cloud computing technology and satellite data processing services at a global scale, such as Google Earth Engine, Amazon Web Service (AWS), Sentinel Hub etc.

This chapter describes the pipeline for retrieving soil moisture from C-band Sentinel-1 SAR data and calibration of the conversion model with CRNS. This method is based on the modified version of the change detection-based approaches to soil moisture estimation techniques using SAR (Bauer-Marschallinger *et al.* 2019, 2021; Hornacek *et al.* 2012). The procedure provided below should serve as a roadmap for scientists, technicians, agronomists, and students from the Members States on estimating soil moisture based on Synthetic Aperture Radar Sentinel-1 C band data. It is divided into three parts. In the first part, a brief description of the different satellite remote sensing data used for this study will be presented. The second part will describe the methodology to retrieve soil moisture from C-band Sentinel-1 data through an image processing technique using Google Earth Engine (GEE) and the construction of a calibrated model between the radar dual-polarisation backscatter signal (VV) and soil water content measured with CRNS. In this step, the free open-source programming language R will be used. Finally, the conclusion and application perspectives will be discussed. The instructions

Table 4.1. Summary of key hydrologic variables available from global remote sensing platforms, dedicated missions/instruments, spatial resolution, temporal resolution, year of satellite launch, and dedicated instrument

Hydrological variable	Missions/instrurrents	Standard spatial resolution (km)	Standard temporal resolution (days)	Launch year	Dedicated measurement
Rainfall	GPM	5	0.125	2014	Y
Snowfall	GPM	5	0.125	2014	N
Evaporation	Terra/MODIS	0.5	1	1999	N
	Aqua/MODIS			2002	
	Suomi/VIIRS			2013	
	Landsat 8			2013	
	Landsat 9			2023	
Runoff	SWOT	0.1	11	2021	Y
Snow cover	Terro/MODIS Aqua/MODIS Suomi/VIIRS	0.5	1	1999 2002 2013	Y
Snow density,depth, or waterequivalent	GCOM-W/AMSR2	30	1	2012	N
Surface soil moisture	SMOS	36	3	2009	Y
	SMAP(radiometer)	36	3	2015	Y
	ASCAT	25	1	2006	N
	GCOM-W/AMSR2	50	1	2012	N
	Sentinel-1A Sentinel-1B	0.1–0.005	12	2014 2016	N N
Deep soil moisture	Biomass	0.2	18 days/yr	2021	N
Surface waterelevation	Jason-3	10	10	2016	N
	SARAL	10	35	2013	N
	SWOT	0.1	11	2021	Y
	ICESat-2	1.5	90	2018	N
Depth togroundwater	–	–	–	–	–
Total groundwater storage	–	–	–	–	–
Terrestrial water storage change	GRACE GRACE-FO	220 180	30 30	2002 2017	Y Y
Water consumption	–	–	–	–	–
Waterquality	–	–	–	–	–
Vegetation/land cover/ irrigatedarea	Terro/MODIS Aqua/MODIS Suomi/VIIRS	0.5	1	1999 2002 2013	y
	Landsat 8 Landsat 9	0.03	16	2013 2023	y
	Sentinel-2A	0.02	10	2015	Y
	Sentinel-2B	0.02	10	2017	Y
	Sentinel-3A	0.3	2	2016	Y
	Proba-V	0.35	2	2013	Y
Vegetation stress	ISS/ECOSTRESS	0.07	4	2018	Y
Photosynthesis	FLEX	0.3	0.5	2022	Y
Water vapour	Aqua/AIRS	13.5	1	2002	N
Integrated water budget	–	–	–	–	–

Note: Critical gaps of daily field scale (~1-10 ha) rainfall and root zone storage remain elusive or impractical. Source: McCabe, M.F., Rodell, M., Alsdorf, D.E., Miralles, D.G., Uijlenhoet, R., Wagner, W., Lucieer, A., Houborg, R., Verhoest, N.E.C., Franz, T.E., Shi, J.C., Gao, H.L. & Wood, E.F. 2017. The future of Earth observation in hydrology. *Hydrol. Earth Sys. Sci.* 21(7): 3879–3914. https://doi.org/10.5194/hess-21-3879-2017

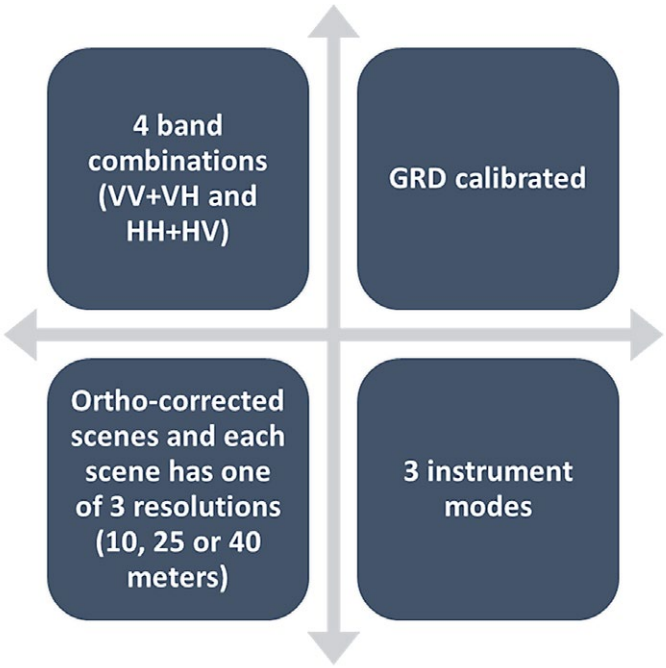

Figure 4.2. Scheme characterizing Sentinel-Radar C-band Satellite imagery of European Space Agency (ESA), used for soil moisture estimation with a combination of the cosmic-ray neutron sensor CRNS

to generate high-resolution soil moisture based on the CRNS and C-band Sentinel-1 in Google Earth Engine can be accessed at https://github.com/mmbaye/SoilMoisutre_Demo.

4.2 Satellite remote sensing data

4.2.1 Sentinel-1 radar microwave data

Sentinel-1 (S1) Ground Range Detected (GRD) is the first of the five missions that the European Space Agency (ESA) implemented under the Copernicus initiative (Torres *et al.* 2012). The S1 mission includes a constellation of two C-band SAR imaging polar-orbiting satellites, providing continuous radar mapping of the globe regardless of the weather. The S1 mission provides data collection of a dual-polarisation instrument (**Figure 4.2**). The C-band SAR has 3-6 days temporal resolution and covers the entire world's landmasses for land monitoring, emergency response, climate change and security. In both ascending and descending orbits, S1 data is collected using a variety of instrument configurations, resolutions, and band combinations (e.g., VV: single co-polarisation, vertical transmit/vertical receive, or VV + VH: dual-band cross-polarisation, vertical transmit/horizontal receive) (Snoeij *et al.* 2009; Torres *et al.* 2012)

4.2.2 Sentinel-2 optical data

Sentinel-2 (S2) data provided by the European Space Agency is also used for this study. They are acquired through two twin satellites (Sentinel-2A and Sentinel-2B), launched separately into a synchronous polar orbit at an altitude of 786 km and evolving at 180° from each other (Drusch *et al.* 2012). Each satellite is equipped with a Multi-Spectral Imager sensor (MSI) covering 13 spectral bands (from 443 nm to 2190 nm) with a field of view of 290 km and a spatial resolution of 10 m (four bands in the visible and near-infrared domains), 20 m (six bands in the near and short-wavelength infra-red domain, NIR and SWIR), and 60 m (three atmospheric correction bands). They monitor the variability of the Earth's surface conditions, or changes in vegetation with the seasons, in a high return time (ten days at the equator with one satellite and five days with the constellation of the two satellites). In this study the Normalized Difference Vegetation Index (NDVI) was estimated using the formula described in **Table 4.2** with the corresponding optical band. This vegetation index will allow users to monitor vegetation biomass over agricultural areas.

Table 4.2. Normalized difference vegetation index (NDVI) required bands and formula

Index name	bands	Formula	Rational
Normalized Difference Vegetation Index (NDVI)	Near-Infra-red (B8) Red (B4)	$\frac{B8 - B4}{B8 + B4}$	The distinction between bare soils and areas covered by vegetation

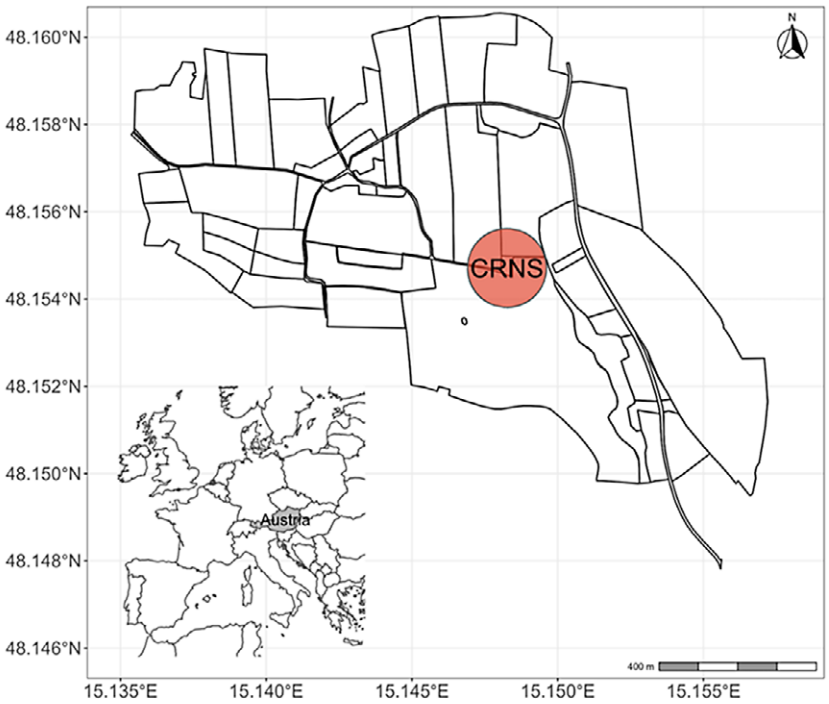

Fig. 4.3. Location of the Cosmic Ray Neutron Sensor (CRNS) within a mixed agricultural land use area in Petzenkirchen (northeast Austria)

NDVI is a measure of the earth's greenness that correlates well with photosynthetically active vegetation. The NDVI is a widely used vegetation index that can be easily calculated using most multispectral sensors as it only requires a red and NIR band. The NDVI scale runs from –1 to 1. Positive NDVI values are closer to 1, bare soil/artificial surfaces have negative NDVI values, water also has negative NDVI values.

4.2.3 CHIRPS precipitation data

Climate Hazards Group InfraRed Precipitation with Station data (CHIRPS) is a 30+ year quasi-global rainfall (daily, pentad and monthly) dataset based on infrared Cold Cloud Duration (Bai *et al.* 2018; Aksu & Akgül, 2020). CHIRPS incorporate 0.05° resolution satellite imagery with in-situ station data to create gridded rainfall time series for trend analysis and seasonal drought monitoring. In this study, precipitation was used as an additional information to understand changes in soil moisture.

4.3 Methodology

4.3.1 Study area

This study was again performed at the field site in the Hydrological Open-Air Laboratory (HOAL) described earlier. HOAL is a cooperation project between the Federal Agency for Water Management (BAW Petzenkirchen) and the Technical University Vienna (TU Vienna). The land use at study site is dominated by cultivated land and the main crops are winter wheat, barley, maize, and rape. A stationary

CRNS is installed at the study site (48.15°N, 15.15°E, elevation 277 m) and soil moisture monitoring has been tracked since December 2013 (**Figure 4.3**).

4.3.2 Methodology of retrieving field scale soil moisture with radar C-band Sentinel-1 and Cosmic Ray Neutron Sensor

The overall methodology to retrieve soil moisture from C-band Sentinel-1 data through an image processing technique using Google Earth Engine (GEE) and the construction of a calibrated model between the radar backscattered coefficient in Vertical-Vertical (VV) polarisation and soil water content measured with CRNS is described in this section. A flowchart of the entire process is shown in **Figure 4.4**, and detailed descriptions of the major steps of the techniques are presented below.

The first phase consists of loading all Sentinel-1 dataset available at the regional scale. After loading all the datasets from Sentinel-1, a different processing steps are carried out using Google Earth Engine (GEE):

- Pre-processing: spatial filtering (selection of the region of interest), temporal filtering, selection of Ascending or Descending mode and spatial resolution;
- Speckle filter: noise speckle (interference) reduction;
- Computation of relative soil moisture: relative soil moisture was estimated using the equation 4.1 proposed by Hornacek *et al.* (2012).

$$\sigma = \frac{\overset{\circ}{\sigma_\theta}(t) - \overset{\circ}{\sigma_{dry}}}{\overset{\circ}{\sigma_{wet}} - \overset{\circ}{\sigma_{dry}}} \qquad 4.1$$

$\overset{\circ}{\sigma_{dry}}$ is the dry reference backscatter [dB], the pixel's backscatter coefficient at entirely dry conditions, $\overset{\circ}{\sigma_{wet}}$ is the wet reference backscatter [dB], the pixel's backscatter coefficient at wet condition.

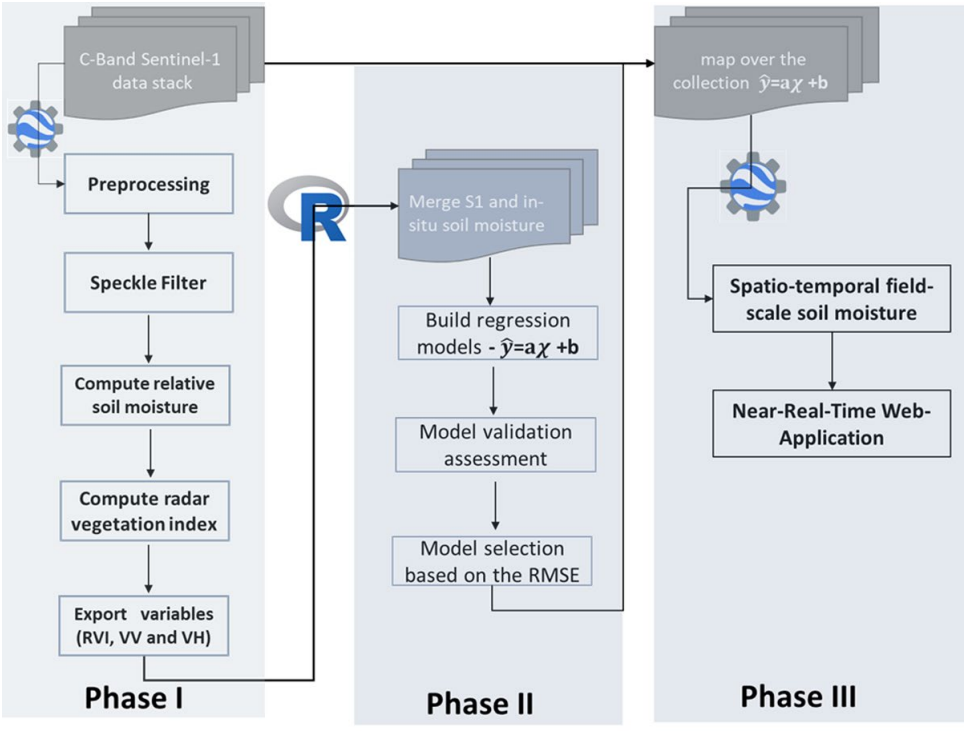

Figure.4.4. Flowchart of the methodology for soil moisture estimation, based on radar C-band Sentinel-1 and Cosmic Ray Neutron Sensor

- Computation of radar vegetation index: various radar vegetation index RVI are estimated using **Equations 4.2 to 4.4**.

$$\sigma_1 = \frac{\sigma_{VV}}{\sigma_{VH}} \quad 4.2$$

$$\sigma_2 = \frac{\sigma_{VV} - \sigma_{VH}}{\sigma_{VV} - \sigma_{VH}} \quad 4.3$$

$$\sigma_3 = \frac{\sigma_{VV} - \sigma_{VH}}{\sigma_{VV}} \quad 4.4$$

$$\sigma_4 = \frac{\sigma_{VV} - \sigma_{VH}}{\sigma_{VH}} \quad 4.5$$

  VV is the single co-polarisation, vertical transmit/vertical receive and VH is the single co-polarisation, vertical transmit/horizontal receive.

- Export variables: extract and export all the radar co-variables discussed above and calculated with the radar bands.

The objective of the second phase is to build a regression model between radar co-variables and the soil moisture data from the CRNS. Thus, it is necessary to combine these two-time series, paying attention to calculate the daily statistics of the in-situ datasets. At this phase, the R software was used. However, it is also possible to do it with other numerical processing computer programme. It is recommended to apply specific filters like the Savitzky-Golay filter before estimating the daily soil moisture statistics. The remaining phases consist of the estimation of the regression model parameters and their validation based on the root mean square error (RMSE) of the different models.

In the last phase (phase 3), the parameters of the regression model were applied to the whole collection of Sentinel-1 images to have a spatio-temporal estimation of the soil moisture at the field scale.

4.3.3 Steps for retrieving large extent soil moisture based on C-band S1 and CRNS

This tutorial consists of blocks of code for step-by-step building soil moisture retrieval using c-Band Radar Sentinel 1 with the support of CRNS. Google Earth Engine (GEE), which is freely accessible, was used together with cloud-based tool for satellite data analysis with a catalogue of satellite imagery and geospatial datasets (Gorelick *et al.* 2017; Tamiminia *et al.* 2020). All satellite data used in this study were processed in this cloud computing platform. A JavaScript application program interface (API) was used to analyse satellite data. However, Python and R versions can also be used.

4.3.3.1 Setting-up the data

The first step is to either load the shapefiles of the study area or manually enter the coordinates of the CRNS site. GPS coordinates were used to define the study area in this example. The recommended procedure comprises of the following four steps:

Step 1. Identification of the CRNS GPS coordinates

Predefining the geographical position of the study site and creating a buffer zone or the footprint around the CRNS location, preferably 10 to 20 hectares in size. Buildings and forests should be avoided as much as possible (see **Figure 4.5**).

Step 2. Radar Vegetation Indices

Defining the function that computes these radar vegetation indices on each Sentinel-1 image. The index bands should be renamed. It is also possible to implement other radar indices. A list of the most used indices in the literature should be proposed. See **Figure 4.6**.

```
Map.setOptions('SATELLITE')
var crnsPosition=ee.Geometry.Point([15.14841,48.15467]);
var region=crnsPosition.buffer(500)
var now=ee.Date(Date.now())
var boxcar = ee.Kernel.circle(10);
Map.centerObject(crnsPosition,15)
Map.addLayer(region,{},'Foot Print')
```

Figure 4.5. Command lines for step 1 (pre-processing)

```
var radarVegetationIndex=function(image){
    var sigma1=image.expression('vv/vh',{'vv':image.select('VV'),'vh':image.select('VH')}).rename('Sigma1')
    var sigma2=image.expression('(vv-vh)/(vv +vh)',{'vv':image.select('VV'),'vh':image.select('VH')}).rename('Sigma2')
    var sigma3=image.expression('(vv-vh)/vv',{'vv':image.select('VV'),'vh':image.select('VH')}).rename('Sigma3')
    var sigma4=image.expression('(vv-vh)/vh',{'vv':image.select('VV'),'vh':image.select('VH')}).rename('Sigma4')
    return image.addBands([sigma1,sigma2,sigma3,sigma4]).copyProperties(image,['system:time_start']);
  }
```

Figure 4.6. Command lines for step 2 (computation of Radar Vegetation Index)

```
var collection = ee.ImageCollection("COPERNICUS/S1_GRD")
                  .filterBounds(region)
                  .filter(ee.Filter.listContains('transmitterReceiverPolarisation', 'VV'))
                  .filter(ee.Filter.listContains('transmitterReceiverPolarisation', 'VH'))
                  .filter(ee.Filter.eq('orbitProperties_pass', 'ASCENDING'))
                  .filterDate(now.advance(-3,'year'),now)
                  .map(function(image){return image.clip(region).select(['VV','VH']).convolve(boxcar)})
                  .map(radarVegetationIndex)


var bands=['Sigma1','Sigma2','Sigma3','Sigma4']
var chart_VVVH = ui.Chart.image.series(collection.select(['VV','VH']), region, ee.Reducer.mean(), 10)
var chart_RVI = ui.Chart.image.series(collection.select(bands), region, ee.Reducer.mean(), 10)

print(
'chart of Radar bands : ',chart_VVVH,
'Chart of Radar Vegetation Index', chart_RVI)
```

Figure 4.7. Command lines for step 3 (Application of RVI function and processing to radar imageries)

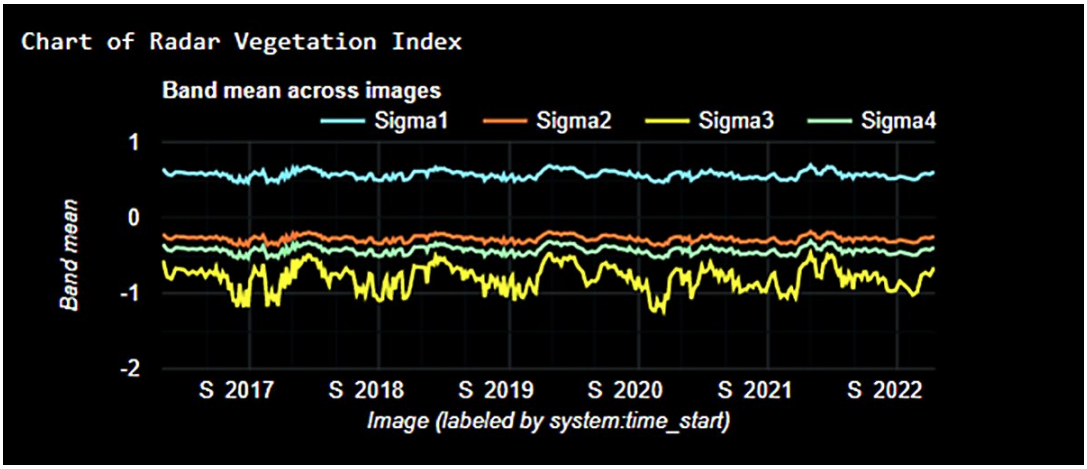

Figure 4.8. Time series of predictor variables over six-years periods

Step 3. Time series Exporting and Visualisation

This step is about the application of different filtering and pre-processing techniques. The boxcar convolution filtering method was used for noise speckle reduction. A series of filtering (temporal filtering, spatial filtering, polarisation filtering and ascending mode) was applied for data reduction. It is important to just keep the ascending mode of the SAR data and the VV polarisation because soil moisture is more sensitive to the VV polarisation than the VH polarisation (Singh *et al.* 2020). In this example, an interval of six years has been considered (see **Figure 4.7).** The rest of the code allows plotting the time series of the variables over the six years. **Figure 4.8** shows an output of this time series which will be exported in CSV format for the development of a conversion model.

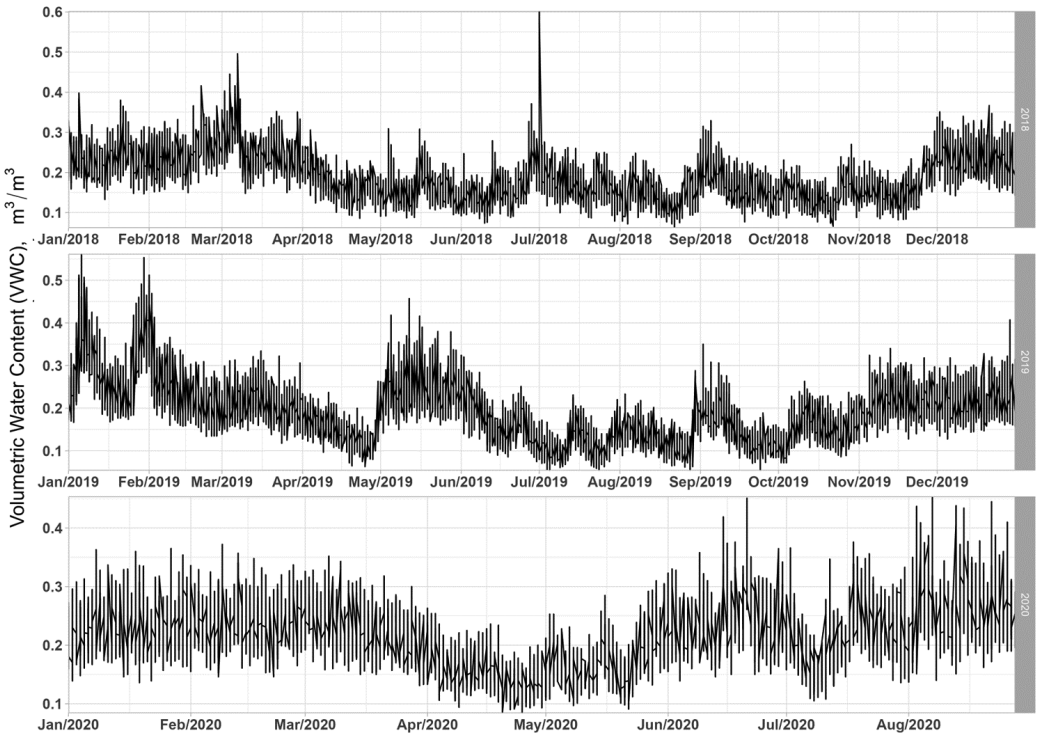

Figure 4.9. Pre-processed time series soil moisture based on the Cosmic Ray Neutron Sensor

4.3.3.2 Model calibration

The calibration process is about to build a calibrated model between the soil moisture data derived from the CRNS and the radar backscatter coefficient (σVV) from Sentinel-1. For the model development, it is necessary to pre-process the raw data of CRNS. This treatment consists of changing the name of the variables, transforming the time variable in date format, and removing the negative measures of the CRNS and the values higher than soil moisture at saturation. For this purpose, the first step in R is to load the corresponding time series SM (soil moisture) dataset. All the code for the calibration purpose can be found on GitHub: https://github.com/mmbaye/SoilMoisutre_Demo. **Figure 4.9** represents the time series of soil moisture measured by the CRNS over three different years. these data have been pre-processed by removing the extreme values.

Some statistical analyses were also performed such as mean, standard deviation, maximum and range per day. The entire data frame has been renamed for ease of use in R. Sentinel-1 data has been available since 2016, and for CRNS since 2015. Thus, for the calibration, only data in 2020 will be considered. Once the data ar\e merged, an estimate of the model parameters is performed. Different types of models can be tested ranging from simple linear regression to non-linear methods or machine learning (Support Vector Machine, Random Forest, XGBoost). In this example, a linear regression model has been proposed by estimating the parameters (a, b) of the model as shown in **Figure 4.10a**. **Figure 4.10** shows the results of the calibration, validation, and prediction of the empirical conversion model. The calibration model with the 2020 data shows an R^2 of 0.81 with an error of about 0.016 m^3/m^3. The predictive error of the model between 2021 and 2022 is of the order of 0.05 m^3/m^3. This increase in prediction error is caused by dense vegetation and snow.

4.3.3.3 High resolution soil moisture map using the model

With the conversion model established, the regression equation is implemented in GEE to convert the VV signal to soil moisture. In this step, the model converts each Sentinel-1 image into soil moisture

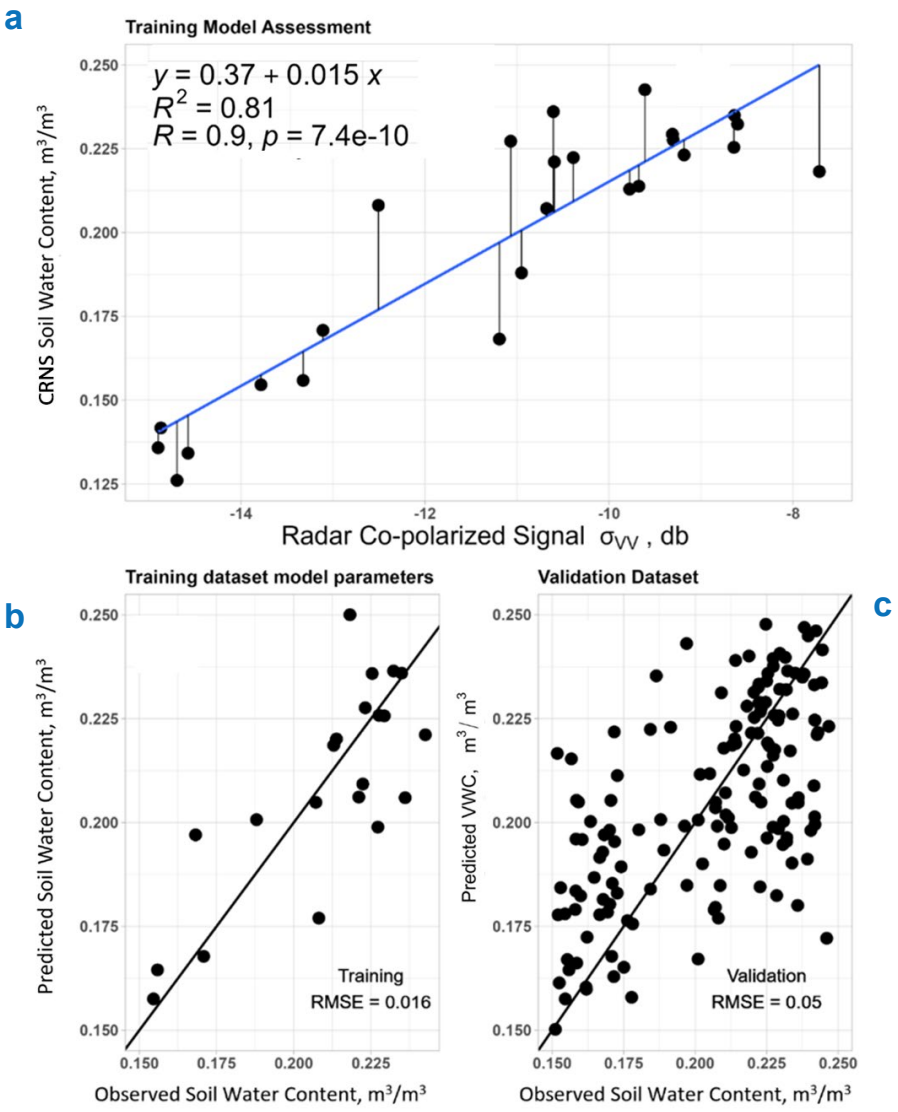

Figure 4.10. Model conversion between radar backscattered coefficient σVV and measured soil water content measured: (a) linear regression model between radar backscattered coefficient σVV and soil water content measured by CRNS; (b)training and validation of the conversion model

information, thus, providing a high spatial resolution soil moisture map as shown in Figure 4.11. This soil moisture map can be used for climate smart agricultural water management.

4.4 Conclusion

In this chapter, a step-by-step algorithm of soil moisture retrieval based on the Cosmic-Ray Neutron Sensor and the C-Band Sentinel-1 was described. The model allows a conversion of Vertical-Vertical (VV) polarisation into soil moisture. The model is calibrated with 2020 CRNS data and validated with data from 2021 to 2022. The results showed the model's good performance with a high correlation for the calibration (R^2 = 0.81) and predicted the soil moisture with an RMSE ranging from 0.016 to 0.05 m^3/m^3. This study is a major step in the monitoring of soil moisture at high spatial and temporal resolution by combining remote sensing and the CRNS based nuclear technology. The preliminary results show the great potential of using nuclear technology such as CRNS for remote sensing calibration of Sentinel-1 (SAR). The code and the guideline to generate high-resolution soil moisture

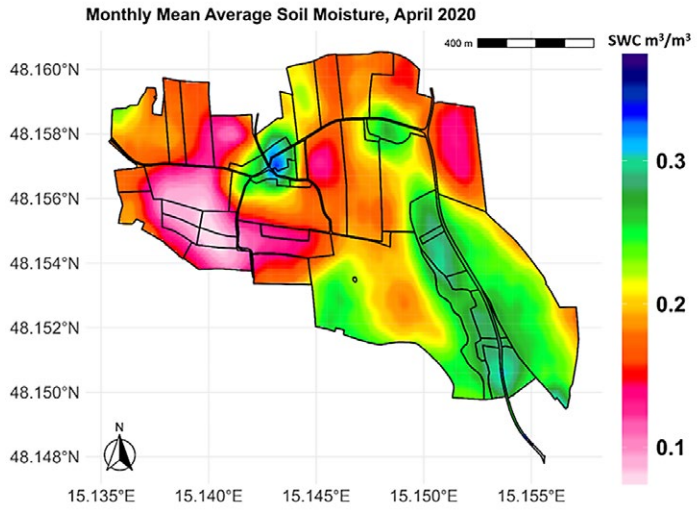

Figure 4.11. Soil moisture map of the mixed agricultural land use area in Petzenkirchen (northeast Austria) where the CRNS has been installed

based on the CRNS and C-band Sentinel-1 in Google Earth Engine are available at: https://github.com/mmbaye/SoilMoisutre_Demo.

References

Aksu, H. & Akgül, M.A. 2020. Performance evaluation of CHIRPS satellite precipitation estimates over Turkey. *Theor. Appl. Climatol.* 142(1): 71–84. https://doi.org/10.1007/s00704-020-03301-5

Bai, L., Shi, C., Li, L., Yang, Y., & Wu, J. 2018. Accuracy of CHIRPS Satellite-Rainfall Products over Mainland China. *Remote Sens.* 10(3): 362. https://doi.org/10.3390/rs10030362

Bauer-Marschallinger, B., Cao, S., Navacchi, C., Freeman, V., Reuß, F., Geudtner, D., Rommen, B., Vega, F.C., Snoeij, P., Attema, E., Reimer, C. & Wagner, W. 2021. The normalised Sentinel-1 Global Backscatter Model, mapping Earth's land surface with C-band microwaves. *Scientific Data*, 8(1): 277. https://doi.org/10.1038/s41597-021-01059-7

Bauer-Marschallinger, B., Freeman, V., Cao, S., Paulik, C., Schaufler, S., Stachl, T., Modanesi, S., Massari, C., Ciabatta, L., Brocca, L. & Wagner, W. 2019. Toward Global Soil Moisture Monitoring With Sentinel-1: Harnessing Assets and Overcoming Obstacles. *IEEE Geosci. Remote. Sens.* 57(1): 520–539. https://doi.org/10.1109/TGRS.2018.2858004

Behari, J., ed. 2005. Dielectric Behavior of Soil. In *Microwave Dielectric Behavior of Wet Soils* (pp. 22–40). Springer Netherlands. https://doi.org/10.1007/1-4020-3288-9_2

Bhogapurapu, N., Dey, S., Mandal, D., Bhattacharya, A., Karthikeyan, L., McNairn, H. & Rao, Y.S. 2022). Soil moisture retrieval over croplands using dual-pol L-band GRD SAR data. *Remote Sens. Environ.* 271: 112900. https://doi.org/10.1016/j.rse.2022.112900

Chan, S.K., Bindlish, R., O'Neill, P.E., Njoku, E., Jackson, T., Colliander, A., Chen, F., *et. al.* 2016. Assessment of the SMAP Passive Soil Moisture Product. *EEE Geosci. Remote. Sens.* 54(8): 4994–5007. https://doi.org/10.1109/TGRS.2016.2561938

Chung, J., Lee, Y., Kim, J., Jung, C., & Kim, S. 2022. Soil Moisture Content Estimation Based on Sentinel-1 SAR Imagery Using an Artificial Neural Network and Hydrological Components. *Remote Sens.* 14(3): 465. https://doi.org/10.3390/rs14030465

Drusch, M., Del Bello, U., Carlier, S., Colin, O., Fernandez, V., Gascon, F., Hoersch, B., Isola, C., Laberinti, P., Martimort, P., Meygret, A., Spoto, F., Sy, O., Marchese, F. & Bargellini, P. 2012.

Sentinel-2: ESA's Optical High-Resolution Mission for GMES Operational Services. *Remote Sens. Environ.* 120: 25–36. https://doi.org/10.1016/j.rse.2011.11.026

Franz, T.E., Wahbi, A., Zhang, J., Vreugdenhil, M., Heng, L., Dercon, G., Strauss, P., Brocca, L. & Wagner, W. 2020). Practical Data Products From Cosmic-Ray Neutron Sensing for Hydrological Applications. *Front. Water* 2. https://www.frontiersin.org/article/10.3389/frwa.2020.00009

Franz, T.E., Zreda, M., Rosolem, R. & Ferre, T.P.A. 2012. Field Validation of a Cosmic-Ray Neutron Sensor Using a Distributed Sensor Network. *Vadose Zone J.* 11(4). vzj2012.0046. https://doi.org/10.2136/vzj2012.0046

Gorelick, N., Hancher, M., Dixon, M., Ilyushchenko, S., Thau, D. & Moore, R. 2017. Google Earth Engine: Planetary-scale geospatial analysis for everyone. *Remote Sens. Environ.* 202: 18–27. https://doi.org/10.1016/j.rse.2017.06.031

Heidbüchel, I., Güntner, A. & Blume, T. 2016. Use of cosmic-ray neutron sensors for soil moisture monitoring in forests. *Hydrol. Earth Sys. Sci.*, 20(3): 1269–1288. https://doi.org/10.5194/hess-20-1269-2016

Hornacek, M., Wagner, W., Sabel, D., Truong, H.-L., Snoeij, P., Hahmann, T., Diedrich, E. & Doubkova, M. 2012. Potential for High Resolution Systematic Global Surface Soil Moisture Retrieval via Change Detection Using Sentinel-1. *IEEE J. Sel. Top. Appl. Earth Obs. Remote Sens.* 5(4): 1303–1311. https://doi.org/10.1109/JSTARS.2012.2190136

Ma, C., Li, X. & McCabe, M.F. 2020. Retrieval of High-Resolution Soil Moisture through Combination of Sentinel-1 and Sentinel-2 Data. *Remote Sens.* 12(14): 2303. https://doi.org/10.3390/rs12142303

Montzka, C., Bogena, H.R., Zreda, M., Monerris, A., Morrison, R., Muddu, S. & Vereecken, H. 2017). Validation of Spaceborne and Modelled Surface Soil Moisture Products with Cosmic-Ray Neutron Probes. *Remote Sens.* 9(2), Article 2. https://doi.org/10.3390/rs9020103

Schrön, M., Köhli, M., Scheiffele, L., Iwema, J., Bogena, H.R., Lv, L., Martini, E., Baroni, G., Rosolem, R., Weimar, J., Mai, J., Cuntz, M., Rebmann, C., Oswald, S.E., Dietrich, P., Schmidt, U. & Zacharias, S. 2017. Improving calibration and validation of cosmic-ray neutron sensors in the light of spatial sensitivity. *Hydrol. Earth Sys. Sci.* 21(10): 5009–5030. https://doi.org/10.5194/hess-21-5009-2017

Singh, A., Gaurav, K., Meena, G.K. & Kumar, S. 2020. Estimation of Soil Moisture Applying Modified Dubois Model to Sentinel-1; A Regional Study from Central India. *Remote Sens.* 2020(12): 2266. https://doi.org/10.3390/rs12142266

Snoeij, P., Attema, E., Davidson, M., Duesmann, B., Floury, N., Levrini, G., Rommen, B. & Rosich, B. 2009. The Sentinel-1 radar mission: Status and performance. *2009 International Radar Conference "Surveillance for a Safer World" (RADAR 2009)*, 1–6.

Stevanato, L., Baroni, G., Cohen, Y., Fontana, C. L., Gatto, S., Lunardon, M., Marinello, F., Moretto, S. & Morselli, L. 2019. A Novel Cosmic-Ray Neutron Sensor for Soil Moisture Estimation over Large Areas. *Agriculture* 9(9): 202. https://doi.org/10.3390/agriculture9090202

Tamiminia, H., Salehi, B., Mahdianpari, M., Quackenbush, L., Adeli, S. & Brisco, B. 2020). Google Earth Engine for geo-big data applications: A meta-analysis and systematic review. *ISPRS J. Photogramm. Remote Sens.* 164: 152–170. https://doi.org/10.1016/j.isprsjprs.2020.04.001

Torres, R., Snoeij, P., Geudtner, D., Bibby, D., Davidson, M., Attema, E., Potin, P., *et al.* 2012. GMES Sentinel-1 mission. *Remote Sens. Environ.* 120: 9–24. https://doi.org/10.1016/j.rse.2011.05.028

Vather, T., Everson, C. & Franz, T.E. 2019. Calibration and Validation of the Cosmic Ray Neutron Rover for Soil Water Mapping within Two South African Land Classes. *Hydrology* 6(3): 65. https://doi.org/10.3390/hydrology6030065

Appendix I
SG filter for temporal smoothing

Matlab code for running main program of SG filter for temporal smoothing of neutron count time series. See supplemental data A for subroutines and datasets.

```
% % % % Trenton Franz

% % % % 4/24/2019

% % % %

% % % % Main program to read in CRNS from Petzenkirchen

%%%%% program updated for HBA


clear all;

close all;

clc;


%%%%%Field name


%%%%Load in Data from text file from CRNS site

%%%%%%Year  Month   Day Day Fraction    Modetared Neutron Counts (cph)
Bare Neutron Counts (cph)   Pressure 1 (mb) Voltage (DCV)   Air Relative
Humidity (%)       Pressure 2 (mb) Neutron Monitor Reference   Intensity
Correction    Water Vapor Correction  Pressure Corretion  Estiamted SWC
(m3/m3)


dat=textread('Petzenkirchen_Data_Hack_20181129.txt');


tdat=datenum(flipud(dat(:,1)),flipud(dat(:,2)),flipud(dat(:,3))+flipud(dat(:,4
)));

n1 = flipud(dat(:,5));

n2 = flipud(dat(:,6));

p1 = flipud(dat(:,11));


h7 = flipud(dat(:,9));

t7 = flipud(dat(:,10));

fsol = flipud(dat(:,15));
```

```
%%%%%remove bad data

t7(find(t7>80|t7<-50))=20;      %%%%% Ext T and RH not added until
6/28/17!!!!!
h7(find(h7>105|h7<0))=50;

n1(find(n1>8000|n1<100))=nan;
n2(find(n2>8000|n2<100))=nan;

%%%%%%%Probe location in field you can use google
%%%%earth to find
csx=15.148415; csy=48.15467;

%%% Use COSMOS Utilities to calculate based off elevation and lat and long
CSF=1.16;

%%%Atmosphere
tref=25;        %%%Reference air temperature (Deg. C)
pref=982;       %%%Reference air pressure (mb, hpa)
rhref=0;        %%%Reference air relative humidity (%)
gama=6.7;       %%%Temperature lapse-rate (monthly climatology): Source
Zweck et al. 2011
lambda=130;     %%%Attenuation rate for Nebraska

% %%%%%%%%%%%%%%%%%%%%%%%%%%%%%%%%%%%%%%%%%%%%%%%%%%%%%%%%%%%%%%%%%%%%%%%%%%%
% %%%%%%%%%%%%%%%%%%%%%%%%%%%%%%%%%%%%%%%%%%%%%%%%%%%%%%%%%%%%%%%%%%%%%%%%%%%
% % % % % % Soil Site Average!!!!!
lw=0.02;              %%%Lattice water, (g/g)
soc=0.005;    %%%Soil organic carbon water equivalent (g/g)
bda=1.42;              %%%Soil bulk density (g/cm3) from Mead
tao=lw+soc;  %%%%Soil water sum(g/g)

sfc=0.40;   %%%Field capacity in (cm3/cm3)
swp=0.25;   %%%Plant Wilting Point in (cm3/cm3)

%%Set upper bound to porosity
```

```
% por=1-bda/2.65;

por=0.6;            %%%Porosity bound reset based on Ammar's
reccomendation.


%%%%%%%%%%%%%%%%%%%%%%%%%%%%%%%%%%%%%%%%%%%%%%%%%%%%%%%%%%%%%%%%%%%%%%%%%%%%%%%

%%%%%%%%%%%%%%%%%%%%%%%%%%%%%%%%%%%%%%%%%%%%%%%%%%%%%%%%%%%%%%%%%%%%%%%%%%%%%%%

%%%%%%%%%%%%%%%%%%%%%%%%%%%%%%%%%%%%%%%%%%%%%%%%%%%%%%%%%%%%%%%%%%%%%%%%%%%%%%%


%%%Calibration Data

swc1=0.276;  %%%%(in g/g)

cd1=datenum(2013,12,12,12,0,0);  %%%Start of calibration, add 6 hours for
average

tw1=(swc1+tao);    %%%%Total water for calibration (g/g)


swc2=24.48/bda/100;  %%%%(in g/g)

cd2=datenum(2014,4,5,12,0,0);  %%%Start of calibration, add 6 hours for
average

tw2=(swc2+tao);    %%%%Total water for calibration (g/g)


swc3=29.26/bda/100;  %%%%(in g/g)

cd3=datenum(2014,4,30,12,0,0);  %%%Start of calibration, add 6 hours for
average

tw3=(swc3+tao);    %%%%Total water for calibration (g/g)


swc4=0.250;  %%%%(in g/g)  %%%guess from rover

cd4=datenum(2016,8,31,12,0,0);  %%%Start of calibration, add 6 hours for
average

tw4=(swc4+tao);    %%%%Total water for calibration (g/g)


swc5=0.271;  %%%%(in g/g)  %%%guess from rover

cd5=datenum(2016,9,8,12,0,0);  %%%Start of calibration, add 6 hours for
average

tw5=(swc5+tao);    %%%%Total water for calibration (g/g)


swc6=0.264;  %%%%(in g/g)  %%%guess from rover

cd6=datenum(2016,9,15,12,0,0);  %%%Start of calibration, add 6 hours for
average

tw6=(swc6+tao);    %%%%Total water for calibration (g/g)
```

```
swc7=0.280;  %%%%(in g/g)  %%%Avg. from gravimetric sampling

cd7=datenum(2016,10,27,12,0,0);  %%%Start of calibration, add 6 hours for
average

tw7=(swc7+tao);    %%%%Total water for calibration (g/g)

swc8=0.267;  %%%%(in g/g)  %%%Avg. from gravimetric sampling

cd8=datenum(2017,3,29,12,0,0);  %%%Start of calibration, add 6 hours for
average

tw8=(swc8+tao);    %%%%Total water for calibration (g/g)


%%summary of calibration

cds=[cd1 cd2 cd3 cd4 cd5 cd6 cd7 cd8]';

swcs=[swc1*bda swc2*bda swc3*bda swc4*bda swc5*bda swc6*bda swc7*bda
swc8*bda]'; %%% cm3/cm3


CI=1./fsol;


%%Variations in water vapor, See Rosolem 2013 J. Hydromet

rhovref=calculate_watervapor(tref,pref,rhref,gama); %%%Temp(C), Press(hPa/
mb), RH(%)

Text=t7;

%%%%%%%%%%%%%%%%%%%%%%%%%%%%

%%%%ONly for Petzen

%%%%%%%%%%%%%%%%%%%%%%%%%%%%

Pext1=p1;

Pext1(find(Pext1>1200|Pext1<700))=nan;

Pext=Pext1;


%%%%%%%%%%%%%%%%%%%%%%%%%%%%

%%%%%%%%%%%%%%%%%%%%%%%%%%%%

%%%%%%%%%%%%%%%%%%%%%%%%%%%%


RHext=h7;

Mod=n1;

Bare=n2;


[rhov,iwv]=calculate_watervapor(Text,Pext,RHext,gama); %%%Temp(C),
```

```
Press(hPa/mb), RH(%), gama

CWV=1.0+0.0054*(rhov-rhovref)*1000;  %%%%correction in g/m3!!!!


%%Pressure variations against the specified average, See Zreda 2012 HESS

Cp=exp((Pext-pref)/lambda);


%%%Corrected Counts

Nc=Mod.*CWV./CI.*Cp./CSF;


%%%Thermal to Fast Ratio

TFR=Bare./Mod;


%%Find counts for calibration

ind21=find(tdat>cd1-6/24 & tdat<=(cd1+6/24));

Ncal1=nanmean(Nc(ind21));

%%%Summary stats

SumN(1,:)=[nanmean(Nc(ind21)) nanmedian(Nc(ind21))
length(ind21) (nansum(Nc(ind21))^0.5)/nansum(Nc(ind21))
nanmean(Nc(ind21))*((nansum(Nc(ind21)))^0.5)/nansum(Nc(ind21))];


ind22=find(tdat>cd2-6/24 & tdat<=(cd2+6/24));

Ncal2=nanmean(Nc(ind22));

%%%Summary stats

SumN(2,:)=[nanmean(Nc(ind22)) nanmedian(Nc(ind22))
length(ind22) (nansum(Nc(ind22))^0.5)/nansum(Nc(ind22))
nanmean(Nc(ind22))*((nansum(Nc(ind22)))^0.5)/nansum(Nc(ind22))];


ind23=find(tdat>cd3-6/24 & tdat<=(cd3+6/24));

Ncal3=nanmean(Nc(ind23));

%%%Summary stats

SumN(3,:)=[nanmean(Nc(ind23)) nanmedian(Nc(ind23))
length(ind23) (nansum(Nc(ind23))^0.5)/nansum(Nc(ind23))
nanmean(Nc(ind23))*((nansum(Nc(ind23)))^0.5)/nansum(Nc(ind23))];


ind24=find(tdat>cd4-6/24 & tdat<=(cd4+6/24));

Ncal4=nanmean(Nc(ind24));

%%%Summary stats

SumN(4,:)=[nanmean(Nc(ind24)) nanmedian(Nc(ind24))
```

```
length(ind24) (nansum(Nc(ind24))^0.5)/nansum(Nc(ind24))
nanmean(Nc(ind24))*((nansum(Nc(ind24)))^0.5)/nansum(Nc(ind24))];


ind25=find(tdat>cd5-6/24 & tdat<=(cd5+6/24));

Ncal5=nanmean(Nc(ind25));

%%%Summary stats

SumN(5,:)=[nanmean(Nc(ind25)) nanmedian(Nc(ind25))
length(ind25) (nansum(Nc(ind25))^0.5)/nansum(Nc(ind25))
nanmean(Nc(ind25))*((nansum(Nc(ind25)))^0.5)/nansum(Nc(ind25))];


ind26=find(tdat>cd6-6/24 & tdat<=(cd6+6/24));

Ncal6=nanmean(Nc(ind26));

%%%Summary stats

SumN(6,:)=[nanmean(Nc(ind26)) nanmedian(Nc(ind26))
length(ind26) (nansum(Nc(ind26))^0.5)/nansum(Nc(ind26))
nanmean(Nc(ind26))*((nansum(Nc(ind26)))^0.5)/nansum(Nc(ind26))];


ind27=find(tdat>cd7-6/24 & tdat<=(cd7+6/24));

Ncal7=nanmean(Nc(ind27));

%%%Summary stats

SumN(7,:)=[nanmean(Nc(ind27)) nanmedian(Nc(ind27))
length(ind27) (nansum(Nc(ind27))^0.5)/nansum(Nc(ind27))
nanmean(Nc(ind27))*((nansum(Nc(ind27)))^0.5)/nansum(Nc(ind27))];


ind28=find(tdat>cd8-6/24 & tdat<=(cd8+6/24));

Ncal8=nanmean(Nc(ind28));

%%%Summary stats

SumN(8,:)=[nanmean(Nc(ind28)) nanmedian(Nc(ind28))
length(ind28) (nansum(Nc(ind28))^0.5)/nansum(Nc(ind28))
nanmean(Nc(ind28))*((nansum(Nc(ind28)))^0.5)/nansum(Nc(ind28))];


% % % ind29=find(tdat>cd9-6/24 & tdat<=(cd9+6/24));

% % % Ncal9=nanmean(Nc(ind29));

% % % %%%%Summary stats

% % % SumN(9,:)=[nanmean(Nc(ind29)) nanmedian(Nc(ind29))
length(ind29) (nansum(Nc(ind29))^0.5)/nansum(Nc(ind29))
nanmean(Nc(ind29))*((nansum(Nc(ind29)))^0.5)/nansum(Nc(ind29))];

% % %

% % % ind210=find(tdat>cd10-6/24 & tdat<=(cd10+6/24));

% % % Ncal10=nanmean(Nc(ind210));
```

```
% % % %%%%Summary stats
% % % SumN(10,:)=[nanmean(Nc(ind210)) nanmedian(Nc(ind210))
length(ind210) (nansum(Nc(ind210))^0.5)/nansum(Nc(ind210))
nanmean(Nc(ind210))*((nansum(Nc(ind210)))^0.5)/nansum(Nc(ind210))];


%%%Calculate N0 values
N0i(1,:)=Ncal1/(0.0808/(tw1+0.115)+0.372);   %%%%N0 (cph)
N0i(2,:)=Ncal2/(0.0808/(tw2+0.115)+0.372);   %%%%N0 (cph)
N0i(3,:)=Ncal3/(0.0808/(tw3+0.115)+0.372);   %%%%N0 (cph)
N0i(4,:)=Ncal4/(0.0808/(tw4+0.115)+0.372);   %%%%N0 (cph)
N0i(5,:)=Ncal5/(0.0808/(tw5+0.115)+0.372);   %%%%N0 (cph)
N0i(6,:)=Ncal6/(0.0808/(tw6+0.115)+0.372);   %%%%N0 (cph)
N0i(7,:)=Ncal7/(0.0808/(tw7+0.115)+0.372);   %%%%N0 (cph)
N0i(8,:)=Ncal8/(0.0808/(tw8+0.115)+0.372);   %%%%N0 (cph)
% % % N0i(9,:)=Ncal9/(0.0808/(tw9+0.115)+0.372);   %%%%N0 (cph)
% % % N0i(10,:)=Ncal10/(0.0808/(tw10+0.115)+0.372);   %%%%N0 (cph)

N0d=nanmean(N0i);

% N0d=2771; %%% Best fit of intercept from local sampling!!!!!!!!

% %
% % %%%%Average Values over certain time period
% % %%%%Starting and ending date of cosmos data rounding to closest hour
value
% % st=datenum(2015, 3, 24, 0, 0, 0);    %%Starting date
% % % en=datenum(2016, 8, 24, 0, 0, 0);    %%%Ending date
% % en=ceil(now);    %%%Ending date

%%%Average Values over certain time period
%%%Starting and ending date of cosmos data rounding to closest hour value
st=datenum(2013, 12, 12, 0, 0, 0);    %%Starting date
en=datenum(2018, 12, 1, 0, 0, 0);    %%Starting date
% en=ceil(now);    %%%Ending date

int=1/24;  %%%interval in days
```

```
ti=[st:int:en]';



% % %%%Standing Wet Biomass Values, Biomass Water Content Values, Dates

% %

% % %%% Specify time for linear interpolation of BWE

% % %%%Beginning time period, emergence date, calibration value,
calibration

% % %%%value, calibration value, harvest date, end time

% %

% % bt=[st en]';

% %

% % %%Standing wet biomass (kg/m2), direct sampling or can get from MODIS
data (William)

% % swb=[0 0]';

% %

% %

% % %%%Biomass water content (g/g), direct sampling or can get from crop

% % %%%coefficients?

% % bwc=[0.75 0.75]';


%%%%Standing Wet Biomass Values, Biomass Water Content Values, Dates


%%%% Specify time for linear interpolation of BWE

%%%%Beginning time period, emergence date, calibration value, calibration

%%%%value, calibration value, harvest date, end time


bt=[st ...

    datenum(2014,5,1,0,0,0) datenum(2014,7,1,0,0,0)
datenum(2014,8,15,0,0,0) datenum(2014,9,15,0,0,0) datenum(2014,10,15,0,0,0)
datenum(2014,11,1,0,0,0)  ...

    datenum(2015,5,1,0,0,0) datenum(2015,7,1,0,0,0)
datenum(2015,8,15,0,0,0) datenum(2015,9,15,0,0,0) datenum(2015,10,15,0,0,0)
datenum(2015,11,1,0,0,0)  ...

    datenum(2016,5,1,0,0,0) datenum(2016,7,1,0,0,0)
datenum(2016,8,15,0,0,0) datenum(2016,9,15,0,0,0) datenum(2016,10,15,0,0,0)
datenum(2016,11,1,0,0,0)  ...

    datenum(2017,5,1,0,0,0) datenum(2017,7,1,0,0,0)
datenum(2017,8,15,0,0,0) datenum(2017,9,15,0,0,0) datenum(2017,10,15,0,0,0)
```

```
datenum(2017,11,1,0,0,0)  ...

    datenum(2018,5,1,0,0,0) datenum(2018,7,1,0,0,0)
datenum(2018,8,15,0,0,0) datenum(2018,9,15,0,0,0) datenum(2018,10,15,0,0,0)
datenum(2018,11,1,0,0,0)  ...

    en]';


%%%Standing wet biomass (kg/m2), direct sampling or can get from MODIS data
(William)

swb=[0 ...

    0 1 3 2 1 0 ...

    0 1 3 2 1 0 ...

    0 1 3 2 1 0 ...

    0 1 3 2 1 0 ...

    0 1 3 2 1 0 ...

    0]';


%%%%Biomass water content (g/g), direct sampling or can get from crop

%%%%coefficients?

bwc=ones(length(swb),1)*0.75;


%%%Biomass water equivalent (mm) assuming vegetion density is 1 and 0.5556

%%%is stochiometric equivalent of cellulose to water

bwei=swb.*(1-bwc).*0.494+swb.*bwc;


%%%% Incoming intensity correction. See Zreda 2012 HESS

bwea=interp1(bt,bwei,ti,'linear');  %%%Linearly interpolate to minute
values for survey period


mr=-4.9506; %%%slope of biomass N0 function from rover

N0r=518.34;  %%%


N0a=N0d.*(mr./N0r.*bwea+1);


%%%Find intensity correction factor for each time period

for i=1:length(tdat)

   if i==1

       ind=find(ti>tdat(i)-1/24 & ti<=tdat(i));
```

```
    else
        ind=find(ti>tdat(i-1) & ti<=tdat(i));
    end

    N0(i,:)=nanmean(N0a(ind));
    bwe(i,:)=nanmean(bwea(ind));

    clear ind

end

int=1/24;  %%%interval in days
tii=[st:int:en]';

%%%Compute daily average water content and site average
for i=1:length(tii)-1
    %%%Neutron Count in Time Interval
    ind1=find(tdat>=tii(i) & tdat<tii(i+1));

    Ncdum=nanmean(Nc(ind1));
    N0dum=nanmean(N0(ind1));
     bwedum=nanmean(bwe(ind1));
     TFRdum=nanmean(TFR(ind1));

     Textdum=nanmean(Text(ind1));
     Pextdum=nanmean(Pext(ind1));
     RHextdum=nanmean(RHext(ind1));


    SWC=((0.0808/(Ncdum/N0dum-.372)-0.115)-tao)*bda;  %%%%

    if SWC>por
       SWC=por;
    end
```

```
    if ~isempty(ind1)
        sswc(i,:)=[(tii(i)+tii(i+1))/2 Ncdum N0dum Textdum Pextdum RHextdum
SWC];
    else
        sswc(i,:)=[(tii(i)+tii(i+1))/2 nan nan nan nan nan nan ];
    end

    clear ind1 Ncdum N0dum SWC

end

% Gap-filling: Linear interpolation if tgap <= 3 hours, and interpolation
based on previous/next 15 days if tgap > 3 hours
% forcing is the data matrix forcing(time,variables)
npoints = 24; % 24 data points per day
nshortmax = 3; % short gap size
ndayslong = 4; % long-gap analysis window

forcing=sswc(:,2:7);

[Xforc,IDXforc] = GapFill(forcing',npoints,nshortmax,ndayslong,-
999999,999999,'forcing');
Xforc = Xforc'; % forcing matrix
IDXforc = IDXforc'; % matrix with gap fill indices
%%%%%Hourly Gap Filled Data
sswc(:,2:7)=Xforc;

% %%%%Remove bad counts
ncf=sswc(:,2);
ncf(find(ncf>1200|ncf<700))=nan;
sswc(:,2)=ncf;

%%%SG Filtered Data
sgf = sgolayfilt(sswc(:,2),3,25);   % SG filter
```

```
SWC1=((0.0808./(sgf./sswc(:,3)-.372)-0.115)-tao).*bda;  %%%%

SWC1(find(SWC1>por))=por;

%%%Summarize data for analyses
[yy mm dd hh min sec]=datevec(sswc(:,1));
dsum=[yy mm dd hh min sswc sgf SWC1];
Luca=dsum(:,[6 9 10 11 14]);

%%%%Plot and figure settings
fs=18;
ms=12;
wd=2;
% %
% % %
% % % % st=datenum(2014, 4, 1, 0, 0, 0);    %%Starting date
% % % % en=datenum(2016, 7, 16, 0, 0, 0);    %%%Ending date

xl=st-1;
xu=en+1;
% % % tick=[datenum(2015,3,22,0,0,0) datenum(2015,4,1,0,0,0)
datenum(2015,4,8,0,0,0) datenum(2015,4,15,0,0,0) datenum(2015,4,22,0,0,0)
datenum(2015,5,1,0,0,0) datenum(2015,5,8,0,0,0) datenum(2015,5,15,0,0,0)
datenum(2015,5,22,0,0,0) datenum(2015,6,1,0,0,0) datenum(2015,6,8,0,0,0)
datenum(2015,6,15,0,0,0) datenum(2015,6,22,0,0,0) datenum(2015,7,1,0,0,0)
datenum(2015,7,8,0,0,0) datenum(2015,7,15,0,0,0) datenum(2015,7,22,0,0,0)
datenum(2015,8,1,0,0,0)];  %%%%
% % % tick=[datenum(2015,4,1,0,0,0) datenum(2015,4,15,0,0,0)
datenum(2015,5,1,0,0,0) datenum(2015,5,15,0,0,0)  datenum(2015,6,1,0,0,0)
datenum(2015,6,15,0,0,0) datenum(2015,7,1,0,0,0) datenum(2015,7,15,0,0,0)
datenum(2015,8,1,0,0,0) datenum(2015,8,15,0,0,0) datenum(2015,9,1,0,0,0)
datenum(2015,9,15,0,0,0) datenum(2015,10,1,0,0,0) datenum(2015,10,15,0,0,0)
datenum(2015,11,1,0,0,0) datenum(2015,11,15,0,0,0) datenum(2016,7,1,0,0,0)
datenum(2016,7,15,0,0,0)];  %%%%
tick=[xl:100:xu];

%%%% Load in Site calibration data for Rainfall and Martin Schron's
%%%% Calibration Method
% % % Matlab Day    SG Filtered SWC     Martin' SWC     Rainfall observed
sitedata=textread('Schron_Rainfall_Petzen.txt');
```

```
figure(1000)
subplot(2,1,1,'Fontsize',fs,'XTick',tick)
hold on
plot(sswc(:,1),sswc(:,2),'k.','markersize',ms)
plot(sswc(:,1),sgf,'r.-','markersize',ms)
hold off
ylabel('Moderated Neutron Counts (cph)','fontsize',fs)
title(,Petzenkirchen CRNS','fontsize',fs+8)
% xlabel('Local Time','fontsize',fs)
datetick('x','dd mmm yy','keepticks')
xlim([xl xu])
% xlim([xl xl+20])
% ylim([0 0.25])
grid on
box on
legend('Corrected Hourly','SG Filtered Hourly')
subplot(2,1,2,'Fontsize',fs,'XTick',tick)
hold on
bar(sitedata(:,1),sitedata(:,4),'k')
hold off
ylabel('Rainfall (mm/day)','fontsize',fs)
title(,Petzenkirchen Rainfall','fontsize',fs+8)
% xlabel('Local Time','fontsize',fs)
datetick('x','dd mmm yy','keepticks')
xlim([xl xu])
% xlim([xl xl+20])
% ylim([0 0.25])
grid on
box on

figure(1001)
subplot(2,1,1,'Fontsize',fs,'XTick',tick)
hold on
plot(sswc(:,1),sswc(:,7),'k.','markersize',ms)
```

```
plot(sitedata(:,1),sitedata(:,2),'r.-','markersize',ms)
plot(sitedata(:,1),sitedata(:,3),'b.-','markersize',ms)
% plot(tdat,SWC2,'b.-','markersize',ms)
hold off
ylabel('Soil Water Content (cm^3/cm^3)','fontsize',fs)
title('Petzenkirchen Soil Water Content','fontsize',fs+8)
datetick('x','dd mmm yy','keepticks')
xlim([xl xu])
% xlim([xl xl+20])
ylim([0.05 0.60])
grid on
box on
legend('Corrected Hourly','SG Filtered Daily (Desilets 2010 EQN)','SG
Filtered Daily (Kohli 2015 EQN)')
subplot(2,1,2,'Fontsize',fs,'XTick',tick)
hold on
bar(sitedata(:,1),sitedata(:,4),'k')
hold off
ylabel('Rainfall (mm/day)','fontsize',fs)
title(,Petzenkirchen Rainfall',fontsize',fs+8)
% xlabel('Local Time','fontsize',fs)
datetick('x','dd mmm yy','keepticks')
xlim([xl xu])
% xlim([xl xl+20])
% ylim([0 0.25])
grid on
box on

figure(1003)
subplot(1,1,1,'Fontsize',fs)
hold on
plot(sitedata(:,2),sitedata(:,3),'k.','markersize',ms)
plot([0 1],[0 1],'r-','linewidth',2)
hold off
xlabel('Soil Water Content, Desilets 2010 EQN (cm^3/cm^3)','fontsize',fs)
ylabel('Soil Water Content, Kohli 2015 EQN (cm^3/cm^3)','fontsize',fs)
```

```
title('Petzenkirchen Soil Water Content Comparison','fontsize',fs+8)
xlim([0 0.6])
ylim([0 0.6])
grid on
box on
axis square
```

Appendix II
SM2RAIN algorithm

Matlab code for running main program of SM2RAIN algorithm for estimating daily rainfall from soil water content time series and input rainfall data. See supplemental data B for subroutines and datasets.

```
%%%%%Program updated for HBA calculations
%%%%%% 3/5/19

clc,clear,close all
dataSM=load('CRNS_Petzenkirchen_HBA.txt');
P=load('P_Petzenkirchen_new.txt');
namefig='CRNS Petzenkirchen';
NDAYS=1;

% SM = sgolayfilt(dataSM(:,7),3,17);

SM=(dataSM(1:1:end,[9]));
DSM=dataSM(1:1:end,1);

D0=fix(dataSM(1,1)+1);
D1=fix(dataSM(end,1)-1);

ID0=find(P(:,1)==D0);
ID1=find(P(:,1)==D1);
PP=P(ID0:ID1,2);
DPP=P(ID0:ID1,1);
DD=(D0:1/24:D1)';

Pint=interp1gap(DPP,PP,DD);
SMint=norma(interp1gap(DSM,SM,DD,2));

AGGR=24*NDAYS;
dataSM2R=[DD,SMint,Pint];
```

```
% [X,R,RMSE,Psim]=cal_SM2RAIN_T(dataSM2R,AGGR,[0.1,0.05,0.1,0.1]',1,namefig);

[X,R,RMSE,Psim,SM]=cal_
SM2RAIN_T(dataSM2R,AGGR,[0.1,0.05,0.1,0.1]',1,namefig);

st=datenum(2013, 12, 12, 0, 0, 0);    %%Starting date
en=datenum(2018, 12, 1, 0, 0, 0);    %%Starting date

int=24/24;  %%%interval in days
tii=[st:int:en]';

tdat=dataSM2R(:,1);

%%%Compute daily average water content and site average
for i=1:length(tii)-1
    %%%Neutron Count in Time Interval
    ind1=find(tdat>=tii(i) & tdat<tii(i+1));

    Pobsdum=sum(dataSM2R(ind1,3));
    Psimdum=sum(Psim(ind1,1));

    if ~isempty(ind1)
        Psum(i,:)=[(tii(i)+tii(i+1))/2 Pobsdum Psimdum];
    else
        Psum(i,:)=[(tii(i)+tii(i+1))/2 nan nan];
    end

    clear ind1 Pobsdum Psimdum

end


[yy mon day hour mm ss]=datevec(Psum(:,1));

Ammar=[yy mon day Psum(:,2:3)];
```

```
fs=20;
ms=12;
wd=2;

st=datenum(2013, 12, 12, 0, 0, 0);    %%Starting date
en=datenum(2018, 12, 1, 0, 0, 0);    %%Starting date

xl=st-1;
xu=en+1;
tick=[xl:100:xu];

figure(2)
subplot(1,1,1,'Fontsize',fs,'XTick',tick)
hold on
bar(Psum(:,1),Psum(:,2),'k')
bar(Psum(:,1),Psum(:,3),'r')
hold off
ylabel('Rainfall (mm/day)','fontsize',fs)
title('Petzenkirchen Rainfall','fontsize',fs+8)
% xlabel('Local Time','fontsize',fs)
datetick('x','dd mmm yy','keepticks')
xlim([xl xu])
% xlim([xl xl+20])
% ylim([0 0.25])
grid on
box on
legend('Precipitation Observed','Precipitation SM2RAIN')
gtext('R = 0.775, KGE = 0.571, BIAS = -0.634, RMSE =3.114','fontsize',fs+8)

figure(3)
subplot(1,1,1,'fontsize',fs)
hold on
plot(Psum(:,2),Psum(:,3),'ko','markersize',ms)
plot([0 60],[0 60],'linewidth',wd)
hold off
```

```
title('Petzenkirchen Rainfall','fontsize',fs+8)
xlabel('Precipitation Observed (mm/day)','fontsize',fs)
ylabel('Precipitation SM2RAIN (mm/day)','fontsize',fs)
box on
grid on
xlim([0 60])
ylim([0 60])
axis square
```

Appendix III
Exponential filter algorithm

Matlab Code for running main program of exponential filter algorithm for estimating root zone soil water content. See supplemental data C for subroutines and datasets.

```
% % % Trenton Franz
% % % 2/27/2019
% % % Main program to compute exponential filter from Petzenkirchen TDT and
% CRNS data following 2016 Peterson HESS
clear all;
close all;
clc;

%%%%Load in processed CRNS data from SG filter download can be linked to
%%%%website and processing
%%%%Load in processed CRNS data from 20131212 to 20181008
crns=textread('pet_CRNS_hourly.txt');

%%%%% Exponential Filter Parameters for shallow CRNS, column 14 is hourly
%%%%% SG Filtered data
th1min=min(crns(:,14));
th1max=max(crns(:,14));

%%%%%Daily averaged values from CRNS, Run daily average code
% % % %  save('Brule_exp_CRNS_Sum_2017.mat','sswc'); Matlab Day and SWC
%%%%load in daily average CNRS for whole time series
load('CRNS_dSum.mat','sswc2');
th1=sswc2(:,2);

%%%%% Exponential Filter Parameters for shallow CRNS time series
th1min=min(crns(:,14));
th1max=max(crns(:,14));

% %%%%Normalize data to Soil Water Index
SWI1=(th1-th1min)./(th1max-th1min);
```

```
%%%%%% Best fit parameters for Exp. Filter
% Depth KGE=    Th2min  Th2max  Topt
param=[30   0.909   0.050   0.680   48.000
    60  0.912   0.155   0.59    62];

%%%%%%%%%%%%%%%%%%%%%%%%%%%%%%%%%%%%%%%%%%%%%%%%%%%%%%%%%%%
%%%%%%%%%%%%%%%%%% 30 cm product %%%%%%%%%%%%%%%%%%
%%%%%%%%%%%%%%%%%%%%%%%%%%%%%%%%%%%%%%%%%%%%%%%%%%%%%%%%%%%

%%%%Optimal filter parameters from calibration data
th2min=param(1,3);
th2max=param(1,4);
T_opt=param(1,5);

%%%Setup filter parameters
K_1=1;
t=1;
SWI_calm=[];
SWI_obsm=SWI1;
SWI_calm(1)=SWI_obsm(1);

%%%%Compute exponential filter
for i=2:length(SWI_obsm)
    if isnan(SWI_obsm(i))
        t=t+1;
        SWI_calm(i)=nan;
        if t==2
        end
    else
        K_2=(K_1)/(K_1+1/exp(t/T_opt));
        if t==1
            Ini=SWI_calm(i-1);
        end

        SWI_calm(i)=Ini+K_2*(SWI_obsm(i)-Ini);
```

```
        K_1=K_2;
        t=1;
    end

end

SWI_30=SWI_calm';
SWC_30=SWI_30*(th2max-th2min)+th2min;

%%%%%%%%%%%%%%%%%%%%%%%%%%%%%%%%%%%%%%%%%%%%%%%%%%%%%%%%%%%%
%%%%%%%%%%%%%%%%%%%%%%%%%%%%%%%%%%%%%%%%%%%%%%%%%%%%%%%%%%%%
%%%%%%%%%%%%%%%%%%%%%%%%%%%%%%%%%%%%%%%%%%%%%%%%%%%%%%%%%%%%
%%%%%%%%%%%%%%%%%%%%%%%%%%%%%%%%%%%%%%%%%%%%%%%%%%%%%%%%%%%%
%%%%%%%%%%%%%%%%%%% 60 cm product %%%%%%%%%%%%%%%%%
%%%%%%%%%%%%%%%%%%%%%%%%%%%%%%%%%%%%%%%%%%%%%%%%%%%%%%%%%%%%
%%%%Optimal filter parameters from calibration data
th2min=param(2,3);
th2max=param(2,4);
T_opt=param(2,5);

%%%Setup filter parameters
K_1=1;
t=1;
SWI_calm=[];
SWI_obsm=SWI1;
SWI_calm(1)=SWI_obsm(1);

%%%%Compute exponential filter
for i=2:length(SWI_obsm)
    if isnan(SWI_obsm(i))
        t=t+1;
        SWI_calm(i)=nan;
        if t==2
        end
    else
        K_2=(K_1)/(K_1+1/exp(t/T_opt));
        if t==1
```

```
            Ini=SWI_calm(i-1);
        end

        SWI_calm(i)=Ini+K_2*(SWI_obsm(i)-Ini);

        K_1=K_2;
        t=1;
    end

end
SWI_60=SWI_calm';
SWC_60=SWI_60*(th2max-th2min)+th2min;
%%%%%%%%%%%%%%%%%%%%%%%%%%%%%%%%%%%%%%%%%%%%%%%%%%%%%%%%
%%%%%%%%%%%%%%%%%%%%%%%%%%%%%%%%%%%%%%%%%%%%%%%%%%%%%%%%
%%%%%%%%%%%%%%%%%%%%%%%%%%%%%%%%%%%%%%%%%%%%%%%%%%%%%%%%
%%%%Summarize all of data
SWCdsum=[sswc2 SWC_30 SWC_60];
[yy mm dd]=datevec(SWCdsum(:,1));
Ammar=[yy mm dd SWCdsum];
 %%%%Plot and figure settings
fs=18;
ms=12;
wd=2;
cmap=flipud(jet(36));
cmap2=flipud(jet(6));
st=datenum(2013, 12, 12, 0, 0, 0);    %%Starting date
en=datenum(2018, 11, 29, 0, 0, 0);    %%%Ending date
xl=st-1;
xu=en+1;
tick=[xl:100:xu];
figure(100)
subplot(1,1,1,'Fontsize',fs,'XTick',tick)
hold on
plot(SWCdsum(:,1),SWCdsum(:,2),'.-','markersize',ms,'color',[cmap2(1,1)
cmap2(1,2) cmap2(1,3)])
plot(SWCdsum(:,1),SWCdsum(:,3),'.-','markersize',ms,'color',[cmap2(2,1)
cmap2(2,2) cmap2(2,3)])
plot(SWCdsum(:,1),SWCdsum(:,4),'.-','markersize',ms,'color',[cmap2(3,1)
```

```
cmap2(3,2) cmap2(3,3)])

title('Exponential Filter Operational Period, Petzenkirchen
CRNS','fontsize',fs)

hold off

ylabel('SWC (cm^3/cm^3)','fontsize',fs)

% xlabel('Local Time','fontsize',fs)

datetick('x','dd mmm yy','keepticks')

xlim([xl xu])

% xlim([xl xl+20])

% ylim([0 0.25])

legend('CRNS (0-20 cm)','Exponential Filter Fit (0-30 cm)','Exponential
Filter Fit (0-60 cm)')

grid on

box on


figure(101)

subplot(4,1,1,'Fontsize',fs,'XTick',tick)

hold on

plot(SWCdsum(:,1),SWCdsum(:,2)*20,'.-','markersize',ms,'color',[cmap2(1,1)
cmap2(1,2) cmap2(1,3)])

% plot(SWCdsum(:,1),SWCdsum(:,3)*60/2.54,'.-','markersize',ms,'color',[cm
ap2(2,1) cmap2(2,2) cmap2(2,3)])

% plot(SWCdsum(:,1),SWCdsum(:,4)*90/2.54,'.-','markersize',ms,'color',[cm
ap2(3,1) cmap2(3,2) cmap2(3,3)])

% plot(SWCdsum(:,1),SWCdsum(:,5)*120/2.54,'.-','markersize',ms,'color',[cm
ap2(4,1) cmap2(4,2) cmap2(4,3)])

% plot(SWCdsum(:,1),SWCdsum(:,6)*150/2.54,'.-','markersize',ms,'color',[cm
ap2(5,1) cmap2(5,2) cmap2(5,3)])

title('Exponential Filter Operational Period, Petzenkirchen
CRNS','fontsize',fs)

hold off

ylabel('Water Storage (cm per 0-20 cm)','fontsize',fs)

% xlabel('Local Time','fontsize',fs)

datetick('x','dd mmm yy','keepticks')

xlim([xl xu])

% xlim([xl xl+20])

% ylim([0 0.25])

% legend('CRNS (0-30 cm)','Exponential Filter Fit (0-60 cm)','Exponential
Filter Fit (0-90 cm)','Exponential Filter Fit (0-120 cm)','Exponential
Filter Fit (0-150 cm)')

grid on
```

```
box on

subplot(4,1,2,'Fontsize',fs,'XTick',tick)

hold on

% plot(SWCdsum(:,1),SWCdsum(:,2)*30/2.54,'.-','markersize',ms,'color',[cm
ap2(1,1) cmap2(1,2) cmap2(1,3)])

plot(SWCdsum(:,1),SWCdsum(:,3)*30,'.-','markersize',ms,'color',[cmap2(2,1)
cmap2(2,2) cmap2(2,3)])

% plot(SWCdsum(:,1),SWCdsum(:,4)*90/2.54,'.-','markersize',ms,'color',[cm
ap2(3,1) cmap2(3,2) cmap2(3,3)])

% plot(SWCdsum(:,1),SWCdsum(:,5)*120/2.54,'.-','markersize',ms,'color',[cm
ap2(4,1) cmap2(4,2) cmap2(4,3)])

% plot(SWCdsum(:,1),SWCdsum(:,6)*150/2.54,'.-','markersize',ms,'color',[cm
ap2(5,1) cmap2(5,2) cmap2(5,3)])

% title('Exponential Filter Operational Period, Petzenkirchen
CRNS','fontsize',fs)

hold off

ylabel('Water Storage (cm per 0-30 cm)','fontsize',fs)

% xlabel('Local Time','fontsize',fs)

datetick('x','dd mmm yy','keepticks')

xlim([xl xu])

% xlim([xl xl+20])

% ylim([0 0.25])

% legend('CRNS (0-30 cm)','Exponential Filter Fit (0-60 cm)','Exponential
Filter Fit (0-90 cm)','Exponential Filter Fit (0-120 cm)','Exponential
Filter Fit (0-150 cm)')

grid on

box on

subplot(4,1,3,'Fontsize',fs,'XTick',tick)

hold on

% plot(SWCdsum(:,1),SWCdsum(:,2)*30/2.54,'.-','markersize',ms,'color',[cm
ap2(1,1) cmap2(1,2) cmap2(1,3)])

% plot(SWCdsum(:,1),SWCdsum(:,3)*60/2.54,'.-','markersize',ms,'color',[cm
ap2(2,1) cmap2(2,2) cmap2(2,3)])

plot(SWCdsum(:,1),SWCdsum(:,4)*60,'.-','markersize',ms,'color',[cmap2(3,1)
cmap2(3,2) cmap2(3,3)])

% plot(SWCdsum(:,1),SWCdsum(:,5)*120/2.54,'.-','markersize',ms,'color',[cm
ap2(4,1) cmap2(4,2) cmap2(4,3)])

% plot(SWCdsum(:,1),SWCdsum(:,6)*150/2.54,'.-','markersize',ms,'color',[cm
ap2(5,1) cmap2(5,2) cmap2(5,3)])

% title('Exponential Filter Operational Period, Petzenkirchen
CRNS','fontsize',fs)

hold off

ylabel('Water Storage (cm per 0-60 cm)','fontsize',fs)
```

```
% xlabel('Local Time','fontsize',fs)

datetick('x','dd mmm yy','keepticks')

xlim([xl xu])

% xlim([xl xl+20])

% ylim([0 0.25])

% legend('CRNS (0-30 cm)','Exponential Filter Fit (0-60 cm)','Exponential
Filter Fit (0-90 cm)','Exponential Filter Fit (0-120 cm)','Exponential
Filter Fit (0-150 cm)')

grid on

box on

subplot(4,1,4,'Fontsize',fs,'XTick',tick)

hold on

plot(SWCdsum(:,1),SWCdsum(:,3)*30,'.-','markersize',ms,'color',[cmap2(1,1)
cmap2(1,2) cmap2(1,3)])

plot(SWCdsum(:,1),SWCdsum(:,4)*60-SWCdsum(:,3)*30,'.-','markersize',ms,'col
or',[cmap2(2,1) cmap2(2,2) cmap2(2,3)])

% title('Exponential Filter Operational Period, Petzenkirchen
CRNS','fontsize',fs)

hold off

ylabel('Water Storage (cm per 30 cm)','fontsize',fs)

% xlabel('Local Time','fontsize',fs)

datetick('x','dd mmm yy','keepticks')

xlim([xl xu])

% xlim([xl xl+20])

% ylim([0 0.25])

legend('0-30cm','30-60cm')

grid on

box on
```

COSMIC RAY NEUTRON SENSING

Water is fundamental to agriculture, and as global food demand surges, sustainable water management has never been more essential. The book titled *Cosmic Ray Neutron Sensing Applications in Agricultural Water Management* introduces Cosmic Ray Neutron Sensor (CRNS) technology as an innovative solution, providing exceptional accuracy in landscape-level soil moisture monitoring — a crucial step for optimizing irrigation and enhancing crop resilience.

Designed for a diverse audience, from beginners to experts, this comprehensive book delivers actionable insights for monitoring soil water content and enhancing water use efficiency. It is an invaluable resource for research institutions, government agencies, and farmers integrating CRNS into sustainable agricultural practices.

Dive into a step-by-step approach to CRNS data processing, from estimating soil moisture in the root zone to validating satellite imagery. Enhance your land management approach and contribute to a sustainable agricultural future with this essential guide to CRNS technology.

Joint FAO/IAEA Centre of Nuclear Techniques in Food and Agriculture

https://www.iaea.org/about/organizational-structure/department-of-nuclear-sciences-and-applications/joint-fao/iaea-centre-of-nuclear-techniques-in-food-and-agriculture

Food and Agriculture Organization of the United Nations

Vienna, Austria

ISBN 978-92-5-139147-1

9 789251 391471

CD2650EN/1/03.25